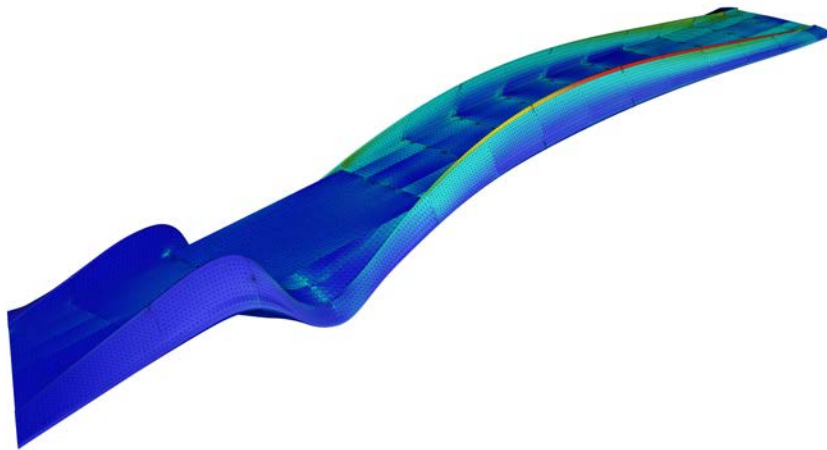




CHALMERS
UNIVERSITY OF TECHNOLOGY



Parametric analysis and stiffness optimisation of FRP pedestrian bridges

Optimisation of hybrid fibre compositions and fibre angles in serviceability limit state

Master's thesis in Structural Engineering and Building Technology

JIMMIE ANDERSSON
GUSTAV GOOD

Department of Civil and Environmental Engineering
Division of Structural Engineering
CHALMERS UNIVERSITY OF TECHNOLOGY
Gothenburg, Sweden 2017
Master's thesis BOMX02-17-8

MASTER'S THESIS BOMX02-17-8

Parametric analysis and stiffness optimisation of FRP pedestrian bridges

Optimisation of hybrid fibre compositions and fibre angles in serviceability limit state

Master's thesis in Structural Engineering and Building Technology

JIMMIE ANDERSSON
GUSTAV GOOD

Department of Civil and Environmental Engineering
Division of Structural Engineering
CHALMERS UNIVERSITY OF TECHNOLOGY
Gothenburg, Sweden 2017

Parametric analysis and stiffness optimisation of FRP pedestrian bridges
Optimisation of hybrid fibre compositions and fibre angles in serviceability limit state
JIMMIE ANDERSSON
GUSTAV GOOD

© JIMMIE ANDERSSON , GUSTAV GOOD, 2017

Master's thesis BOMX02-17-8
Department of Civil and Environmental Engineering
Division of Structural Engineering
Chalmers University of Technology
SE-412 96 Gothenburg
Sweden
Telephone: +46 (0)31-772 1000

Cover:
von Mises stress analysis of Kaponjärbron

Chalmers Reproservice
Gothenburg, Sweden 2017

Parametric analysis and stiffness optimisation of FRP pedestrian bridges
Optimisation of hybrid fibre compositions and fibre angles in serviceability limit state
Master's thesis in Structural Engineering and Building Technology
JIMMIE ANDERSSON
GUSTAV GOOD
Department of Civil and Environmental Engineering
Division of Structural Engineering
Chalmers University of Technology

ABSTRACT

FRP (Fibre Reinforced Polymer) bridges come in many different sizes and shapes, and often involve complex geometry. This, combined with anisotropic material behaviour, means building a structural analysis model of the bridge becomes time consuming, and making early design decisions difficult. Therefore, parametric analysis, where the analysis model is generated based on a set of changeable parameters, could be a suitable method for evaluating performance.

The decisive factors in almost all cases when designing FRP pedestrian bridges are the serviceability demands. The fibres used in FRP can be made of different materials but glass fibre is the dominant one used today. Since glass fibres have comparatively low stiffness, bridges often need to be stiffened with carbon fibres. The downside with carbon fibres is the high price and it is therefore critical to minimise the amount of carbon fibre used. By using parametric analysis, it is possible to optimise the position of the carbon fibres and its cover area.

In this thesis the possibilities of using parametric modelling for analysing and optimising existing or proposed FRP pedestrian bridges have been investigated. By developing our own parametric FE-solver, we were able to quickly make models of several FRP pedestrian bridges, and apply optimisation algorithms to improve performance in serviceability limit state. Optimisations include global placement of carbon fibre laminates, alignment of fibre directions, and improving geometry shapes. Three case studies were performed; Kaponjärbron in Gothenburg, a bascule bridge in Fredrikstad and Arkitektbron in Gothenburg.

Results show that there are considerable performance gains to be made with all of the suggested optimisation methods, on a case by case basis. The methods made different significance of improvement in the three case studies, and it is difficult to see a certain pattern when one method is useful or not. Conclusively, we see a clear advantage in using parametric analysis for pedestrian FRP bridges in terms modelling time, flexibility and possibility to run iterative optimisations.

Keywords: FRP, Shell analysis, Carbon fibre, Glass fibre, Finite element method, Parametric analysis

Parametrisk analys och optimering av gångbroar i FRP
Optimering av olika fibertyper och fibervinklar i bruksgränstillstånd
Examensarbete inom masterprogrammet Structural Engineering and Building Technology
JIMMIE ANDERSSON
GUSTAV GOOD
Institutionen för bygg- och miljöteknik
Avdelningen för Konstruktionsteknik
Chalmers tekniska högskola

SAMMANFATTNING

FRP-broar (Fibre Reinforced Polymer) finns i många olika storlekar och former, och har ofta komplexa former. Detta, kombinerat med dess anisotropa materialegenskaper, gör det tidskrävande att bygga en analysmodell av bron, och tidiga beslut svåra. På grund av detta kan parametrisk analys, där analysmodellen genereras baserat på förändringsbara parametrar, vara en lämplig metod för att utvärdera prestandan.

Den avgörande faktorn i nästan alla fall är kraven i bruksgränstillstånd för bron. Fibrerna som används i FRP broar kan vara av flera olika typer, men glasfibrer är den dominerande fibertypen i dagsläget. Eftersom glasfibrer har jämförelsevis låg styvhet behövs broar ofta styvas upp med kolfiber. Nackdelen med kolfiber är det höga priset och det är därför kritiskt att kunna minimera mängden. Genom att använda parametrisk analys är det möjligt att optimera kolfiberns placering och täckyta.

I det här exjobbet har vi tittat på fördelarna med att använda parametrisk modellering för analysering och optimering av existerande och föreslagna FRP-gångbroar. Genom att utveckla vår egen parametriska FE-lösare hade vi möjligheten att snabbt kunna modellera flera FRP-gångbroar, och applicera optimerings-algoritmer för att förbättra prestandan i bruksgränstillståndet. Optimeringarna inkluderade global placering av kolfiberlaminat, fibervinklar och geometri. Tre fallstudier utfördes; Kaponjärbron i Göteborg, en klaffbro i Fredrikstad och Arkitektbron i Göteborg.

Resultat visar att det finns stora prestandaförbättringar att göra med de föreslagna optimeringsmetoderna, från fall till fall. Metoderna resulterade i olika stora förbättringar i fallstudierna, och det är svårt att se ett mönster när en metod ska användas eller inte. Slutligen så ser vi en klar fördel med att använda parametrisk analys för FRP-gångbroar i avseende på modelleringstid, flexibilitet och möjlighet att utföra iterativa optimeringar.

Nyckelord: FRP, Skalanalys, Finita elementmetoden, Kolfiber, Glasfiber, Parametrisk analys

CONTENTS

Abstract	i
Sammanfattning	ii
Contents	iii
Preface	vii
Nomenclature	ix
Abbreviations	xi
1 Introduction	1
1.1 Background	1
1.2 Problem description	1
1.3 General aim	2
1.4 Method	2
1.5 Limitations	2
1.5.1 FE-tool	3
2 Fibre composites	4
2.1 Composite materials	4
2.1.1 Fibres	4
2.1.2 Matrices	6
2.2 Composite laminates	7
2.2.1 Sandwich panels	9
2.3 Manufacturing methods	10
2.3.1 Vacuum assisted resin transfer molding	10
2.4 Shell bridges in FRP	11
2.4.1 Pont y Ddraig	12
2.4.2 Bascule footbridge - Fredrikstad	12
2.4.3 Ooypoort pedestrian bridge	13
3 Theory	14
3.1 Laminated composites	14
3.1.1 Laminate stiffness	14
3.1.2 Laminate stresses	15
3.2 The Finite Element Method	16
3.2.1 Shell elements	16
3.2.2 Element definition	17
3.3 Parametric analysis	21
3.3.1 Example: Parametric supports under a loaded disc	21
3.4 Rhinoceros 3D	22
3.4.1 Grasshopper 3D	22
3.4.2 Karamba 3D	24

3.4.3	Galapagos	24
3.5	Stiffness optimisation	24
3.5.1	Carbon fibre placement	24
3.5.2	Fibre orientations	25
4	Development of an FE-tool	26
4.1	The C# language	26
4.2	Code structure	26
4.3	General solution methodology	27
4.4	Meshing	28
4.5	MiStrAn	28
4.5.1	Class structure	28
4.5.2	Solver routine	29
4.5.3	Results	30
4.6	Tortoise	31
4.6.1	Assemble component	31
4.6.2	Align material axis to curves-component	31
4.6.3	Analyse component	32
4.6.4	Visualise results component	32
4.6.5	Section component	33
4.7	Verification of tool	33
4.7.1	Complex geometry with isotropic materials	33
4.7.2	Composite beam	34
5	Case studies	37
5.1	Kaponjärbron	37
5.1.1	Modelling	37
5.1.2	Model verification	42
5.1.3	Demands	43
5.1.4	Initial analyses	44
5.1.5	Optimisation	49
5.1.6	Fibre angle alignment	56
5.1.7	Comments	58
5.2	Bascule bridge in Fredrikstad	59
5.2.1	Modelling	60
5.2.2	Demands	65
5.2.3	Analysis	65
5.2.4	Optimisation	67
5.2.5	Comments	71
5.3	Arkitektbron	71
5.3.1	Modelling	72
5.3.2	Demands	76
5.3.3	Analysis	77
5.3.4	Optimisation	78
5.3.5	Comments	84

6 Discussion	85
6.1 FRP and bridges	85
6.2 Parametric analysis	85
6.3 Optimisation techniques	85
6.3.1 Case studies	85
6.3.2 Carbon fibre optimisation	86
6.3.3 Fibre angle optimisation	86
6.4 FE-solver	86
6.4.1 Performance	86
6.4.2 Verification	87
7 Further investigations	88
7.1 Eigenfrequency optimisation	88
7.2 Element definitions	88
7.3 Ultimate limit state	88
7.4 Second order effects	88
References	89
Appendix A Tortoise components	91
Appendix B C# types	97
Appendix C Tortoise accessibility	98

PREFACE

This master thesis has been written for the Department of Civil Engineering and Building Technology, Division of Structural Engineering, at Chalmers University of Technology in collaboration with the Ramböll Bridge Division in Gothenburg, during the spring of 2017. We would like to thank Mikael Nummedal who let us write the thesis at the Ramböll office and always made sure we got what we needed.

Supervisors for this thesis have been Georgi Nedev (Ramböll) and Erik Olsson (Chalmers) and we would like to thank them for taking the time to help us throughout this project. Examiner has been Reza Haghani Dogaheh and we would like to thank him for the help with initiating the idea of the thesis.

Finally, we would like to thank Alf Jensen at FiReCo, for sharing his knowledge and experience in FRP, and Thore Berntsson with co-workers, for having us at their workshop to show and explain the production process.

NOMENCLATURE

Roman upper case letters

A	Extensional stiffness matrix
B	Coupling stiffness matrix
\mathbf{B}	Shape function derivative matrix
\mathbf{D}	Constitutive matrix
D	Bending stiffness matrix
E	Young's modulus
E_L	Longitudinal Young's modulus
E_T	Transverse Young's modulus
G_d	Permanent action
G_{LT}	In-plane shear modulus
I	Second moment of inertia
\mathbf{K}	Global stiffness matrix
\mathbf{K}^e	Element stiffness matrix
$\bar{\mathbf{K}}^e$	Element stiffness matrix, local coordinates
\mathbf{K}_{FF}	Global stiffness matrix, reduced to free dof's
L	Theoretical span length
\mathbf{M}	Global mass matrix
\mathbf{M}_{FF}	Global mass matrix, reduced to free dof's
\mathbf{M}^e	Element mass matrix
\mathbf{N}	Global shape function matrix
N_i	In plane shape function for node i
N_{ij}	Out of plane shape function for node i and dof j
\mathbf{P}	Polynomial function matrix
\underline{Q}	Lamina stiffness matrix
\bar{Q}	Reduced lamina stiffness matrix
S	Laminate stiffness matrix
S_d	Variable load
\mathbf{T}	Partial transformation matrix
\mathbf{T}_g	Transformation matrix

Roman lower case letters

\mathbf{a}	Global displacement vector
\mathbf{a}_F	Global displacement vector, reduced to free dof's
\mathbf{a}_m	Element displacement from the first eigenmode vector
\mathbf{f}	Global force vector
\mathbf{f}_b	Global reaction force vector
\mathbf{f}_F	Global force vector, reduced to free dof's
\mathbf{f}_ℓ	Global load vector
f	Frequency
$f_{1,vert}$	First vertical frequency
$f_{1,hor,vrid}$	First horizontal frequency

h_k	Distance from mid plane of laminate to upper surface of k :th lamina
h_{k-1}	Distance from mid plane of laminate to lower surface of k :th lamina
l_i	Element side length opposite node i
q_{fk}	Characteristic distributed pedestrian load
\mathbf{r}	Reaction force vector
t	Element thickness
t_{cf}	Carbon fibre section thickness
\mathbf{u}	In-plane displacement field
u_i	Displacement in u-direction at node i
v_i	Displacement in v-direction at node i
w	Vertical deflection field
w_i	Vertical deflection at node i

Greek upper case letters

Δ	Element area
----------	--------------

Greek lower case letters

α_i	Rotation around α -axis at node i
β_i	Rotation around β -axis at node i
γ_i	Rotation around γ -axis at node i
γ_n	Rotation around z-axis
γ_{xy}	Shear strain
ϵ	Strain
ϵ_x^0	Mid-plane strain in x-direction
ϵ_y^0	Mid-plane strain in y-direction
θ	Fibre angle of a lamina
κ_x	Curvature in x-direction
κ_y	Curvature in y-direction
κ_{xy}	Curvature in xy-direction
λ	Eigenvalue
μ	Element side length fraction
ν_{LT}	Major Poisson's ratio
ν_{TL}	Minor Poisson's ratio
ρ	Density
σ	Stress
σ_1	Largest principal stress
σ_2	Smallest principal stress
σ_x	Stress in x-direction
σ_y	Stress in y-direction
σ_{vM}	von Mises Stress
τ_{xy}	In plane shear stress
τ_{xy}^0	Mid-plane shear stress

Special characters

∇	Gradient operator
$\tilde{\nabla}$	Nabla-Tilde operator

ABBREVIATIONS

API	Application programming interface
bc	Boundary condition
CFRP	Carbon fibre reinforced polymer
CST	Constant strain triangle
dof	Degree of freedom
FE	Finite element
FEM	Finite element modelling
First freq	First vertical eigenfrequency
FRP	Fibre reinforced polymer
GFRP	Glass fibre reinforced polymer
NURBS	Non-uniform rational basis spline
PAN	Polyacrylonitrile
RX	Rotation around x-axis
RY	Rotation around y-axis
RZ	Rotation around z-axis
SLS	Serviceability limit state
ULS	Ultimate limit state
VARTM	Vacuum assisted resin transfer molding
z-def	Maximum vertical deformation

1 Introduction

1.1 Background

FRP (Fibre Reinforced Polymer) is a composite material consisting of fibres and a polymer matrix, where the fibres contribute with strength and stiffness, while the matrix transfers the loads and protects the fibres against environmental attacks. The advantages of building bridges in FRP materials include high strength to weight ratio, low maintenance cost, low carbon dioxide emissions, corrosion resistance and the possibility to build complex geometrical shapes (Valbona Mara & Harryson, 2013). Despite the advantages FRP is rarely used as a structural material in the building industry, even though the material has gained a lot of success in other industries, as the boat- and space industry. Reasons for the absence of FRP structures includes a higher price than other common structural materials, and difficulties in design, since there is a lack of proper building standards today. However, with the prices of both carbon fibres and glass fibres constantly dropping and new FRP building standards under development, FRP is currently gaining more interest in the building industry. FRP has been around for some years as a construction material for bridges in Europe, and there are hundreds of FRP bridges already built. However in Sweden, building bridges in FRP is not common, and as of today (April 2017), there are a few FRP-bridges in the design stage, but only a single bridge with FRP as the main structural material has been built in Malmö (Mattsson, 2017).

Since FRP materials come at a higher price it is important to use the fibres to their full potential, for example by combining different fibre types and fibre angles. FRP can be combined in many different ways and allows many possibilities due to the amounts of available configurations. By efficient use of the material and in the right context, FRP can be a viable choice in place of common structural materials, such as steel or concrete. There is especially large potential to use FRP as the main structural material in movable bridges and bridges supported on weak ground due to the light weight of the material. FRPs can also be suitable materials in bridges where corrosion can be of significance due to their high corrosion resistance.

Since FRP is not widely used in the building industry, there is a general shortage of software tools able to analyse the material in a construction environment. *BRIGADE/Plus* is an FE-package with the functionality to do so, but it does not supply good tools for complex geometry.

1.2 Problem description

FRP bridges come in many different sizes and shapes, and can involve complex geometry. This, combined with the anisotropic material behaviour of composites, means building a structural analysis model of the bridge becomes time consuming, and making early design decisions difficult. This can lead to some rushed decisions, for example locking down the geometry or laminate configurations too early.

The decisive factors in almost all cases are the serviceability demands of the bridge. The fibres used in FRP can be made of different materials, but glass fibre is the dominant one used today. Since glass fibres have low stiffness another option is to use carbon fibres. The downside with carbon fibres is the high price and it is therefore not widely used. Designing a bridge with a combination of both glass fibres and carbon fibres, using the advantages of both materials, can improve the efficiency of

the bridge while keeping costs down. However, extensive analysis is needed to determine where the carbon fibre should be placed to be as efficient as possible, and to minimise the amount of carbon fibres used.

1.3 General aim

The aim is to conclude if optimising the combination of glass fibres and carbon fibres, along with fibre alignment and placement of said carbon fibres, can improve the performance of an FRP-bridge in serviceability limit state. This seen from both a structural efficiency and economical perspective. Through the development of an FE-tool within the software *Grasshopper*, the aim is to be able to quickly assess the performance of a free form FRP bridge with respect to dynamic demands and deflection in an early design stage using a range of different material settings and layouts. By developing a parametric tool the geometry and other input data can constantly be changed without the need of constantly making completely new models. This can hopefully make work more efficient in an early design stage, and provide the possibility to make major changes without creating too much of a burden. By doing the parametric modelling in *Grasshopper* more accurate models can be created than for example *BRIGADE/Plus*, modelled at a much faster rate.

1.4 Method

The work will be divided into three main parts:

1. A literature study on fibre reinforced polymers. This part is done to gain more knowledge about the material, to see what limitations and possibilities there are, and to find examples where our tool could be useful.
2. Development of an FE-tool. Firstly, information will be gathered to see what theories the FE-tool needs to be based on, that is most suitable within the time range. The tool will be programmed in the language *C#* and made accessible in *Grasshopper*. *C#* was chosen for its ease of use, our previous knowledge from earlier projects and the fact that *Grasshopper* is written in *C#* helps with the integration. The FE-solver will be programmed independent of the *Grasshopper* interface, which means that it is possible to use the solver itself in other software. Once the tool is finished it will be verified with other FE-tools in *Grasshopper*, and software that can also handle anisotropic materials.
3. A number of case studies. These will be performed on existing or proposed FRP bridges to assess the performance and usability of the tool, as well as showcase the potential of parametric analysis and the optimisation theories.

1.5 Limitations

The thesis will only treat the fibre types glass fibres and carbon fibres, since these are the most commonly used in the building industry today. This does not apply to the FE-tool, which can analyse almost any material.

Analysed structures will only be evaluated on deformation and eigenfrequencies since those are the most common limiting factors. Serviceability limit state loads will be the only loads taken into

consideration. No analyses with ultimate limit state loads will be performed. This thesis will only investigate pedestrian bridges, and only bridges where the load carrying structure is of shell type.

1.5.1 FE-tool

The FE-tool will only be able to calculate shell elements, beam and bar elements are not available. The shell elements are based on the Kirchhoff plate theory, which is suitable only for thin shells, where the out of plane shear deformation is not of significance. Only linear analysis will be performed, and second order effects are not taken into consideration.

2 Fibre composites

2.1 Composite materials

A composite material is a combination of two or more materials, usually with different properties. Examples include concrete, metal composites, and plywood where the grains are directed in alternating directions to give higher strength (Damberg, 2001). In this thesis the composite material *fibre reinforced polymers*, where fibres are combined with a polymer matrix, is investigated.

2.1.1 Fibres

The most common fibre material is glass fibres, due to their good mechanical properties and low price. There are also other fibre types such as aramid- and carbon fibres with higher strength and stiffness, but these also comes with a higher price. The lack of stiffness in glass fibres sometimes makes it necessary to combine these fibres with carbon fibres to increase the stiffness of the structure to meet the deformation demands. When talking with producers and engineers working with fibre reinforced polymer, it was concluded that aramid fibres were very rarely used. The widely used fibres are glass fibres and carbon fibres, therefore this thesis will only handle those two fibre types.

The fibres can be divided into continuous and discontinuous fibres. Continuous fibres typically have a large length-diameter ratio and an organised pattern. Unidirectional layers, woven cloth and helical winding are all types of continuous fibres and can be seen in Figure 2.1. Discontinuous fibres are much shorter than continuous fibres and usually somewhat random in orientation, which reduces their stiffness and strength in a single direction. Discontinuous fibres are cheaper than continuous fibres and are therefore used where cost is the main driver and continuous fibres are used when high strength and stiffness is required (Campbell, 2010). Chopped fibres and discontinuous fibre mats are examples of discontinuous fibres and can be seen in Figure 2.2.

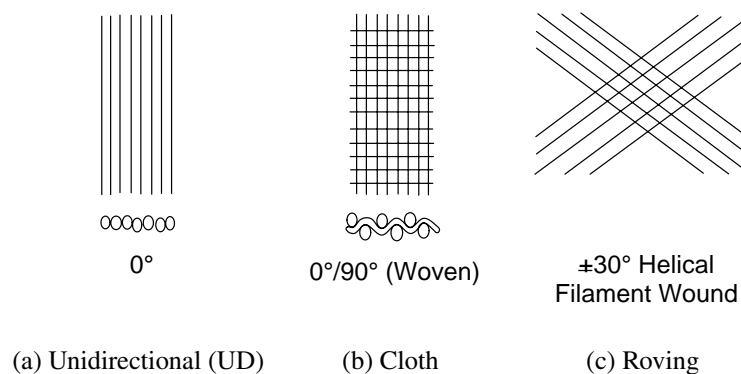


Figure 2.1: Types of continuous fibres.

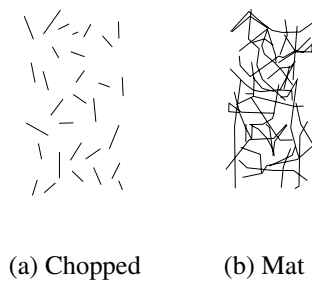


Figure 2.2: Types of discontinuous fibres.

Glass fibres

Glass fibres are today the most commonly used fibre reinforcement in polymer composites. Glass fibres have gained popularity due to its corrosion resistance, high tensile strength and low price. By changing the composition of the the glass, different fibres can be produced, but the most common type is E-glass (Electrical Grade) (Damberg, 2001). Throughout this thesis only glass fibre of type E-glass with the properties in Table 2.1 will be considered. Since the fibres are a reinforcement material, it is appropriate to compare its properties with the properties of steel. Glass fibres only weighs roughly one third of steel, and only has a third the Young's modulus of steel. The tensile strength of the E-glass, for a finished product, is around four to five times stronger than conventional steel, with a virgin tensile strength of 3448 MPa, with finished products having 50%-75% of this strength. This is the strength of the fibres only, and when the fibres are mixed with the matrix a strength of approximately 1100 MPa can be expected with a fibre volume of 45 % according to a example product stated in Agarwal, Broutman, and Chandrashekhara (2015).

When glass fibre is the only fibre type in a fibre reinforced polymer laminate, the composite is usually shortened *GFRP*, which this thesis will refer to. Due to its low stiffness FRP bridges with glass fibre reinforcement usually have difficulties fulfilling the Serviceability Limit State (SLS) demands for deformation and eigenfrequencies, but have less problem fulfilling the Ultimate Limit State (ULS) demands since the strength of the glass fibres is even greater than steel.

The price of GFRP is depending on location and is frequently changing over time, but according to the master thesis by Chlostá (2012), a GFRP laminate roughly costs 1.25 – 2.5 EUR/kg while normal construction steel costs between 0.6 – 0.7 EUR/kg. GFRP is roughly 2-3 times more expensive than steel, but close enough to be a compatible option. It is also expected that the price of GFRP will decrease in a close future (Chlostá, 2012).

Table 2.1: Properties of E-glass fibres (Agarwal, Broutman, & Chandrashekhara, 2015)

Property	E-Glass
Density	2540 kg/m ³
Young's modulus	72.4 GPa
Tensile strength*	3448 MPa
Range of diameter	3–20 µm
Coefficient of thermal expansion	5 10 ⁻⁶ /°C

*Virgin value, finished products range from 50%-75% of virgin value

Carbon fibres

Carbon fibre is a fibre reinforcement material characterised by high strength, low density and high stiffness. It is considerably more expensive than glass fibres and is therefore not as widely used. In the master thesis of Chlosta (2012) it was stated that carbon composite costs around 10 – 45 EUR/kg which is at least 8 times as expensive as glass fibre laminates. Carbon fibres can be made of either polyacrylonitrile (PAN) or pitch, where PAN fibres are more common and usually have higher strength (Damberg, 2001).

Carbon fibre reinforced polymers are often referred to as *CFRP*. Carbon fibres are usually applied on structures where the deformation or vibration requirements cannot be reached with only glass fibres. Since carbon fibres are so expensive it is common to change only certain parts of the structure to use the carbon fibre as efficient as possible. When designing a GFRP-bridge with carbon fibre parts, usually the parts of the section furthest away from the neutral axis are changed from glass fibres to carbon fibres, since this is an efficient way to increase the stiffness with as little carbon fibres as possible. Despite the high price there are bridges constructed with only carbon fibre laminates.

Table 2.2: Properties of PAN carbon fibres (Agarwal, Broutman, & Chandrashekhara, 2015)

Property	PAN
Density	1770–1960 kg/m ³
Young's modulus	230–595 GPa
Tensile strength	1925–6200 MPa
Range of diameter	5–8 µm
Coefficient of thermal expansion*	–0.75 to –0.4 10 ⁻⁶ /°C

*Axial expansion

2.1.2 Matrices

The fibres themselves are not usable in engineering applications due to their small cross sections. Instead they are embedded in a polymer matrix which serves the main tasks of binding the fibres together, transferring loads to the fibres and protecting the fibres. The matrix has a large impact on properties like compression, shear and transverse modulus. Polymers are the most widely used matrices, mainly due to its low cost, easy processability and good chemical resistance (Agarwal et al., 2015). There are mainly two types of polymers, *Thermosetting* and *Thermoplastic*.

Thermosetting

Thermosets are often delivered as a liquid that hardens when mixed with a catalyst or heated. Thermosets are often the widely used due to its high heat resistance, good chemical resistance and good mechanical properties. The main downsides are a slow hardening process and difficulties to recycle the material. Two examples of thermosets are epoxy and polyester (Damberg, 2001).

Thermoplastic

Thermoplastics start softening and melting at high temperatures, usually around 80 – 200 °C and becomes solid when the temperature is lowered again. This process is reversible, and the material can be reshaped if required. Examples of thermoplastics are polystyrene, polyethylene and polycarbonate (Damberg, 2001).

2.2 Composite laminates

A fibre reinforced laminate consist of several stacked laminae with a matrix bonding them together. A lamina is a very thin layer of unidirectional- or woven fibres in a matrix material. Since the fibres in each lamina can be orientated in different directions a large number of different combinations can be achieved. Each layer of lamina is very thin, typically around 0.1 mm (Agarwal et al., 2015). The fibre directions of the different laminae can be altered to obtain different properties of the laminate. Fibre composites can be categorised into single-layer and multilayer composites.

Single-layer laminates

Single-layer laminates can despite its name be made from multiple laminae, but all layers have the same orientation and properties, and the whole laminate can be consider as one single layer. A laminate is classed as single layer if it is made with discontinuous fibres even though the planar fibre orientation may not be uniform through the thickness, or if the laminate is made from non-woven mats with random orientation (Agarwal et al., 2015). Single-layer laminates are desired if only high strength and stiffness are required in one direction and the demands in the transverse direction is low.

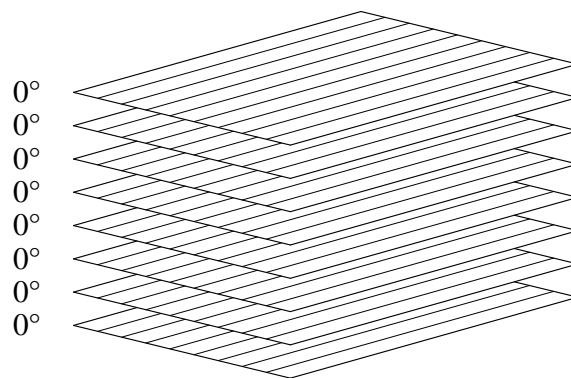


Figure 2.3: Lay-up of unidirectional laminae forming a single layer laminate.

Multilayer laminates

In structural applications multilayer laminates are the most used type of laminates. Usually there are strength and stiffness demands in several directions, and to reach these requirements the laminae can have different thicknesses and be orientated in different directions (Damberg, 2001). Just as in single-layer laminates multiple laminates are joined together with a matrix. It is desired to stack the laminae symmetrical around the neutral axis to avoid warping.

When describing the lamina orientations in a laminate each lamina is denoted by the angle between the fibre direction and the first material axis. If the laminate consists of different fibre types it should be noted next to the angle. An example of a multilayer laminate can be seen in Figure 2.4.

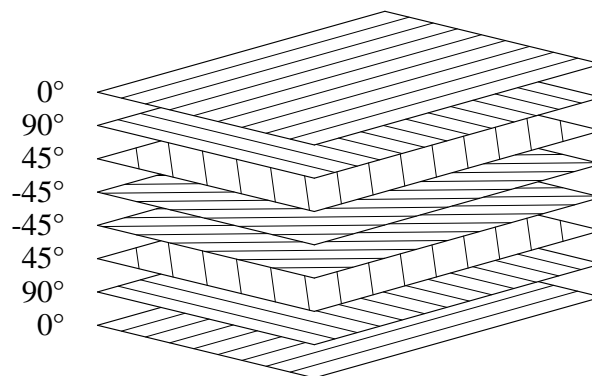


Figure 2.4: Lay-up of laminae with different directions forming a multi-layer laminate.

Hybrid laminates

Hybrid laminates are a multilayered composite where more than one type of fibre is used in the matrix. A hybrid composite can have a mixture of fibres in the same lamina (Agarwal et al., 2015), but this is not very common and in this thesis only hybrids with the same fibre type in each lamina will be considered. Although hybrids can consist of many different types of fibres a common combination is a mixture of glass fibres and carbon fibres, and this is the combination that will be further used in this thesis.

By combining carbon fibres with glass fibres a hybrid composite can be achieved that has the advantages of both fibre types. The glass fibres improves the impact properties and increases the strain when it fails in tension. The carbon fibres helps improving the stiffness, which the glass fibres are lacking (Summerscales & Short, 1978).

Glass fibres and carbon fibres have different thermal properties, where glass fibre is expanding and carbon fibre is shrinking when temperature is increased, see Table 2.1 and Table 2.2 (Agarwal et al., 2015). To prevent undesirable warping due to these thermal contradictions the lay-up of the fibres are usually symmetric around the neutral axis. In the book by Summerscales and Short (1978) it is stated that there are several ways to construct the hybrid, but the main types are:

1. **Mixed fibre tows:** Fibre types are randomly mixed within the resin, in no specific layers.
2. **Mixed fibre ply:** Each layer has a mixture of the different fibres, for example by using woven or knitted hybrid tapes.
3. **Individual fibre ply:** Each layer consists of one fibre type. The layers are mirrored around the neutral axis.

4. **Carbon fibre shell with glass fibre core:** Special case of 3. where the outer layers are made of carbon fibres and the inner layers of glass fibres. This type of sandwich panel is used throughout the case studies in this thesis.
5. **Reinforced with rods or webs:** Another refinement of 3. where the outer layers are made of a positioned carbon fibre web/rod, on a continuous glass fibre base.

The different hybrid types can be seen in Figure 2.5.

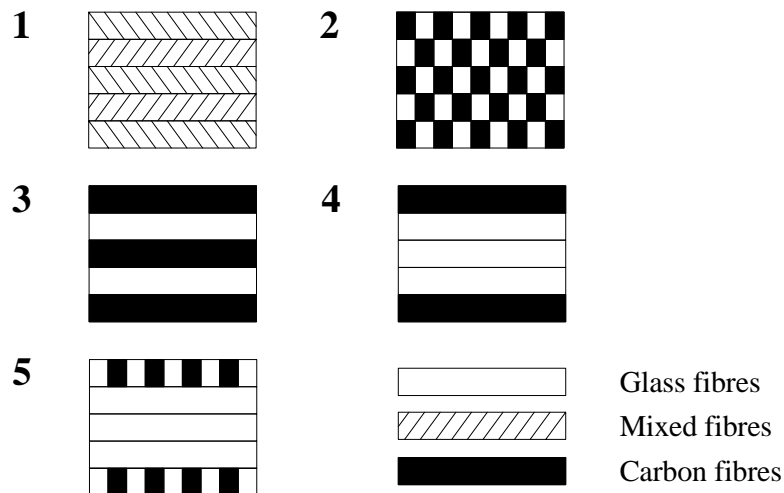


Figure 2.5: Lay-up of hybrid laminate of carbon fibres and glass fibres.

2.2.1 Sandwich panels

Thin shell structures usually need stiffeners along the plates to stiffen them against out of plane deformations. This is necessarily not the cheapest and easiest solution, another method is to use sandwich panels when there are high demands on stiffness and low weight. A sandwich panel typically consists of two thin, stiff and strong face sheets separated by a thick, light and weaker core as can be seen in Figure 2.6. The core are usually made of structural foams, honeycombs or balsa wood. The face material can either be metallic materials such as steel and aluminium or non-metallic materials, commonly plywood, cement or fibre composites (Tarek K.Hassan & Rizkalla, 2003). By using a sandwich panel one can achieve a structure with high stiffness, low weight, good stability and with fewer details. The downsides with a sandwich panel is that it can be difficult to make non destructive tests and sometimes the panel needs reinforcement of certain parts to handle the transfer of the exterior loads.

A sandwich panel acts similar to an I-beam in bending. The skins of the panel corresponds to the flanges of the I-beam, with one of the skins in compression and the other in tension. The core has the same task as the web in the beam, to transfer the shear loads and increase the bending stiffness of the shell by separating the faces from the neutral axis. The core also helps preventing local out of plane buckling (Damberg, 2001).

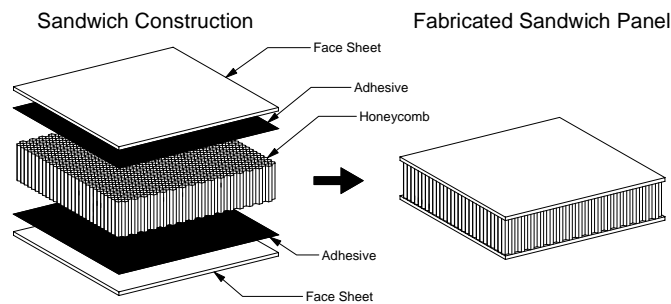


Figure 2.6: Structure of a honeycomb sandwich panel.

2.3 Manufacturing methods

There are many different methods to produce FRP laminates. The choice of manufacturing method depends on many factors such as technical-, environmental- and economical aspects. Since this thesis focuses on shell elements in free form bridges not all methods are applicable. Some methods do not allow fibres orientation in specific directions and these methods are not suitable load bearing bridge elements. The most common techniques can be summed up as the following: hand-lay up techniques (hand-lay up and spray-up), bag molding processes, resin transfer molding, vacuum assisted resin transfer molding, filament winding, pultrusion and preformed molding compounds. After investigating the different methods and talking with producers, several methods were disregarded and what we found to be the most suitable methods for these types of bridges are either hand lay-up technique or vacuum assisted resin transfer molding, VARTM. The VARTM method is a fast and cheap method, but sometimes in complex geometries certain layers need to be hand laid-up to make the resin fully penetrate all parts. Still the most suitable and probable method for producing free form shell bridges would be the VARTM method and this method will be the only one described in this thesis.

2.3.1 Vacuum assisted resin transfer molding

The following section describes the process of producing an FRP-structure using the VARTM method. The pictures in this section were taken during a study trip to Thore Berntsson boat builders, where a small rescue boat was about to be built.

Depending on what surface texture is desired a gel coat can be applied on the mold. The gel coat becomes the outer surface of the laminate when it is completed. Once the gel coat has dried the different fibre layers can be attached to the mold, see Figure 2.7a. Once all the fibres are put into place, small pipes are distributed evenly along the surfaces to help the vacuum process and the resin to spread. A plastic bag is then attached along the edged of the form and sealed. Once the bag is in place vacuum is applied to the outlet of the mold creating a large pressure difference, see Figure 2.7b. The resin is connected to the vacuum bag with a plastic pipe via an inlet to the vacuum bag. The resin then impregnates the fibres due to the pressure difference, shown in Figure 2.8a. When enough resin has saturated the fibres, the inlet to the bag is closed and the resin is allowed to cure. An example of a cured part can be seen in Figure 2.8b. Once the resin has cured the bag is removed and different elements can be glued together if needed.



(a) Fibres attached to the mold

(b) Vacuum applied to the plastic bag

Figure 2.7: Stages of vacuum assisted resin transfer molding.



(a) Resin started to impregnate the fibres

(b) A cured part

Figure 2.8: Stages of vacuum assisted resin transfer molding.

2.4 Shell bridges in FRP

Hundreds of fibre composite bridges have been completed all around Europe, both bridges entirely made of FRP or with FRP parts. The bridges in this section all have fibre composite shells forming the main load bearing structure.

2.4.1 Pont y Ddraig

The Pont y Ddraig (The dragon's bridge) or Foryd harbour Lifting bridge as it is also known as is a cyclist and pedestrian bridge situated in the County Denbighshire in Wales. The bridge is designed by Ramböll with detailed design by Gurit composites, and was completed in 2013. It is divided into two spans, each span 32 m long and made of glass fibre reinforced polymer. Both spans are movable. The bridge decks are hinged on a central caisson and lifted by cables that are connected to the central mast (News, 2013). The bridge in its opened and closed state can be seen in Figure 2.9.



Figure 2.9: Pont y Ddraig bridge. Courtesy of Dawnus and www.plastics.gl.

The use of moulded FRP as the main material of the bridge instead of e.g. steel or concrete was an essential choice to save as much weight as possible. This is especially a good choice for a movable bridge to make the lifting cycles fast and energy efficient (News, 2013). The GFRP components were designed as sandwich panels, consisting of two glass fibre laminates, bonded to a foam core panel. The top deck is supported by transverse bulkheads and stiffeners with a centered longitudinal diaphragm along the whole deck, shown in Figure 2.10. Unidirectional carbon fibres in the longitudinal direction was added on the top deck and along the deepest points of the deck soffit to provide enough stiffness.

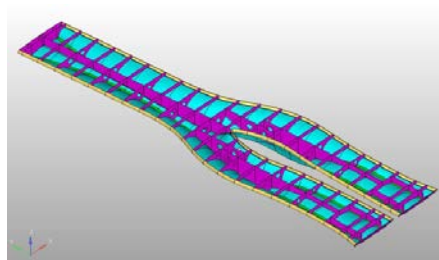


Figure 2.10: FE-model of bridge. Courtesy of www.plastics.gl.

2.4.2 Bascule footbridge - Fredrikstad

The bascule footbridge in Fredrikstad is a movable bridge with a span of 56 m. It was designed by Griff kommunikasjon AS and was completed in 2003. The bridge does not have any counter weights for the opening mechanism, but instead one large hydraulic cylinder on each side pushing the bridge upwards. By using FRP composites as the main load carrying material the weight of each movable

part could be reduced to 20 tons where 9 tons are FRP. The bridge is built as a double curved box girder with longitudinal and transverse stiffeners inside. The panels are partly single skin and partly sandwich configurations. The bridge deck is a sandwich structure with carbon fibre reinforcement and a balsa core. The bottom flange of the girder is a carbon fibre single skin laminate, while the internal stiffeners are a combination of glass fibres and carbon fibres. All FRP parts of the bridge except the translucent side panels are made by vacuum assisted resin infusion (FiReCo, 2014).



(a) Closed state



(b) Opened state

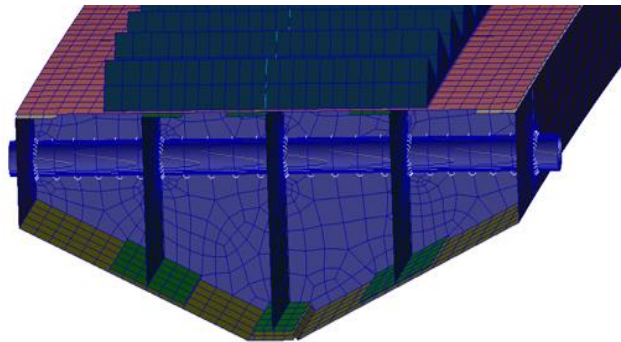
Figure 2.11: Bascule bridge in Fredrikstad. Courtesy of FireCo.

2.4.3 Ooypoort pedestrian bridge

The Ooypoort pedestrian bridge is designed by Olaf Gipser and is situated near the city of Nijmegen in Netherlands. It was completed in 2012 and spans a total of 56 m. It is made completely by vacuum infused glass fibre reinforced polymer. Advantages by using FRP for this bridge included low weight, durability and low maintenance costs. The bridge has an outer shell with three longitudinal stiffeners and transverse stiffeners evenly distributed along the bridge (Dongyu-Fiberglass, 2014).



(a) View of the bridge



(b) Cross section of an FE-model

Figure 2.12: Ooypoort pedestrian bridge. Courtesy of www.compositesworld.com

3 Theory

3.1 Laminated composites

3.1.1 Laminate stiffness

The stiffness in different directions of a laminate depends on the configurations and angles of the laminae. Number of laminae, thickness of each lamina, fibre materials and fibre orientation all effect the stiffness of the laminate. To take this into account a laminate stiffness matrix S can be derived. The following chapter, explained by Agarwal et al. (2015), shows how to obtain the stiffness matrix.

The first step in calculating the laminate stiffness matrix is to calculate reduced stiffness terms for each lamina. From the predetermined properties of a lamina; longitudinal elastic modulus E_L , transverse elastic modulus E_T , major Poisson's ratio ν_{LT} and in-plane shear modulus G_{LT} , the stiffness terms Q_{ij} can be determined.

$$Q_{11} = \frac{E_L}{1 - \nu_{LT}\nu_{TL}} \quad (3.1)$$

$$Q_{22} = \frac{E_T}{1 - \nu_{LT}\nu_{TL}} \quad (3.2)$$

$$Q_{12} = \frac{\nu_{TL}E_L}{1 - \nu_{LT}\nu_{TL}} \quad (3.3)$$

$$Q_{66} = G_{LT} \quad (3.4)$$

where the minor Poisson's ratio, ν_{TL} , is calculated as:

$$\nu_{TL} = \frac{E_T\nu_{LT}}{E_L} \quad (3.5)$$

With the stiffness terms known it is possible to calculate the transformed lamina reduced stiffness terms \bar{Q}_{ij} based on the fibre angle, θ , of the lamina:

$$\bar{Q}_{11} = Q_{11}m^4 + Q_{22}n^4 + 2(Q_{12} + 2Q_{66})m^2n^2 \quad (3.6)$$

$$\bar{Q}_{22} = Q_{11}n^4 + Q_{22}m^4 + 2(Q_{12} + 2Q_{66})m^2n^2 \quad (3.7)$$

$$\bar{Q}_{12} = (Q_{11} + Q_{22} - 4Q_{66})n^2m^2 + Q_{12}(m^4 + n^4) \quad (3.8)$$

$$\bar{Q}_{66} = (Q_{11} + Q_{22} - 2Q_{12} - 2Q_{66})n^2m^2 + Q_{66}(m^4 + n^4) \quad (3.9)$$

$$\bar{Q}_{16} = (Q_{11} + Q_{22} - 2Q_{66})m^3n - (Q_{22} - Q_{12} - 2Q_{66})n^3m \quad (3.10)$$

$$\bar{Q}_{26} = (Q_{11} + Q_{22} - 2Q_{66})n^3m - (Q_{22} - Q_{12} - 2Q_{66})m^3n \quad (3.11)$$

where

$$m = \cos \theta$$

$$n = \sin \theta$$

Once the reduced stiffness is calculated, determine for the k :th lamina, the distance h_k from the mid plane of the laminate to the upper surface of the lamina, and the distance h_{k-1} from the mid plane to the lower surface of the lamina, as seen in Figure 3.1.

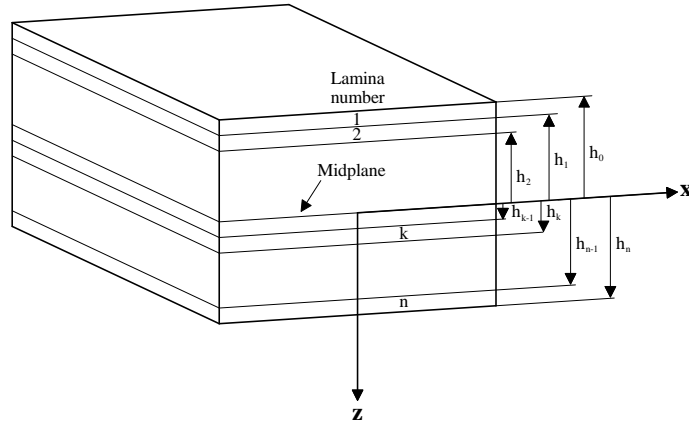


Figure 3.1: Multilayered laminate geometry.

All previous steps should be performed for each lamina in the laminate, once these are calculated the *extensional stiffness matrix* A , *coupling stiffness matrix* B and *bending stiffness matrix* D can be described as:

$$A_{ij} = \sum_{k=1}^n (\bar{Q}_{ij})_k (h_k - h_{k-1}) \quad i, j = 1, 2, 6 \quad (3.12)$$

$$B_{ij} = \frac{1}{2} \sum_{k=1}^n (\bar{Q}_{ij})_k (h_k^2 - h_{k-1}^2) \quad i, j = 1, 2, 6 \quad (3.13)$$

$$D_{ij} = \frac{1}{3} \sum_{k=1}^n (\bar{Q}_{ij})_k (h_k^3 - h_{k-1}^3) \quad i, j = 1, 2, 6 \quad (3.14)$$

Where n is the number of laminae in the laminate. For a shell which has both membrane stiffness and bending stiffness, the laminate stiffness S can be written:

$$S = \begin{bmatrix} A & B \\ B & D \end{bmatrix} \quad (3.15)$$

Note that the *coupling stiffness matrix*, B , is zero for symmetrical stacking of laminae about mid-plane, which is usually desired to avoid warping of the plate (Roylance, 2000).

3.1.2 Laminate stresses

The strains in a laminate vary linearly even though the laminae can have different properties, due to the assumption that no slip occur between the laminae. In an isotropic material, a linear strain distribution would result in a linear stress variation as well. In a laminate where the laminae have different elastic properties, each lamina has a constant stiffness, \bar{Q} . This gives a linear stress distribution over each lamina, but the stress distribution over the laminate consist of several linear segments. When adjacent laminae have different properties, there will be a stress discontinuity (Agarwal et al., 2015). An example can be seen in Figure 3.2.

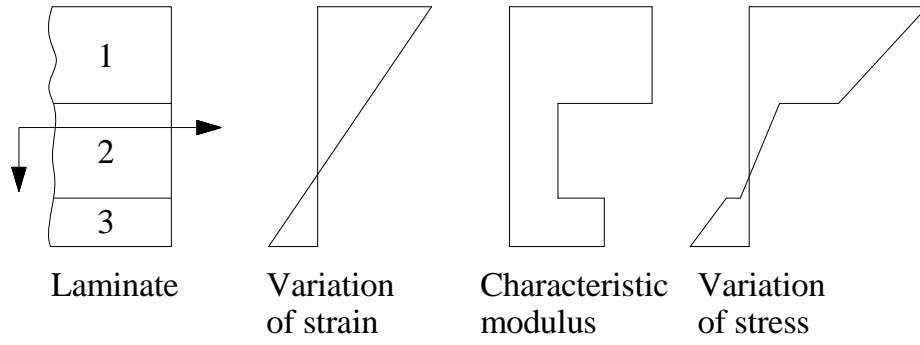


Figure 3.2: Strain and stress distribution in a three ply laminate.

Once the reduced lamina stiffness terms, \bar{Q}_{ij} , mid-plane strains, ϵ^0 , mid-plane shear strain, γ_{xy} , and the curvature κ are known for the laminae the stresses for each lamina can be calculated. Stresses for the k :th lamina are calculated as follows:

$$\begin{bmatrix} \sigma_x \\ \sigma_y \\ \tau_{xy} \end{bmatrix} = \begin{bmatrix} \bar{Q}_{11} & \bar{Q}_{12} & \bar{Q}_{16} \\ \bar{Q}_{12} & \bar{Q}_{22} & \bar{Q}_{26} \\ \bar{Q}_{16} & \bar{Q}_{26} & \bar{Q}_{66} \end{bmatrix}_k \begin{bmatrix} \epsilon_x^0 \\ \epsilon_y^0 \\ \gamma_{xy}^0 \end{bmatrix} + z \begin{bmatrix} \bar{Q}_{11} & \bar{Q}_{12} & \bar{Q}_{16} \\ \bar{Q}_{12} & \bar{Q}_{22} & \bar{Q}_{26} \\ \bar{Q}_{16} & \bar{Q}_{26} & \bar{Q}_{66} \end{bmatrix}_k \begin{bmatrix} \kappa_x \\ \kappa_y \\ \kappa_{xy} \end{bmatrix} \quad (3.16)$$

where z is the distance from mid-plane to lamina.

3.2 The Finite Element Method

The Finite Element Method is a method designed to discretise differential equations, widely used in structural mechanics. These differential equations are assumed to hold over a certain region, which may be one, two or three dimensional. In finite element modelling, regions are divided into smaller parts, or elements, and approximations that hold over a *finite element* are sought, rather than the entire region. If we want to approximate displacement field \mathbf{u} over a region, we may use the finite element approximation:

$$\mathbf{u} = \mathbf{N}\mathbf{a} \quad (3.17)$$

where \mathbf{N} is the global shape function matrix, and the displacement vector \mathbf{a} contains the displacements at the nodal points.

This can be used to obtain a global system of equations:

$$\mathbf{K}\mathbf{a} = \mathbf{f} \quad (3.18)$$

where \mathbf{K} is the global stiffness matrix, and \mathbf{f} is the global force vector.

The displacement vector \mathbf{a} is sorted into *degrees of freedom* (dof), which are translations or rotations in a specific direction at the position of a node (Ottosen & Petersson, 1992). Large simulations may contain millions of degrees of freedom, and can require efficient methods to solve in a reasonable amount of time.

3.2.1 Shell elements

Shells are curved structures where one dimension is significantly smaller than the other, e.g. an egg shell. In FE-analysis, we use shell elements to model these type of structures. A simple shell

element is essentially a flat element with membrane and plate action, that has 3 translational degrees of freedom, and 3 rotational degrees of freedom in each node.

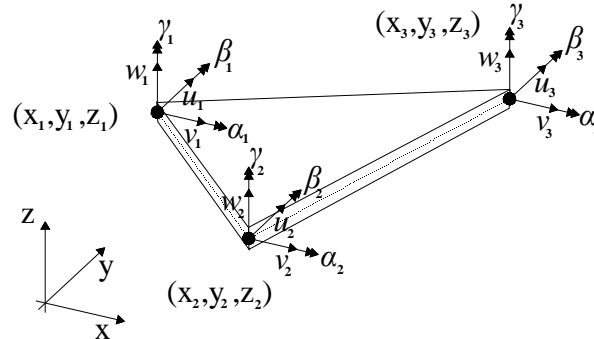
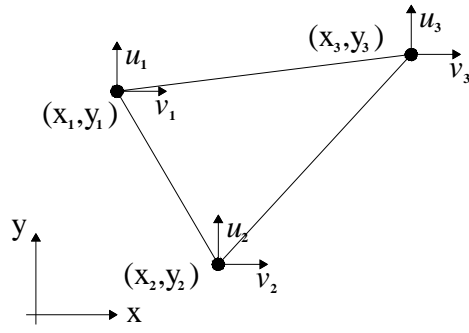


Figure 3.3: Triangular shell element and its degrees of freedom.

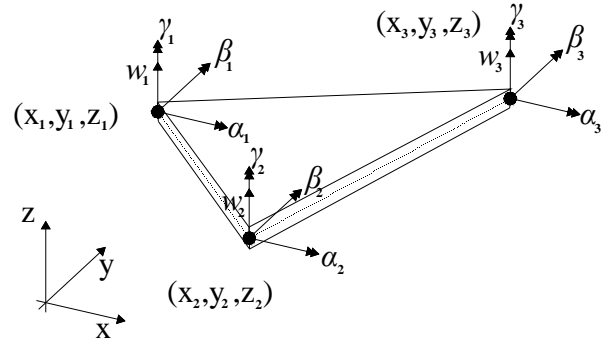
3.2.2 Element definition

Since free form curved shapes are common in FRP bridge design, it was decided to use only triangular elements throughout this project. It is generally regarded as complicated to create quad meshes for curved shapes. Moreover, quad mesh faces can always be divided into triangles, but not vice versa.

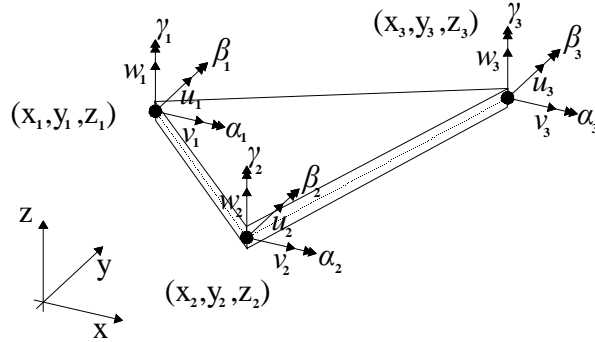
The element chosen for this project is a combination of the Constant Strain Triangle (or CST) and a standard triangular Kirchhoff bending plate. The Kirchhoff plate bending theory disregards out of plane shear deformations, however in the shell structures with thin thicknesses analysed in this thesis, the error from this approximation can be considered small and therefore acceptable. The definition was taken in its entirety from Zienkiewicz and Taylor (2000).



(a) CST-element



(b) Triangular Kirchhoff plate element.



(c) Triangular shell element

Figure 3.4: Two kinds of elements, the CST-element and the Kirchhoff plate element is combined to form a triangular shell element.

As seen in Figure 3.4 the 6 dof CST-element is combined with the 12 dof Kirchhoff element to form a 18 dof shell element. However stiffness for the rotations around the z-axis, denoted γ_n , are not calculated. They are instead given a sufficiently small arbitrary stiffness to fulfil equilibrium conditions.

Shape functions, bending deformations

Analogous to Equation (3.17), the vertical deformations from bending over an element can be expressed as:

$$[w] = \mathbf{N}^e \mathbf{a}^e \quad (3.19)$$

where:

$$\mathbf{N}^e = \begin{bmatrix} N_{11} & N_{12} & N_{13} & N_{21} & N_{22} & N_{23} & N_{31} & N_{32} & N_{33} \end{bmatrix} \quad (3.20)$$

$$\mathbf{a}^e = [w_1 \quad \alpha_1 \quad \beta_1 \quad w_2 \quad \alpha_2 \quad \beta_2 \quad w_3 \quad \alpha_3 \quad \beta_3]^T \quad (3.21)$$

The shape functions, \mathbf{N}_i , can be described as:

$$\mathbf{N}_i = \begin{bmatrix} P_i - P_{i+3} + P_{k+3} + 2(P_{i+6} - P_{k+6}) \\ -b_j(P_{k+6} - P_{k+3}) - b_k P_{i+6} \\ -c_j(P_{k+6} - P_{k+3}) - c_k P_{i+6} \end{bmatrix} \quad (3.22)$$

where i, j, k are cyclic permutations of 1, 2, 3.

The polynomial functions \mathbf{P} are defined as:

$$\begin{aligned} \mathbf{P} = & [L_1, L_2, L_3, L_1 L_2, L_2 L_3, L_3 L_1, \\ & L_1^2 L_2 + \frac{1}{2} L_1 L_2 L_3 (3(1 - \mu_3)L_1 - (1 + 3\mu_3)L_2 + (1 + 3\mu_3)L_3), \\ & L_2^2 L_3 + \frac{1}{2} L_1 L_2 L_3 (3(1 - \mu_1)L_2 - (1 + 3\mu_1)L_3 + (1 + 3\mu_1)L_1), \\ & L_3^2 L_1 + \frac{1}{2} L_1 L_2 L_3 (3(1 - \mu_2)L_3 - (1 + 3\mu_2)L_1 + (1 + 3\mu_2)L_2)] \end{aligned} \quad (3.23)$$

where

$$\mu_i = \frac{l_k^2 - l_j^2}{l_i^2} \quad (3.24)$$

and l_i is the length of the triangle side opposite node i .

This definition is based on area coordinates, such that:

$$L_i = \frac{a_i + b_i x + c_i y}{2\Delta}, \quad (3.25)$$

$$\Delta = \text{element area} = \frac{1}{2}(b_1 c_2 - b_2 c_1) \quad (3.26)$$

$$a_i = x_j y_k - x_k y_j \quad (3.27)$$

$$b_i = y_j - y_k \quad (3.28)$$

$$c_i = x_k - x_j \quad (3.29)$$

$$i = 1, 2, 3$$

i, j, k as positive cyclic permutations

Shape functions, in-plane deformations

Analogous to Equation (3.17), the in-plane deformations over an element can be expressed as:

$$\mathbf{u} = \mathbf{N}^e \mathbf{a}^e \quad (3.30)$$

where

$$\mathbf{N}^e = \begin{bmatrix} N_1 & 0 & N_2 & 0 & N_3 & 0 \\ 0 & N_1 & 0 & N_2 & 0 & N_3 \end{bmatrix} \quad (3.31)$$

$$\mathbf{a}^e = [u_1 \quad v_1 \quad u_2 \quad v_2 \quad u_3 \quad v_3]^T \quad (3.32)$$

The shape functions, N_i can be described as:

$$\begin{aligned} N_i &= L_i \\ i &= 1, 2, 3 \end{aligned} \quad (3.33)$$

Stiffness matrix and coordinate transformation

The stiffness matrix for the triangular shell element is defined as

$$\bar{\mathbf{K}}^e = \int_{\Omega} \mathbf{B}^T \mathbf{D} \mathbf{B} d\Omega \quad (3.34)$$

where \mathbf{D} is the constitutive matrix. When analysing FRP, the constitutive matrix is replaced by the laminate stiffness matrix, S , expressed in Equation (3.15). The \mathbf{B} -matrix is defined as:

$$\mathbf{B} = \tilde{\nabla} \mathbf{N}^e \quad (\text{for in plane deformations}) \quad (3.35)$$

$$\mathbf{B} = (\tilde{\nabla} \nabla) \mathbf{N}^e \quad (\text{for out of plane deformations}) \quad (3.36)$$

where the operators ∇ and $\tilde{\nabla}$ are defined as:

$$\nabla = \begin{bmatrix} \frac{\partial}{\partial x} \\ \frac{\partial}{\partial y} \end{bmatrix} \quad (3.37)$$

$$\tilde{\nabla} = \begin{bmatrix} \frac{\partial}{\partial x} & 0 \\ 0 & \frac{\partial}{\partial y} \\ \frac{\partial}{\partial y} & \frac{\partial}{\partial x} \end{bmatrix} \quad (3.38)$$

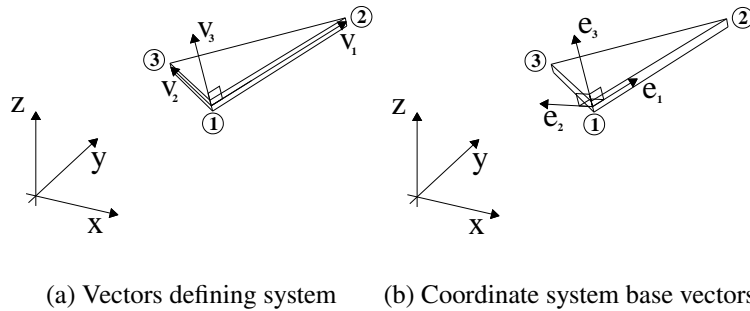


Figure 3.5: Element local coordinate system

As seen in Figure 3.5, the local coordinate system of the elements is based on the vectors \mathbf{v}_1 , \mathbf{v}_2 , and \mathbf{v}_3 , where:

$$\mathbf{v}_1 = \begin{bmatrix} x_2 - x_1 \\ y_2 - y_1 \\ z_2 - z_1 \end{bmatrix}, \quad \mathbf{v}_2 = \begin{bmatrix} x_3 - x_1 \\ y_3 - y_1 \\ z_3 - z_1 \end{bmatrix}, \quad \mathbf{v}_3 = \mathbf{v}_1 \times \mathbf{v}_2 \quad (3.39)$$

$$\mathbf{e}_1 = \frac{\mathbf{v}_1}{|\mathbf{v}_1|}, \quad \mathbf{e}_3 = \frac{\mathbf{v}_3}{|\mathbf{v}_3|}, \quad \mathbf{e}_2 = \mathbf{e}_3 \times \mathbf{e}_1 \quad (3.40)$$

Using this coordinate system, we can construct a transformation matrix, \mathbf{T}_g , which is used to transform the stiffness matrix to global coordinates in the following manner:

$$\mathbf{K}^e = \mathbf{T}_g \bar{\mathbf{K}}^e \mathbf{T}_g^T \quad (3.41)$$

where

$$\mathbf{T}_g = \begin{bmatrix} \mathbf{T} & 0 & 0 & 0 & 0 & 0 \\ 0 & \mathbf{T} & 0 & 0 & 0 & 0 \\ 0 & 0 & \mathbf{T} & 0 & 0 & 0 \\ 0 & 0 & 0 & \mathbf{T} & 0 & 0 \\ 0 & 0 & 0 & 0 & \mathbf{T} & 0 \\ 0 & 0 & 0 & 0 & 0 & \mathbf{T} \end{bmatrix} \quad (3.42)$$

$$\mathbf{T} = [\mathbf{e}_1 \quad \mathbf{e}_2 \quad \mathbf{e}_3] \quad (3.43)$$

Mass matrix

The element mass matrix, denoted \mathbf{M}^e , is calculated as follows:

$$\mathbf{M}^e = \mathbf{T}_g \bar{\mathbf{M}}^e \mathbf{T}_g^T \quad (3.44)$$

$$\bar{\mathbf{M}}^e = \int_{\Omega} \rho \mathbf{N}^e T \mathbf{N}^e T d\Omega \quad (3.45)$$

where ρ is the density of the material, and t is the thickness of the element.

3.3 Parametric analysis

The process of defining a model on parameters rather than static values is called *parametric analysis*. This type of analysis is used to systematically examine the behaviour of the output of the model as the inputs vary (Analytica, 2014). By using parametric analysis, the entire model does not have to be rebuilt if the input data or demands change, and different alternatives can easily be explored by simply adjusting the parameters.

Ansys (2010) writes:

"... [Parametric analysis] makes it possible to quickly evaluate hundreds of designs in batch processes to explore the complete design space so that we know we have the best possible design."

Parametric analysis is a wide spread practice in the automotive industry and in product development (Ansys, 2011), but the construction industry does not seem to have caught on yet. Little software for parametric analysis is available for construction today, but some examples include *Karamba*, *Kangaroo*, and a *Grasshopper*-plugin for *Tekla*.

3.3.1 Example: Parametric supports under a loaded disc

A disc is loaded in the centre with an arbitrary point load. The parameters t_A and t_B control the position of support *A* and *B* respectively along the rim (where $t = 1$ means a full rotation along the disc). Some of the deflected shapes can be seen in Figure 3.6.

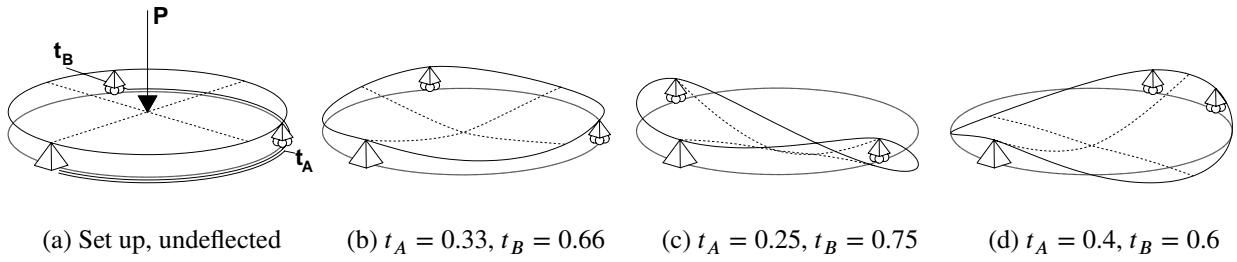


Figure 3.6: Deflected shapes, parametric supports under a loaded disc.

The solution space can be seen in Figure 3.7, where z-axis represents deflection. Marked with black dots are the optimum solutions in terms of deflection, being $t_A = \frac{1}{3}, t_B = \frac{2}{3}$ and $t_A = \frac{2}{3}, t_B = \frac{1}{3}$. Note that results are only collected from $t_{A,B} = 0.05$ to $t_{A,B} = 0.95$ since rigid body motion will occur at $t_{A,B} = 0$ and $t_{A,B} = 1$.

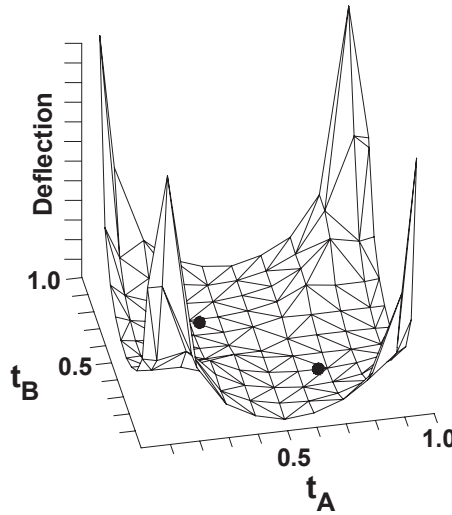


Figure 3.7: Solution space for the disc. The dots show the optimal solution for minimal deflection.

3.4 Rhinoceros 3D

Rhinoceros 3D (or simply *Rhino*) is a 3d modelling software capable of handling complicated NURBS (Non-Uniform Rational B-Spline) curves and surfaces, while still being lightweight, user friendly and offers a large software developer kit (Novedge, 2017). The latter has led to the development of a large number of plugins for *Rhino*. One of the most popular plugins, *Grasshopper 3D*, is described below.

3.4.1 Grasshopper 3D

Grasshopper 3D (or simply *Grasshopper*) is an algorithmic modelling plugin for *Rhino* (Rutten, 2017). It uses visual programming to generate primarily geometry, but also other kinds of data such as number data, audio and moving pictures. It uses *Rhino's* powerful API (Application Programming Interface) to show geometry representation in the view port of *Rhino*. Instead of programming by writing lines of text, the user connects wires between components, which sends data between them.

Grasshopper has a large following, an active forum, and many available plugins for download (Rutten, 2017).

Example: Mobius Strip

Figure 3.8 shows a simple *Grasshopper*-script that produces the mobius strip seen in Figure 3.9. As seen in the image, the data is sent on-wards by wires. The *Circle*-component, for instance, creates a circle and sends it on to the *Perp Frames*-component which creates perpendicular frames along the curve. Parameters controlling the shape in this example are; radius of circle, number of section planes, and number of rotations. This is a powerful and easy way to generate parametric and complex geometry.

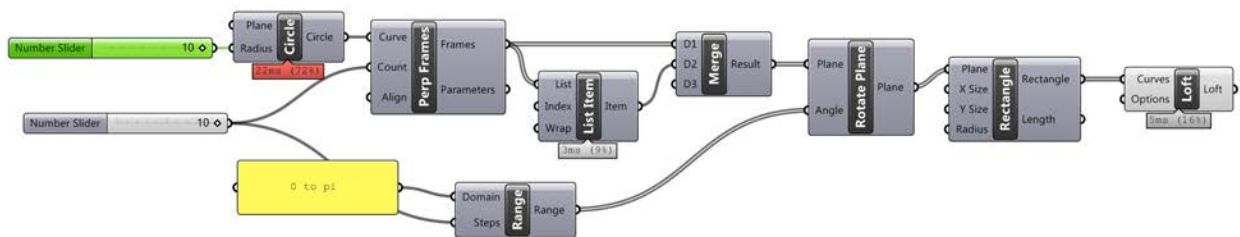


Figure 3.8: Simple mobius strip script in *Grasshopper*.

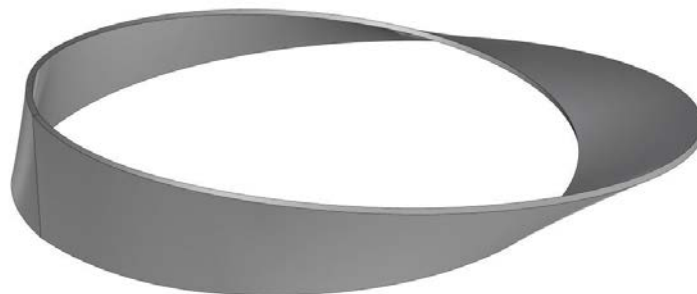


Figure 3.9: Geometry output from script above.

The components used in this script are described in the list below (David Rutten, 2014):

- *Circle*
Creates a circle defined by base plane and radius.
- *Perp Frames*
Generates a number of equally spaced, perpendicular frames (or planes) along a curve.
- *Range*
Creates a range of numbers.
- *List Item*
Retrieve a specific item from a list. Used to duplicate the first plane in this instance. It needs to be first and last in the list in order to create a closed strip.
- *Merge*
Merge a number of data streams.

- *Rotate plane*
Performs plane rotation around the vertical axis.
- *Rectangle*
Creates a rectangle on a plane.
- *Loft*
Create a lofted surface through a set of section curves.

3.4.2 Karamba 3D

Karamba 3D (or simply *Karamba*) is a commercial parametric structural engineering plugin for *Grasshopper*. By supplying components for analysis to *Grasshopper*, it can perform detailed structural analysis on models containing bars, beams, and shells (karamba3d, 2016). *Karamba* is currently (May 2017) only able to handle isotropic materials.

3.4.3 Galapagos

Galapagos is an evolutionary solver for *Grasshopper*. It provides an interface to maximise or minimise a variable, or *fitness*, dependant on a number parameters (Rutten, 2016). A script is built in *Grasshopper* that produces some sort of variable (e.g. deflection, area, stress) dependant on a set of parameters, or *genes*, and let *Galapagos* minimise or maximise the variable by changing said parameters. When running the solver, *Galapagos* initially tries a number of random values for supplied *genes*. In the next iteration, it cherry picks sets of *genes* that perform well according to the *fitness-criteria*, and "mate" these by producing combinations of said gene-sets. This is done iteratively until the solver times out.

A detailed explanation on evolutionary solver principles can be found in Rutten (2010).

3.5 Stiffness optimisation

3.5.1 Carbon fibre placement

For a GFRP structure that cannot meet the required deformation criteria, there is a need to stiffen the structure. There are different ways to achieve this, one way is to increase the GFRP section. This is however not always sufficient and it is therefore often necessary to add carbon fibres, which have a much greater stiffness, at strategic places.

The general approach for placing the carbon fibres today is based on the flexural rigidity, EI , of the section. Since the second moment of inertia, I , is larger further away from the neutral axis the carbon fibre, with a higher Young's modulus, is placed as far away of from the neutral axis a possible.

In this thesis the stiffness optimisation is based on Hooke's law for elastic materials:

$$\sigma = \epsilon E \quad (3.46)$$

where

E = Young's modulus

σ = Stress

ϵ = strain

Same equation rewritten:

$$\frac{\sigma}{E} = \epsilon \quad (3.47)$$

To minimise the strain for each element, the Young's modulus, should be large when the stresses are large, and does not need to be large when stresses are low. Based on this, the optimisation idea is to put carbon fibres on the elements with the highest stresses.

To receive the largest stresses an analysis of the structure with a uniform material is done to see how the stresses act in its natural form in the structure. The elements in the mesh with the highest stresses are selected and the material of those elements is changed to carbon fibres, which is much stiffer than the glass fibre. The amount of chosen elements and their carbon fibre thickness is dependent on how much carbon fibre weight is desired and best suitable for each structure.

3.5.2 Fibre orientations

Since carbon fibre is an anisotropic material the strength differs in different directions. The strongest direction is along the fibres, assuming a unidirectional lamina. As explained in previous chapter it is desired to maximise the Young's modulus to get as small strains as possible.

To find in what directions the fibres should be aligned, the direction of the highest principal stress in each elements needs to be found for an isotropic material. If the fibres are angled in the same direction as the principal stress, the strain will be as small as possible. The principal stress angle θ , the angle between the elements local x-axis and the largest principal stress is calculated as follows:

$$\theta = \frac{1}{2} \tan^{-1} \left(\frac{2\tau_{xy}}{\sigma_x - \sigma_y} \right) \quad (3.48)$$

where:

$$\sigma_x = \text{Stress in x-direction.} \quad (3.49)$$

$$\sigma_y = \text{Stress in y-direction} \quad (3.50)$$

$$\tau_{xy} = \text{In plane shear stress} \quad (3.51)$$

The first material axis for each element is then changed to these angles, but this pattern is usually quite unorganised and not possible to construct. A more realistic way to align the directions based on this pattern is explained in Section 4.6.2.

4 Development of an FE-tool

Since *Grasshopper* was chosen for this project as a parametric tool, only *Karamba* was available for FE-analysis. However, as mentioned in Section 3.4.2, *Karamba* has not implemented anisotropic materials - a fundamental feature in analysis of FRP structures. This forced the decision to design and code our own FE-solver. Although it demands a lot of effort, this does provide the advantages listed below:

- Complete transparency of the calculations being done.
- Control over element definitions and stiffness calculations.
- Ability to customise results output.
- Performance by limiting the solver to only perform the calculations needed for the task.

4.1 The C# language

C# (pronounced C-sharp) is a modern object-orientated, type sensitive, imperative programming language developed by Microsoft . It implements automatic garbage collection which makes it relatively easy to use (Tutorialspoint, 2014). Objects are defined by *classes* which serves as a description of how the object works and what properties it has. While some languages benefit from higher performance (like C++ or C), C#'s ease of use makes it popular within the Windows environment.

C# was used exclusively throughout this project, based on the advantages listed below:

- Ease of use.
- The fact that *Grasshopper* is written in C# makes integration easier.
- Wide online support.
- Previous knowledge from earlier projects.

All code was written using *Visual Studio Express*, a free code editor and platform provided by Microsoft.

4.2 Code structure

The macro structure of the code can be seen in Figure 4.1. Code developed by us in this project is lumped into two parts; *Tortoise* (*Grasshopper* plugins are usually named after animals and this plugin analyses shells) and *MiStrAn* (short for Minimalistic Structural Analysis). A brief explanation of the different components of the macro structure is listed below:

- *Rhino* is accessible by the user and functions as a geometry tool by providing *Grasshopper* with geometrical input, and serves as a platform to receive geometrical output from *Grasshopper*.
- *Grasshopper* is the parametric user platform for the solver. It supplies a wide range of functionality in terms of geometry manipulation.
- *Tortoise* is the *Grasshopper*-plugin and user interface developed by us for this project. It provides components accessible from *Grasshopper* and additionally performs some of the solver's geometrical tasks in order to take advantage of *Rhino*'s vast geometrical library.
- *MiStrAn* is the FE-solver developed by us for this project. It generates stiffness matrices, assembles the system of equations and returns the results from the analysis.

- **PARDISO** is a solver for large systems of linear equations, developed and provided free of charge by Intel. It is used to solve the general system of equations and eigenvalue problems generated by *MiStrAn*.
- **ALGLIB** is a linear algebra code library. It is used in this project to handle matrix operations such as multiplication and subtraction of large sparse matrices.

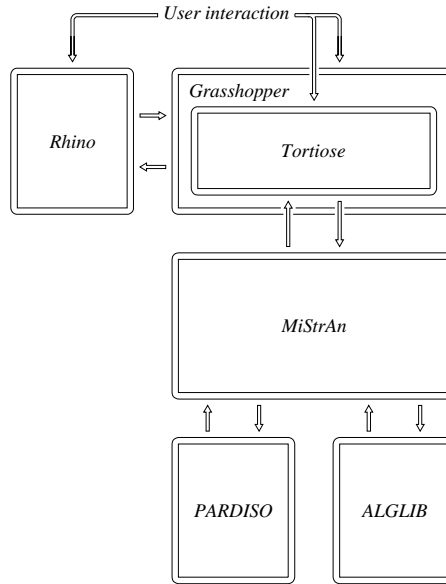


Figure 4.1: Macro structure of code.

4.3 General solution methodology

The general methodology for analysing a structure is described briefly below:

1. Geometry is defined by surfaces in either *Grasshopper* and/or *Rhino*.
2. A mesh is generated in *Grasshopper* from the geometry using *Karambas* component *Mesh Breps*.
3. Boundary conditions, loads, and sections are defined in *Grasshopper* using *Tortoise*.
4. The structure is assembled using *Tortoise* and sent to *MiStrAn* for analysis.
5. *MiStrAn* generates laminate stiffness matrices S , element stiffness matrices \mathbf{K}^e , element load vectors \mathbf{f}^e , and element mass matrices \mathbf{M}^e .
6. *MiStrAn* assembles global stiffness matrix \mathbf{K} , global load vector \mathbf{f} , global mass matrix \mathbf{M} , and boundary condition matrix \mathbf{bc} .
7. *PARDISO* solves the system of equations $\mathbf{K}\mathbf{a} = \mathbf{f}$, and eigenvalue problem $(\mathbf{K}_{FF} - \lambda\mathbf{M}_{FF})\mathbf{v} = \mathbf{0}$
8. *MiStrAn* performs post processing on results to produce stresses etc.
9. Stresses, deflections and other results are sent to *Tortoise* for visualisation in grasshopper.

4.4 Meshing

The process of dividing a region into finite elements, or an element mesh, is often referred to as *meshing*. This is a complicated task with many parameters to consider, such as element aspect ratio, element size etc. Throughout this project, *Karamba's Mesh Breps*-component was used for meshing. This component utilises Delaunay-triangulation and algorithms for controlling the aspect ratio of elements, all very suitable for FE-analysis. A mesh generated by the *Mesh Breps*-component can be seen in Figure 4.2.

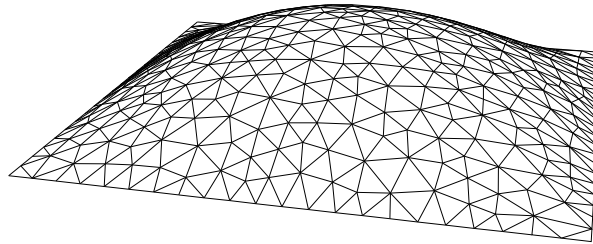


Figure 4.2: Mesh generated by *Karamba's Mesh Breps*-component.

4.5 MiStrAn

As described in Section 4.2, *MiStrAn* is the central FE-solver designed and developed by us for this project. It is based on standard finite element theory described in Section 3.2, and at the time only implements shell elements. It is designed for 3D space, does all calculations in SI units, and is limited to linear problems. It depends on the commercial packages *PARDISO* and *ALGLIB* for solving equations and matrix operations respectively.

4.5.1 Class structure

As described in Section 4.1, *C#* is an object orientated language where objects are defined by classes. The class structure set up for *MiStrAn* can be seen in Figure 4.3. The different *C#* types are explained in Appendix B. A small explanation for each class follows:

- **Structure**
Main class for containing the whole structural definition. Assembles global stiffness matrix and handles results. Abbreviations: K = stiffness matrix, M = mass matrix, f = load vector, bc = boundary condition matrix, a = displacement vector, r = reaction force vector.
- **Node**
Holds information for a single node in the structure.
- **ShellElement**
Stores information for a single shell element. Produces the elements stiffness matrix, mass matrix, and load vector contribution. Abbreviations: D = constitutive matrix.
- **Section**
Holds information of one or several elements section. Produces constitutive matrix for the shell elements.
- **Load**
Stores load information.

- **Support**

Stores information of support conditions for a node. Abbreviations: X = locked in x-direction, RX = locked in rotation around x-axis etc.

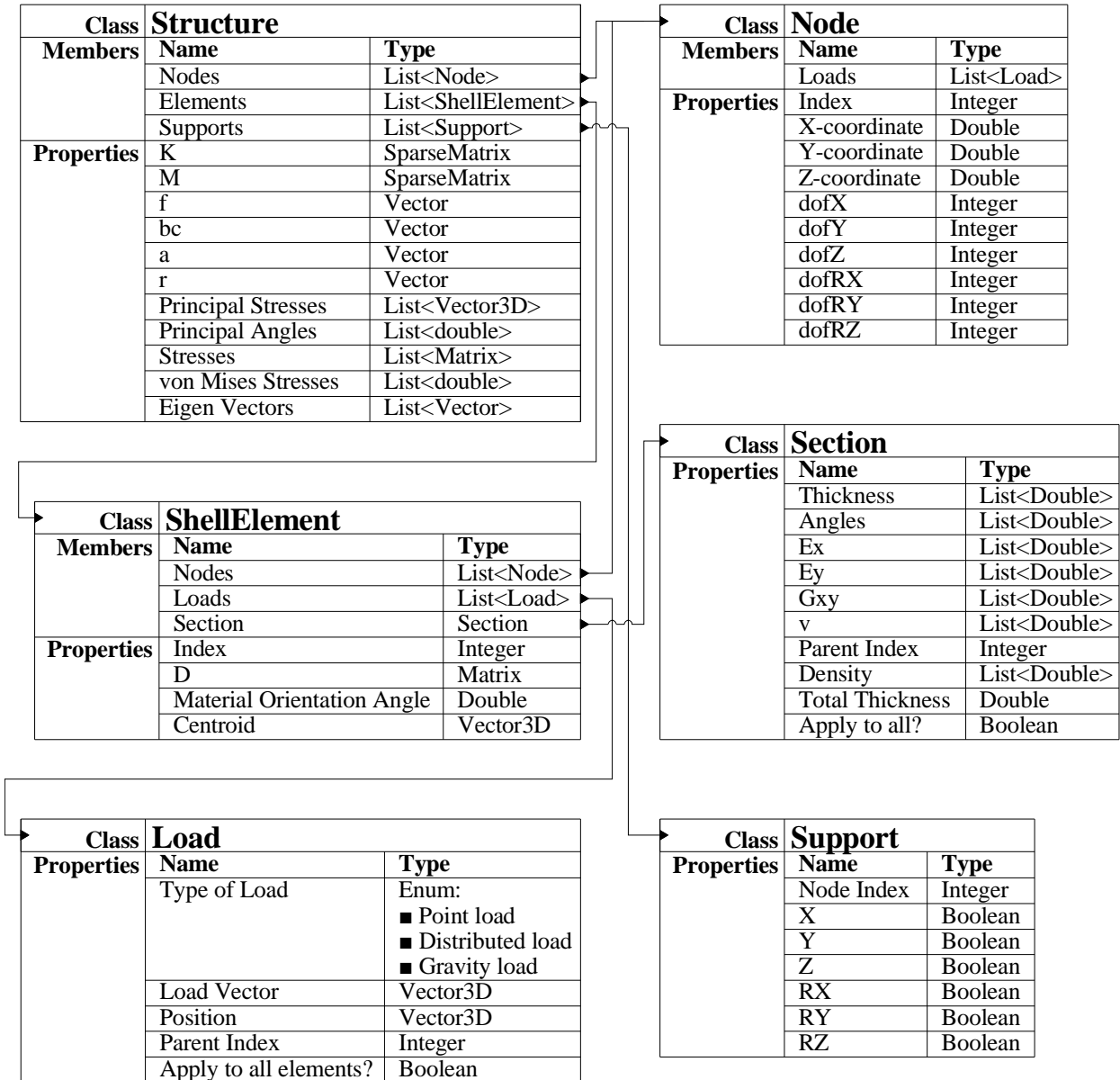


Figure 4.3: *MiStrAn* class structure.

4.5.2 Solver routine

When solving the system of equations, the global stiffness matrix, **K**, and the global mass matrix, **M**, is first assembled in the Structure-class. The following system is then sent to *PARDISO* for solving the displacement vector:

$$\mathbf{K}_{FF} \mathbf{a}_F = \mathbf{f}_F \quad (4.1)$$

where F are free degrees of freedom. The reaction forces, \mathbf{f}_b are then calculated by the following expression:

$$\mathbf{f}_b = \mathbf{K}\mathbf{a} - \mathbf{f}_\ell \quad (4.2)$$

where \mathbf{f}_ℓ is the load vector. For dynamics, *PARDISO* solves the following generalised eigenvalue problem:

$$(\mathbf{K}_{FF} - \lambda \mathbf{M}_{FF})\mathbf{v} = \mathbf{0} \quad (4.3)$$

where \mathbf{v} is the eigenvector or mode shape, and λ is the eigenvalue. The eigenfrequency, f , is then calculated with the following expression:

$$f = \frac{\sqrt{\lambda}}{2\pi} \quad (4.4)$$

The information is then sent back to *MiStrAn* where the results are generated.

4.5.3 Results

Results generated by *MiStrAn* include:

- Nodal displacements
- Lamina stresses
- von Mises stresses
- Principal stresses
- Principal directions
- Reaction forces
- Eigenfrequencies
- Mode shapes

Lamina stresses for the k :th lamina are calculated using Equation (3.16), where:

$$\begin{bmatrix} \epsilon_x^0 \\ \epsilon_y^0 \\ \gamma_{xy}^0 \\ \kappa_x \\ \kappa_y \\ \kappa_{xy} \end{bmatrix} = \mathbf{B}\mathbf{a}^e \quad (4.5)$$

von Mises stresses are calculated as follows:

$$\sigma_{vM} = \sqrt{\sigma_x^2 - \sigma_x\sigma_y + \sigma_y^2 + 3\tau_{xy}^2} \quad (4.6)$$

Principal stresses are calculated as follows:

$$\sigma_{1,2} = \frac{\sigma_x + \sigma_y}{2} \pm \sqrt{\frac{(\sigma_x - \sigma_y)^2}{2} + \tau_{xy}^2} \quad (4.7)$$

The principal directions are calculated using the principal angle, θ , the angle between the elements local x-axis and the largest principal stress, which is obtained with the following expression:

$$\theta = \frac{1}{2} \tan^{-1} \left(\frac{2\tau_{xy}}{\sigma_x - \sigma_y} \right) \quad (4.8)$$

4.6 Tortoise

As described in Section 4.2, *Tortoise* is the *Grasshopper*-plugin and user interface developed by us for this project. Since *Rhino* offers some powerful geometry functionality, *Tortoise* also handles some of the geometrical task needed for this project.

Being a *Grasshopper*-plugin, *Tortoise* exists only within the *Grasshopper*-environment and is divided into components available for the user on the canvas. A few of the main components used in an analysis are described below. A complete list of components in *Tortoise* can be seen in Appendix A.

4.6.1 Assemble component

This component assembles the mesh, supports, loads and sections into a structure. The supports, loads and sections are *Tortoise* types and are generated by their respective *Tortoise* component. Once a structure is assembled it can be modified and analysed in other *Tortoise* components.

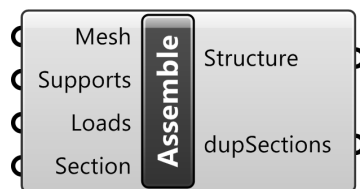


Figure 4.4: *Assemble*-component.

4.6.2 Align material axis to curves-component

If not altered, the material axis in each element (corresponding to 0° orientation angle in a laminate) will coincide with the local element x-axis. This is not very suitable when the mesh is generated by an automatic algorithm, since the local axis systems can not be considered to be aligned in a sensible way.

To handle this, a default material orientation axis is generated that is aligned with the global x-axis, seen in Figure 4.6a. For simple geometry, this may be a suitable setting, but for more complex geometry, a more refined approach is needed.

With this in mind, an algorithm to align the element material axis to arbitrary NURBS-curves was developed, with the result seen in Figure 4.6b. The algorithm is implemented in the *Align Material Axis To Curves*-component, which can be seen in Figure 4.5.

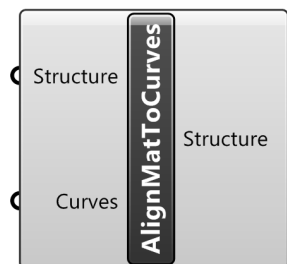


Figure 4.5: *Align Material Axis to Curves*-component.

The algorithm works in the following way:

1. Create a number of material axis orientation curves and add to the pool.
2. Loop through all elements and assign them to the curve closest to their centroid.
3. For each element, find closest point on assigned curve.
4. Align material axis to curve tangent at said point.

Closest points and tangents of NURBS-curves are available and utilised through the *Rhino-API*.

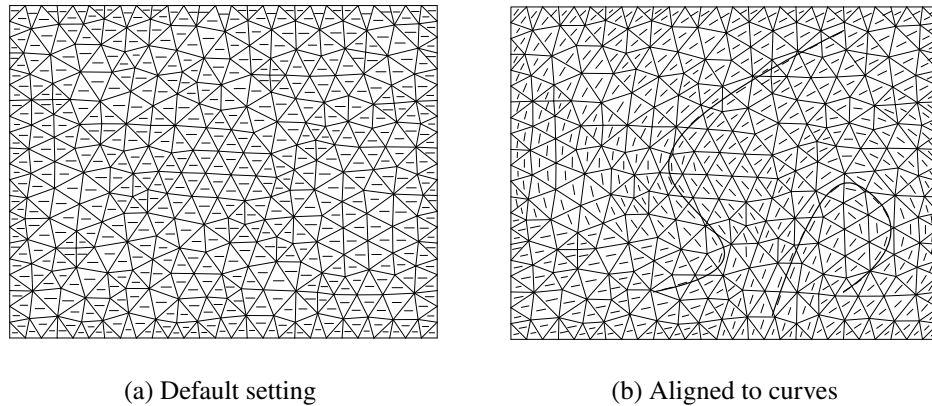


Figure 4.6: Material orientation axis for a rectangular mesh.

4.6.3 Analyse component

The *Analyse*-component performs the main analysis of an assembled structure and provides results. The component outputs reaction forces, stresses, rotations and displacements for all the nodes in the structure. The analysed structure can then be visualised in different components or further analysed in other components.

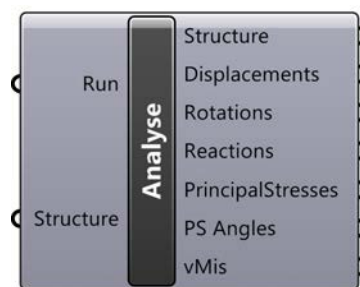


Figure 4.7: *Analyse*-component.

4.6.4 Visualise results component

The *Visualise results*-component displays either a von Mises stress plot or a deformation plot from an analysed structure. The component has input options for scaling the deformed mesh or to set stress limits in the stress plot.

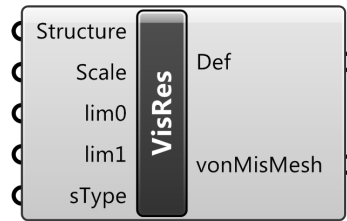


Figure 4.8: *Visualise Results*-component.

4.6.5 Section component

The *Section*-component assigns material properties and thickness for one or multiple elements. The component can handle both isotropic- and laminate materials. Figure 4.9 shows an example of a three ply laminate, consisting of outer carbon fibre plies and a middle glass fibres ply.

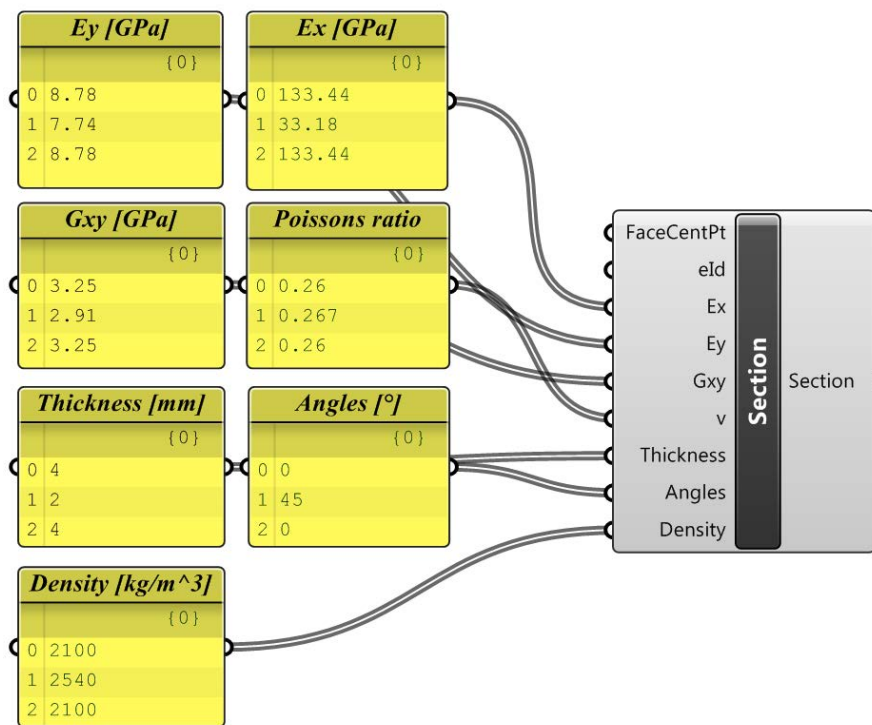


Figure 4.9: *Section*-component.

4.7 Verification of tool

Verification has been done analytically and with the commercial software *Karamba* and *BRIGADE/Plus*. Several other comparisons except these presented in this chapter have been done throughout the process and have shown similar results.

4.7.1 Complex geometry with isotropic materials

Since building complex geometry is extremely time consuming in *BRIGADE/Plus* such verification has been done with *Karamba*. However, *Karamba* can only handle isotropic materials, and therefore

steel was chosen for verification. In all three case studies in this thesis a verification of the geometry was performed with *Karamba*. For all the three cases the results of *Tortoise* and *Karamba* correspond well. These results are presented in each case study.

4.7.2 Composite beam

BRIGADE/Plus was used to verify that the composite material module was correctly implemented. A 10 meter long cantilever I-beam was modelled in this test. The beam was fully fixed in six points on one edge and had two point loads acting on the other edge, as seen in Figure 4.10. Each point load had a magnitude of 50 kN and acted in positive z-direction. No self weight was included. The mesh size in both the *BRIGADE/Plus* and the *Tortoise* model was 62.5 mm, which can be considered small enough but still a reasonable size to keep the computational time down. Larger mesh sizes were also used which gave similar results.

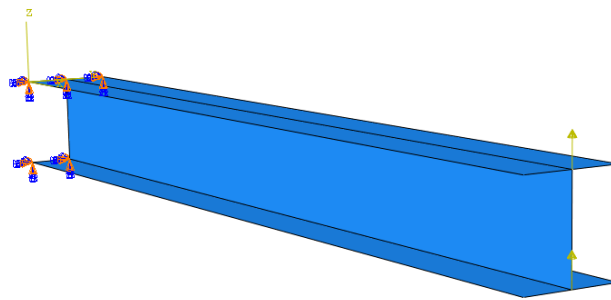


Figure 4.10: Loads and constraints acting on the beam.

The composite material was a five ply laminate, two glass fibre plies and three carbon fibre plies, acting with the strong direction in longitudinal axis. The material properties in Table 4.1 were used:

Table 4.1: Material properties used in model

Property	Glass fibres	Carbon fibres
Longitudinal E-modulus [GPa]	45	142
Transversal E-modulus [GPa]	12	10.3
Shear modulus [GPa]	5.5	7.2
Poisson's ratio [-]	0.19	0.27

The configuration for the laminates can be seen in Table 4.2.

Table 4.2: Laminate configuration

Laminate*		
45°	C/Ep	1 mm
-45°	G/Ep	2 mm
90°	C/Ep	1 mm
-45°	G/Ep	2 mm
45°	C/Ep	1 mm

* C= Carbon fibres, G=Glass fibres, Ep= Epoxy

The maximum obtained deformations in the analysis can be seen in Table 4.3.

Table 4.3: Deformation verification between *BRIGADE/Plus* and *Tortoise*

Max def	BRIGADE/Plus	Tortoise	Difference
Z-axis [mm]	428.7	439.8	2.6%
Y-axis [mm]	12.3	11.7	4.7 %
X-axis [mm]	31.5	30.6	3.0 %

The deformed mesh for *BRIGADE/Plus* and *Tortoise* viewed from the side can be seen in Figure 4.11.

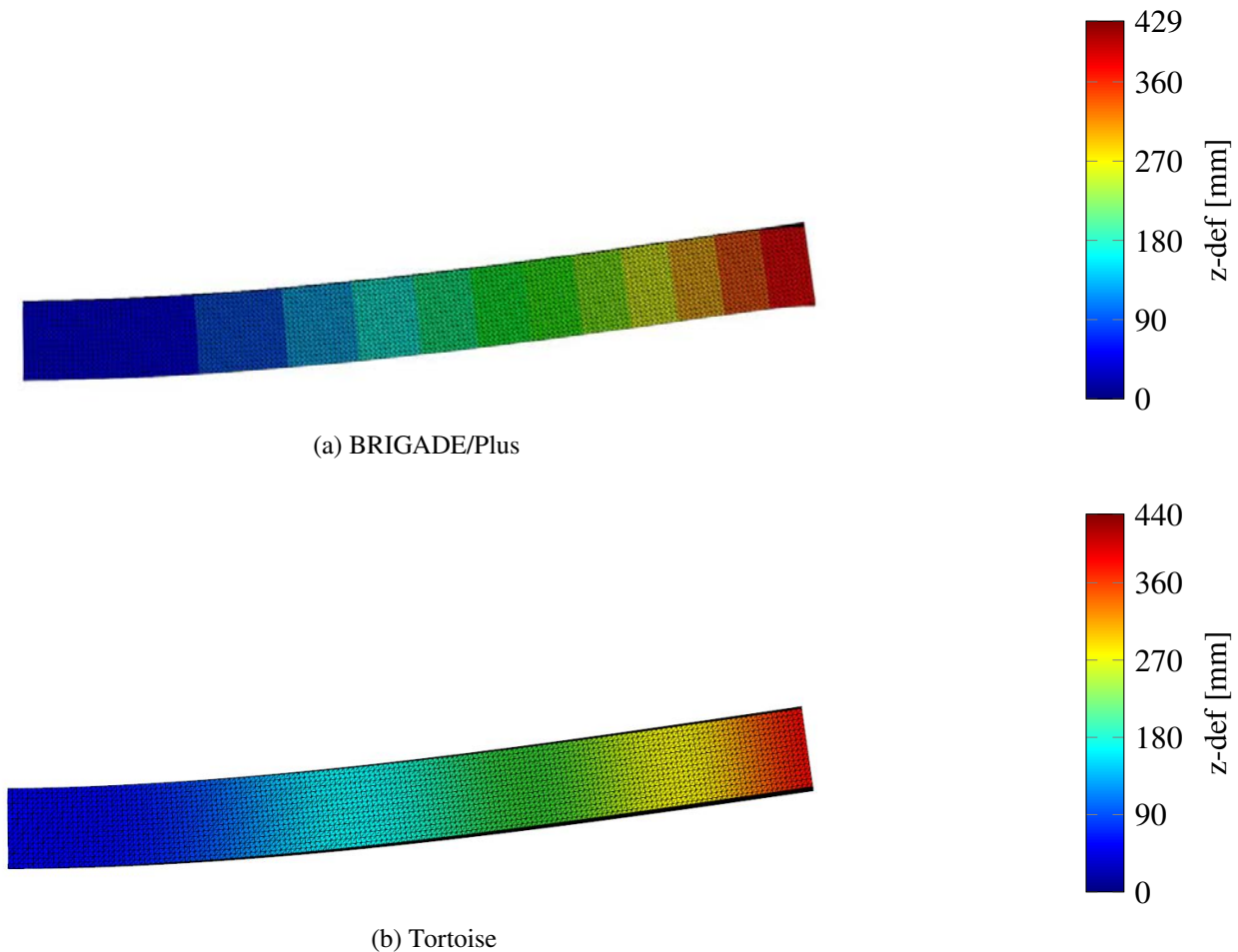


Figure 4.11: Deformed meshes, scaled by 2.3.

The deformation results show a small difference between *BRIGADE/Plus* and *Tortoise*, 2.6% - 4.7%. This difference is probably due to *BRIGADE/Plus* using a different element definition.

Next, a comparison of the stresses between *Tortoise* and *BRIGADE/Plus* was done. The obtained results can be seen in Table 4.4, and the plotted von Mises stresses can be seen in Figure 4.12.

Table 4.4: Maximum stresses comparison

Stresses	BRIGADE/Plus	Tortoise	Difference
von Mises [MPa]	1862.3	1862.2	0.005%
Principal (Abs.) [MPa]	1904.2	1906.1	0.1 %

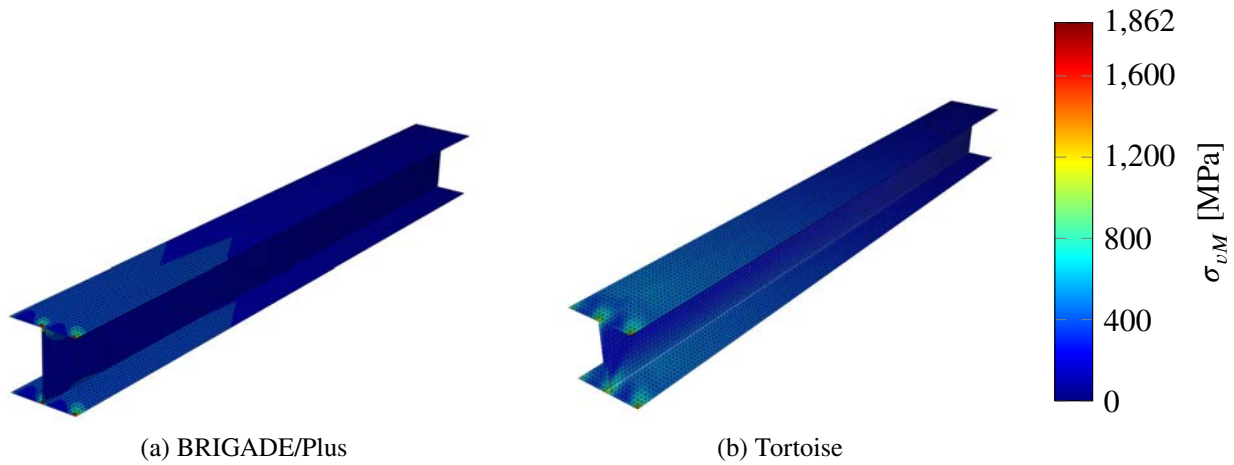


Figure 4.12: von Mises stress plots.

Both the results and the overall behaviour for both the stresses and deformations of the models correspond well. It can be concluded that *Tortoise* performs well in cases similar to this and the composite material module seems to be correctly implemented.

5 Case studies

In order to assess the performance and usability of the tool, as well as showcase the potential of parametric analysis and our optimisation theories, three case studies of existing or planned FRP bridges were performed. The results and the methodology of these case studies are presented in this chapter.

5.1 Kaponjärbron

Kaponjärbron is a 45.1 m long and 3 m high shell structure bridge, currently in the design stage, spanning over the Rosenlund canal in Gothenburg. The bridge consists of a main span on two supports and a cantilever part on the south side. The main span between the north side and the support in the canal is 34.3 m long, and the cantilever part is 10.8 m long. If the bridge is built it will be the second bridge in Sweden with fibre reinforced polymers as the main structural material (Ramböll, 2016). FRP was chosen as the main material due to the challenging geotechnical combined with the bad state of the current canal walls. Therefore the bridge is designed with an extra support in the canal and is only supported by the canal walls on the north side. Figure 5.1 shows a rendered image of the proposed Kaponjärbron.



Figure 5.1: Rendered image of Kaponjärbron. Courtesy of Ramböll.

5.1.1 Modelling

Materials

The materials used in this analysis are E-Glass fibres/Epoxy, Carbon fibres/Epoxy and foam. Table 5.1 list all the material properties for the different materials used throughout the analysis. The foam

material has been assigned no stiffness or strength, and is only used to create distance in the sandwich panel.

Table 5.1: Material properties (Agarwal, Broutman, & Chandrashekhara, 2015)

Property	E-Glass/Epoxy	Carbon/Epoxy	Foam
E_L [GPa]	38.6	138.0	0.0
E_T [GPa]	8.27	8.96	0.0
G_{LT} [GPa]	4.14	7.1	0.0
ν [-]	0.26	0.3	0.5
ρ [kg/m ³]	2100	2100	0.0

The main ply arrangement for all laminates in the first analysis can be seen in Table 5.2. The configuration is based on the master thesis by Chiv and Vocal (2014).

Table 5.2: Laminate configuration

Laminate*		
0°	G/Ep	4 mm
45°	G/Ep	0.25 mm
-45°	G/Ep	0.25 mm
90°	G/Ep	0.25 mm
0°	Foam	30 mm
90°	G/Ep	0.25 mm
-45°	G/Ep	0.25 mm
45°	G/Ep	0.25 mm
0°	G/Ep	4 mm

* G=Glass fibre, Ep=Epoxy

The laminate is rather unidirectional with the two thickest plies in 0° direction, combined with six other thinner plies in transverse and diagonal directions. The laminate is a sandwich panel with a 30 mm thick layer of foam in the centre. The foam layer increase the laminates bending stiffness. The additional distance to the neutral axis does not have a large impact on the global behaviour of the bridge since membrane action is dominating, but it has great significance locally, especially the short span above the middle support, see in Figure 5.2. For this part the foam thickness is increased to 120 mm and the thickness of the outermost plies have been increased to 6 mm each. The configuration can be seen in Table 5.3.

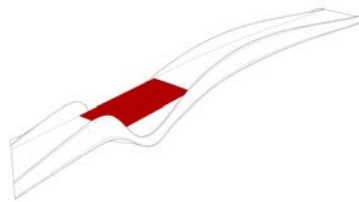


Figure 5.2: Bridge part extra vulnerable for local bending.

Table 5.3: Laminate configuration of small bridge deck part.

Laminate*		
0°	G/Ep	6 mm
45°	G/Ep	0.25 mm
-45°	G/Ep	0.25 mm
90°	G/Ep	0.25 mm
0°	Foam	120 mm
90°	G/Ep	0.25 mm
-45°	G/Ep	0.25 mm
45°	G/Ep	0.25 mm
0°	G/Ep	6 mm

* G=Glass fibre, Ep=Epoxy

When carbon fibres were introduced, the outermost glass fibre plies were substituted to carbon fibre plies with varying thickness. Carbon fibres were chosen to substitute the glass fibre plies instead of being added on top, since glass fibres plies with same direction as the carbon fibre plies would give minimal contribution to the strength and stiffness. The configuration for the hybrid laminate can be seen in Table 5.4.

Table 5.4: Hybrid laminate configuration.

Laminate*		
0°	C/Ep	t mm
45°	G/Ep	0.25 mm
-45°	G/Ep	0.25 mm
90°	G/Ep	0.25 mm
0°	Foam	30 mm
90°	G/Ep	0.25 mm
-45°	G/Ep	0.25 mm
45°	G/Ep	0.25 mm
0°	C/Ep	t mm

* C=Carbon fibre, G=Glass fibre, Ep=Epoxy, t =varying thickness

Mesh

The geometry was provided in the form of a *Rhino*-model from Ramböll. The geometry had to be simplified somewhat to be able to produce a mesh that could be used for analysis. Figure 5.3 shows the geometry after the modifications.

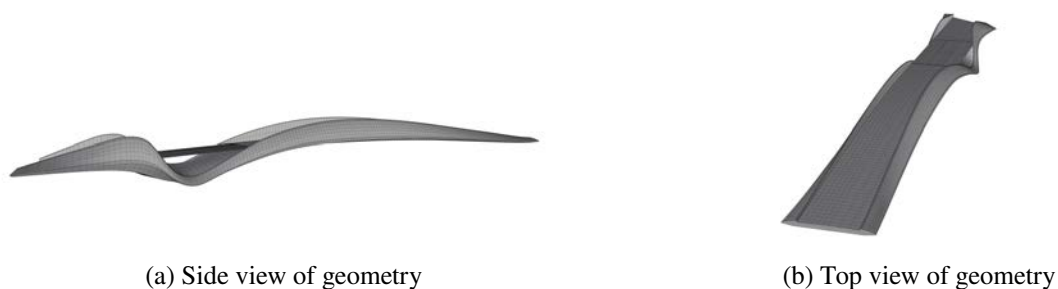


Figure 5.3: Geometry used for the analyses.

To prevent large local deformations in the bridge deck and local buckling, stiffeners were added, both longitudinal and transversely. The amount and position of stiffeners were based on investigations from the master thesis by Chiv and Vocal (2014). The geometry for the stiffeners can be seen in Figure 5.4.

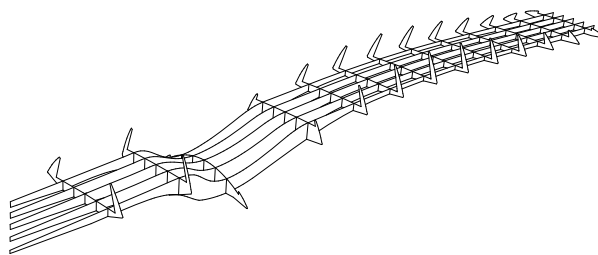


Figure 5.4: Transverse and longitudinal stiffeners in the bridge.

To find a mesh size that is accurate enough but can be analysed within a reasonable computational time, a convergence study of the mesh size was done. Figure 5.5 shows the result of the study. The GFRP-material and section from Section 5.1.1 was used and applied with gravity load on the entire structure.

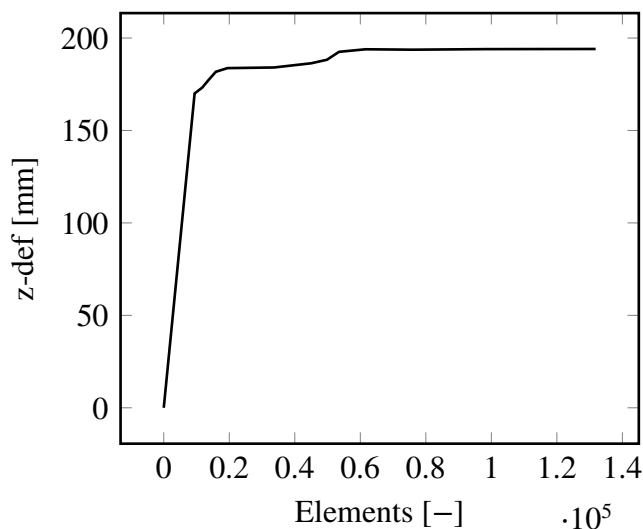


Figure 5.5: Vertical deflection for meshes with different element sizes

Due to the lack of symmetry in the structure the entire model needed to be included in the analysis. The model converges at around 60000 elements. The convergence curve is not fully smooth and has a steeper part around 50000 elements. This could depend on the complex geometry causing imperfections in the mesh. The mesh component used for this analysis was the *Karamba* meshing component *Mesh Breps*.

It was chosen that a mesh with an element side length 0.2 m which corresponds to about 73000 elements was suitable for this model with regards to accuracy and run-time. This mesh size will be used throughout the analyses of this bridge. Figure 5.6 shows a picture of the model with the proposed mesh.



Figure 5.6: Plot of the meshed geometry.

Loads

The bridge was loaded with a pedestrian distributed load on the bridge deck, and a permanent action G_d from the self weight. The pedestrian characteristic distributed load, q_{fk} , can be calculated from EN-1991-2:2003 (2003) Section 4.3.5, which gives:

$$q_{fk} = 5 \text{ kN/m}^2$$

The pedestrian load was regarded as a leading frequent load in this case. When analysing in service-ability limit state the variable actions Q_d from Table A2.6 in EN-1991-2:2003 (2003) gives:

$$Q_d = \psi_{1,1} q_{fk}$$

where $\psi_{1,1} = 0.4$ from Table 2.6 in EN-1990:2002/A1 (2002). The total variable load in this case would then be:

$$Q_d = 2 \text{ kN/m}^2$$

Q_d is applied on the entire bridge deck.

Other loads as wind load and concentrated loads on the bridge deck, representing a snowplough, have been neglected due to causing mostly local deformations. This case study was not mainly focused on making an exact model with the right load cases, but instead model a reasonable case for comparative purposes. It was concluded that the chosen load case was representative enough.

Boundary conditions

The bridge was supported in two places by two supports in each position, the first being located on the northern edge of the canal and the second in the canal itself, minimising the load effect on the canal edges. The south side of the bridge has a cantilevering end. A total of four supports were modelled, and the two supports in the canal are locked in longitudinal-, transverse- and vertical-direction but are free to rotate in all directions. The two supports on the edge of the canal are locked in transverse- and vertical direction, but are free to move in longitudinal direction and rotate in all directions, which can be seen in Figure 5.7.



Figure 5.7: Support conditions.

5.1.2 Model verification

The analysed model was compared with the commercial software *Karamba*. Since anisotropic materials cannot be analysed in *Karamba*, or any other FE-analysis software in *Grasshopper*, a steel material was used, with a section of 20 mm and with the steel properties in Table 5.5.

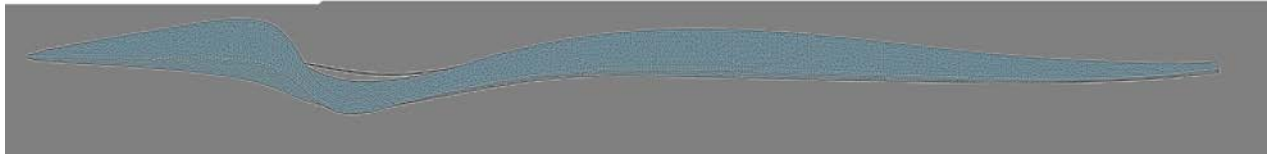
Table 5.5: Material properties

Property	Steel
E_L [GPa]	210
E_T [GPa]	210
G_{LT} [GPa]	79.3
ν [-]	0.3
ρ [kg / m ³]	7800

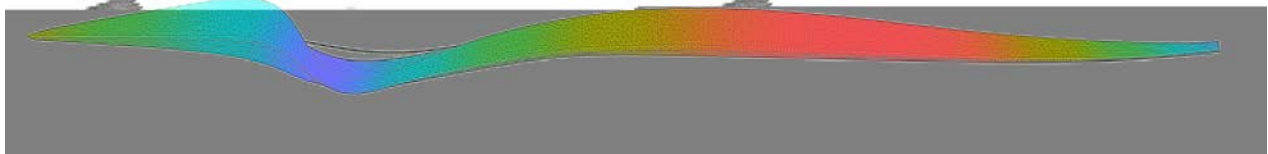
No direct comparison with an anisotropic FRP material can be done with *Karamba*, but models with anisotropic materials have been compared with *BRIGADE/Plus* and can be considered reliable. The model used in *Tortoise* and *Karamba* had 72878 elements and both analysers used the same mesh. The bridge was loaded with self weight only. The obtained results from the analyses can be seen in Table 5.6.

Table 5.6: Result comparison between *Karamba* and *Tortoise*

	Karamba	Tortoise	Difference
z-def [mm]	60.9	59.2	-2.8%
First freq [Hz]	2.41	2.42	+0.4 %



(a) Karamba



(b) Tortoise

Figure 5.8: Deformation comparison, scaled by 10.

Comparing the results in Table 5.6, the difference between *Tortoise* and *Karamba* in maximum vertical deflection and first eigenfrequency are within reasonable limits. The deformation plots look very similar and have the same deformation pattern. The model can be considered verified.

5.1.3 Demands

During this analysis only serviceability demands will be considered since this is governing in most cases when designing FRP-bridges. The allowed vertical deflection when loaded by variable loads and self weight is limited to:

$$L/400$$

where:

$$L = \text{Theoretical span length in meter}$$

according to B.3.4.2.2 in TRVK-Bro-11 (2011). In this case the allowed deformation is 86 mm for the main span.

Demands on vibrations needs to be fulfilled and according to Carlsson (2015) the following demands were set for Kaponjärbron :

$$\begin{aligned} f_{1,vert} &\geq 3.5 \text{ Hz} \\ f_{1,horvrid} &\geq 1.75 \text{ Hz} \end{aligned}$$

where:

$$\begin{aligned} f_{1,vert} &= \text{First vertical frequency.} \\ f_{1,horvrid} &= \text{First horizontal frequency.} \end{aligned}$$

5.1.4 Initial analyses

The first analysis is performed with the glass fibre section, displayed in Table 5.2. Table 5.7 shows the results from the first analysis and the minimum requirements.

Table 5.7: Analysis of first model compared with demands

	First analysis	Demands	Utilisation
z-def [mm]	187	84	223%
First freq [Hz]	1.83	3.5	191 %
First horizontal freq [Hz]	4.29	1.75	41%

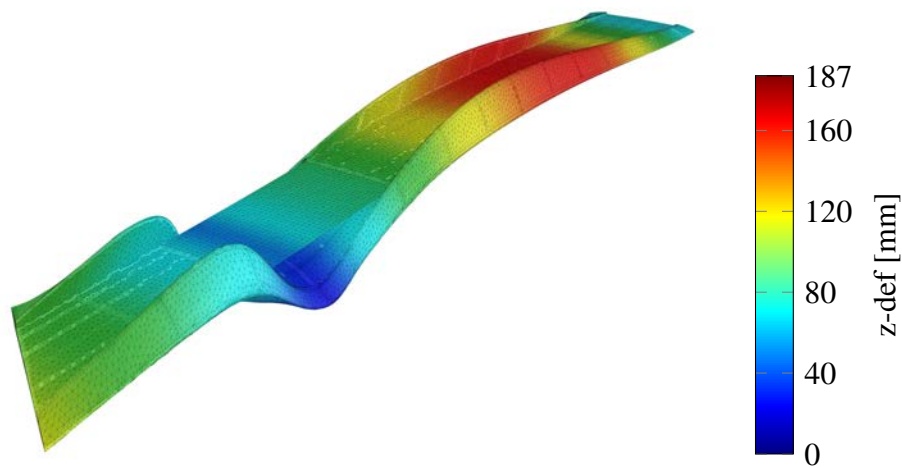


Figure 5.9: Deformation plot from first analysis, scaled by 1.

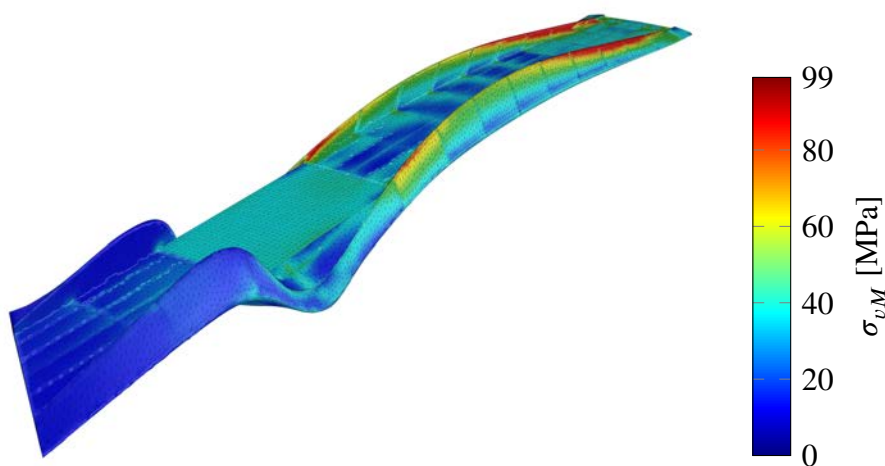


Figure 5.10: von Mises stress plot from first analysis.

The deformation plot looks as expected, no extreme local deformation occurs and the largest deformations are in the main span. The cantilever part of the bridge has some upwards deformations. If the main span is deflecting down, the cantilever will be deflecting upwards as a result. By making the main span more stiff, the cantilever will deform less as well. For this load case it can be seen that the parapets take highest stresses. The bridge deck over the main span experience slightly higher stresses close to the stiffeners. The cantilever part experiences very low stresses.

Since the bridge does not meet the requirements for vertical deformation and first eigenfrequency for this load case, some design modifications had to be done. To increase the stiffness of the bridge, carbon fibre can be added at certain places, but as little as possible to keep the costs down. In the master thesis by Chiv and Vocal (2014), carbon fibres were added underneath the bridge deck and on top of the parapets. An approximation of their carbon fibre placement can be seen in Figure 5.11. This carbon fibre arrangement will be referred to as *original design*.

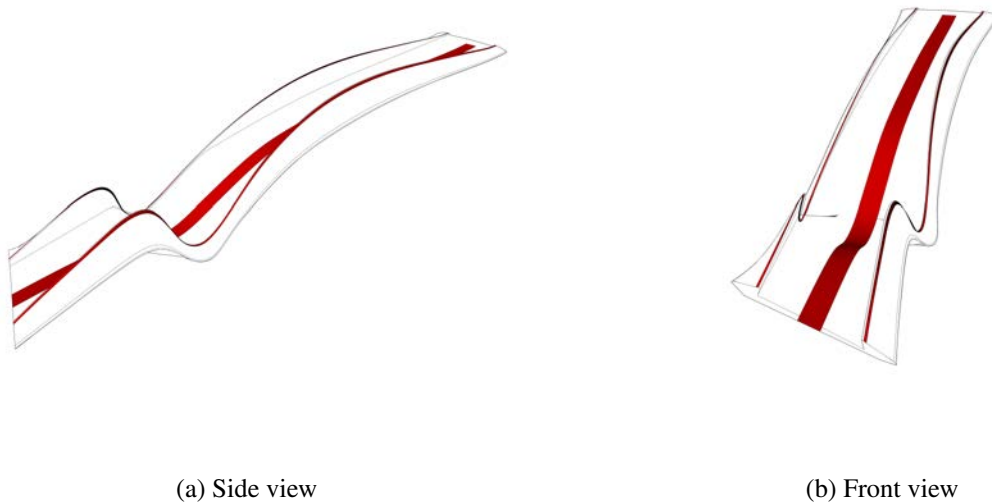


Figure 5.11: Placement of carbon fibre elements.

The carbon fibre strips were modelled with the sectional dimensions $900 \text{ mm} \times 50 \text{ mm}$ and $130 \text{ mm} \times 20 \text{ mm}$ under the bridge deck and on the parapets respectively. In total, 4.75 t of carbon fibre was used in our model and was spread out over 51.94 m^2 . The following results were obtained:

Table 5.8: Initial model improved with CFRP, compared with the demands

	Improved model	Demands	Utilisation
z-def [mm]	107	84	127%
First freq [Hz]	2.35	3.5	149 %
First horizontal freq [Hz]	4.31	1.75	41%

The first eigenmode is shown in Figure 5.12 and deformation plots can be seen in Figure 5.13.



Figure 5.12: First eigenmode.

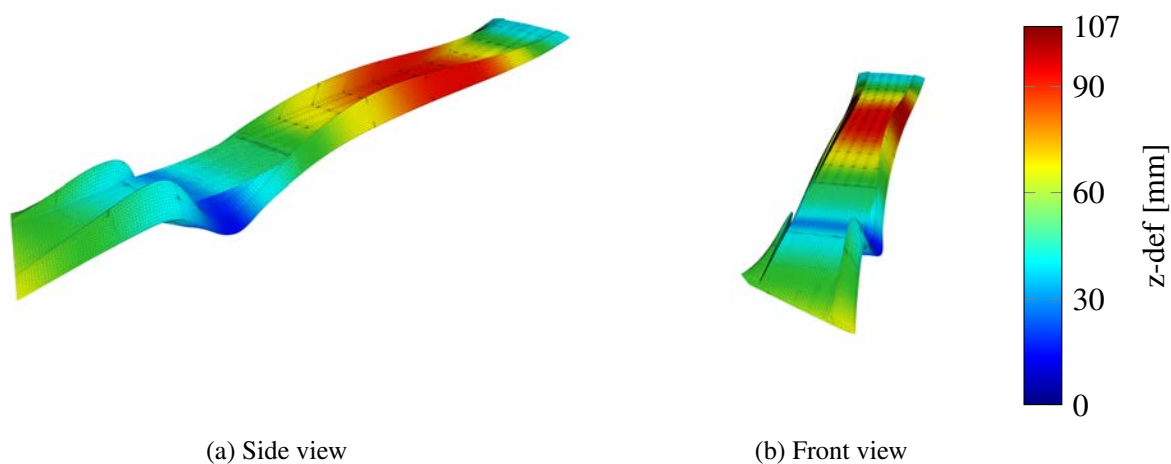


Figure 5.13: Deformation plots, scaled by 10.

Deformation behaviour is very similar to the model where no carbon fibre were used. The stress plots can be seen in Figure 5.14.

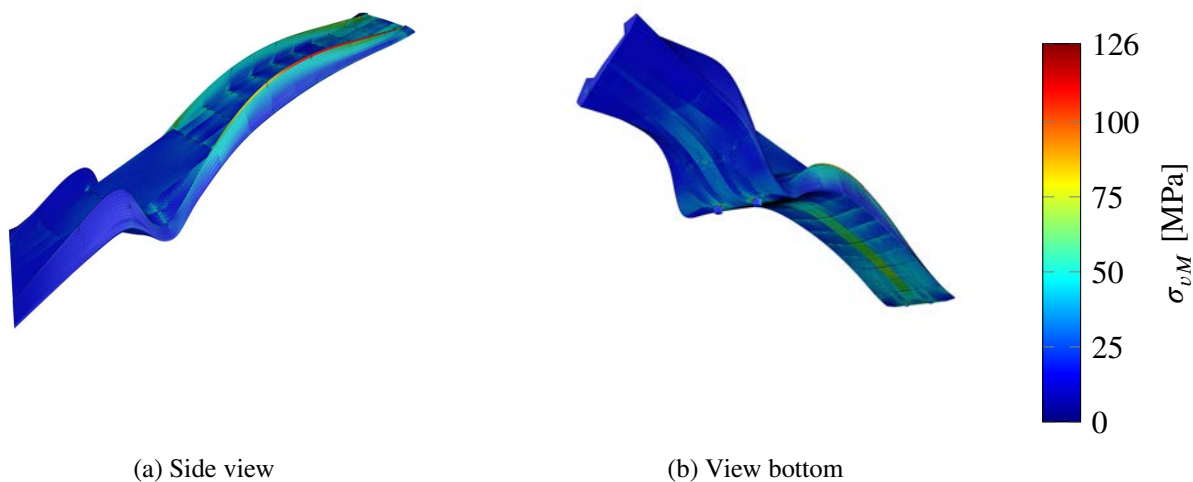


Figure 5.14: von Mises stress plots.

As seen in the stress plots, the carbon fibre parts are experiencing higher stresses. The elements on the parapets are taking much higher stresses than the carbon fibre under the deck. The elements with carbon fibre close to the free end experience much lower stresses than the carbon parts on the parapets, just as much as pure glass fibre elements. To see how much the carbon fibres at the south side of the middle supports actually contributed to decreasing the deformation and increasing the lowest eigenfrequency another analysis was made where the carbon fibres were removed from these areas, illustrated in Figure 5.15.

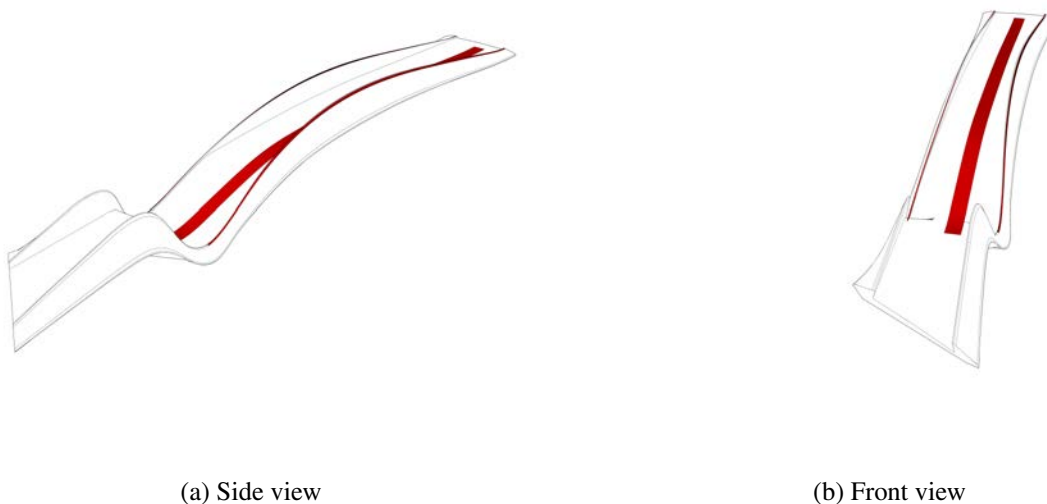


Figure 5.15: Placement of the reduced carbon fibres.

Table 5.9 shows a comparison of the reduced carbon fibre placement and the original placement. Even though the model with reduced carbon fibre amount has 1.14 t less carbon fibre, the maximum vertical deformation difference was only 0.6 mm. By removing these carbon fibre parts large amount of money can be saved without almost any loss in performance.

Table 5.9: Compared results from original model and model with reduced amount of carbon fibres

	Original	Reduced	Difference
Weight CFRP [t]	4.75	3.61	-24 %
z-def [mm]	106.7	107.3	+0.6%
First freq [Hz]	2.35	2.36	+0.4 %

Since the cantilever part of the bridge also has requirements for maximum vertical deformation it is important to see how it is affected by the reduced amount of carbon fibre. To get the maximum downward deformation only the cantilever part of the bridge deck is loaded. Table 5.10 shows the maximum vertical deformation for the cantilever part with the different carbon fibre layouts.

Table 5.10: Deformation of cantilever part, when loaded with pedestrian load

	z-def [mm]
Original	-25.7
Reduced CFRP	-28.7
No CFRP	-31.7

The removed carbon fibre does affect the vertical deformation for the cantilever part, but it is not significant. The decrease compared to the suggested layout is 12% compared to the reduced layout.

The largest deformation for the cantilever part does not occur when the cantilever part of the deck is loaded, but when the main span is fully loaded instead. Table 5.11 shows the deformation results for the cantilever edge when only the main span is fully loaded.

Table 5.11: Deformation of cantilever part, loaded at main span

	z-def [mm]
Original	+125.4
Reduced CFRP	+122.9

Note that the deformation in this case is positive. The reduced carbon fibre configuration does not increase the deformation significantly, only about 2%. What seems to be important is to reduce the deflection of the main span, which will in turn decrease the deformation of the cantilever. Therefore, the deformation of the cantilever part was not taken into further account during this case study and only the maximum deformation over the main span was considered.

It was investigated where else carbon fibre could be reduced without increasing the deformation at the main span. Since the bottom carbon strip was not very stressed at any section an analysis was made where the entire carbon bottom strip was also removed, only leaving the strips on the parapets.



Figure 5.16: Placement of the further reduced carbon fibre elements.

Table 5.12 shows the results from this analysis.

Table 5.12: Comparison of original model and model with further reduced CFRP

	Original	Reduced	Difference
Weight CFRP [t]	4.75	0.47	-90%
z-def [mm]	106.7	128.1	+20%
First freq [Hz]	2.35	2.15	+8.5 %

The maximum vertical deformation was only increased by 20% while only using 10% of the original carbon fibre weight. There seems to be a large potential to use the carbon fibres more efficiently than the suggested arrangement. In Section 5.1.5 it will be investigated how to optimise the carbon amount and placement, to fully utilise the carbon fibres.

5.1.5 Optimisation

Carbon fibre placement

The model have been optimised in several aspects to minimise the deflection and increase the eigenfrequencies. One aspect is to see if the carbon fibre can be placed on different locations to be more efficient. As seen in Figure 5.14 a large part of the carbon fibre elements were barely stressed and not utilised properly. An analysis was done to see where the elements with the highest stresses were located, and the carbon fibres were placed on these elements. Three different models were then made based on the previous analysis in Section 5.1.4. All three models had the same amount of carbon fibre as the original analysis (4.75 t), but with different thickness and area configurations. The carbon fibre thickness is constant for all the elements it was applied on. The following models were analysed:

- *Model 1*, with the same total CFRP area as the original model, 51.9 m².
- *Model 2*, with the same CFRP thickness as the bottom CFRP strip of the original model.
- *Model 3*, with the same CFRP thickness as the parapet CFRP strips of the original model.

The different arrangement can be seen in Table 5.13.

Table 5.13: Different carbon fibre arrangements

	CFRP thickness [mm]	CFRP area [m ²]	CFRP weight [t]
Model 1	43.5	51.9	4.75
Model 2	50	45.2	4.75
Model 3	20	113.1	4.75

Note that the CFRP section thickness is divided in two plies and depending on production method and material properties the maximum thickness per ply that can be infused without risk of defects can be limited. (Agarwal et al., 2015). This hybrid laminate set up can be seen in Table 5.4. The top and bottom ply of the laminate is changed from the original 4 mm to new thicknesses, depending on which model that is being analysed, same procedure as in Section 5.1.4. The selection of elements

where the carbon laminate should be applied was done in the *GetStressedElements*-component and the different arrangements can be seen in Figure 5.17.

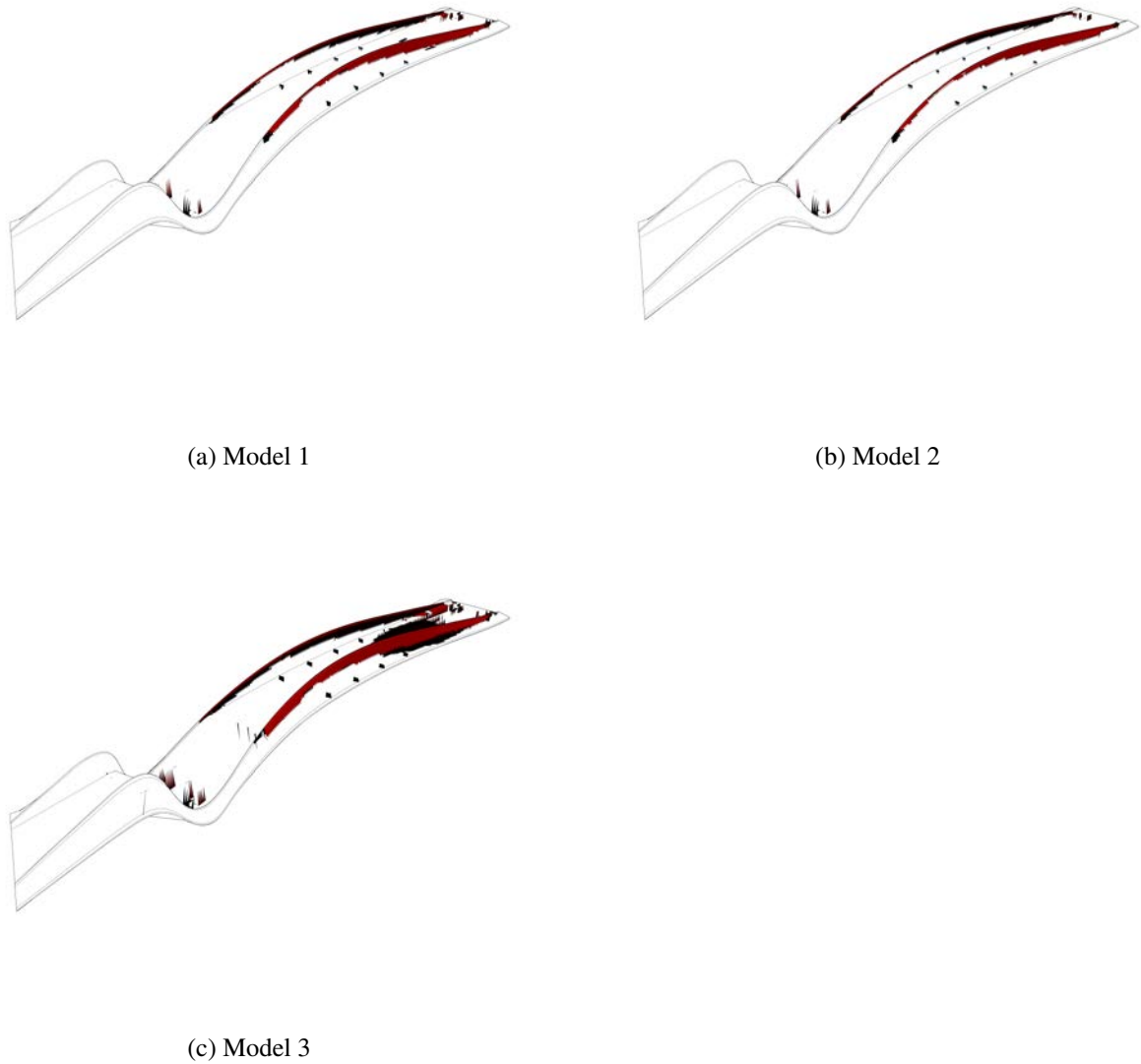


Figure 5.17: Carbon fibre placement based on the elements experiencing highest stresses.

The highest stressed elements are placed mostly at the top of the parapets. In *Model 3* it can be seen that once the parapets are covered with carbon fibre, the next area with highly stressed elements are the north side of the bridge deck. An analysis was done for each model and Table 5.14 shows the results.

Table 5.14: Results for different CFRP configurations

	z-def [mm]	First freq [Hz]
Model 1	67	2.60
Model 2	67	2.59
Model 3	63	2.68

Model 3 performed best in both vertical deformation and first eigenfrequency. Table 5.15 shows the improvement compared with the original carbon fibre placement from Section 5.1.4.

Table 5.15: Results for the original design and the Model 3 design

	Original	Model 3	Difference
z-def [mm]	106.7	63	-41%
First freq [Hz]	2.35	2.68	+14%

Based on the results from Table 5.15 it seems that placing the carbon fibre based on the highest stressed elements is more efficient than the original placement, in regards of deformation at the main span. There are a few similarities, but placing most of the carbon fibre on the parapets of the main span made a great difference, since elements at the cantilevering end are not stressed as much.

Since the results between the three different models differed slightly it was suitable to make an optimisation analysis of the ratio between area of carbon elements and the carbon fibre section thickness of those elements to get the optimal use of the 4.75 t carbon fibre used in the analyses so far. The analysis was performed with *Galapagos*. For this analysis a coarser mesh around 33000 elements was used due to the long computational time of this kind of analysis, since *Galapagos* could iterate thousands times to find the best solution.

Galapagos changed configurations of the total area of carbon fibre elements and the section thickness of the carbon fibre elements so the total mass of carbon fibre was kept 4.75 t. Figure 5.18 shows the result from this analysis.

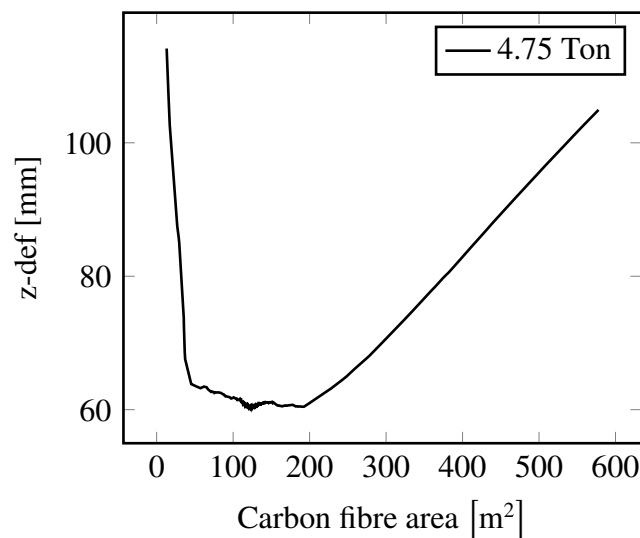


Figure 5.18: Deformation with different configurations of CFRP area and CFRP section thickness, where total CFRP weight is constant.

The laminate area of the entire bridge is 852.4 m². Values when the carbon fibre area had exceeds 600 m² were removed from the graph. The smallest deformation in this case, 60 mm, occurred when the carbon fibre elements had a total area of 124.1 m² and a carbon fibre section thickness of 18.2 mm, which gives 9.1 mm thickness per outer ply. Table 5.16 shows the results for the optimal ratio between carbon fibre elements area and carbon fibre thickness per element, compared with the *Model 3*, which was the best result from previous analysis.

Table 5.16: Result comparison of optimised carbon fibre design and Model 3

	Model 3	Optimised	Difference
CFRP area [m ²]	113.1	124.1	-
CFRP thickness [mm]	20.0	18.2	-
z-def [mm]	63	60	-4.8%
First freq [Hz]	2.68	2.73	+1.9%

As can be seen in Table 5.16 the carbon fibre area and carbon fibre section thickness for *Model 3* was quite a good initial guess, but if using *Model 1* or *Model 2* the maximum vertical deformation difference would have been almost 12% which is significant amount. This configuration is the optimal use for this amount of carbon fibres, but if the allowed amount of carbon fibres changes this composition might not be the best any more. Figure 5.19 shows an investigation of the deformation versus the ratio of carbon fibre area for a few different carbon fibre amounts.

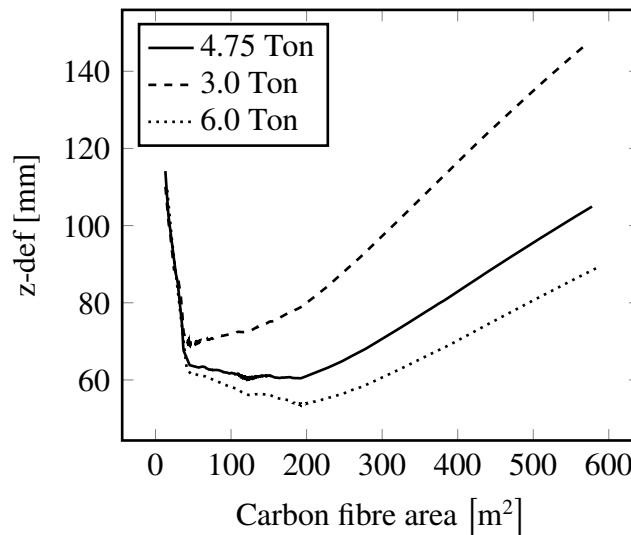


Figure 5.19: Deflection with different configurations of carbon fibre area and carbon fibre section thickness, the total carbon weight is constant for each curve.

By trying out a few different amounts a general pattern for this specific structure can be seen. For all the three different amounts it is very beneficial to use more than 40 – 45 m² and less than 185 – 190 m² of carbon fibre area to get a good usage of the carbon fibres in regards of deformation over the main span. To get the best solution, an optimisation should be done for that specific carbon fibre amount. Other factors also need to be taken into consideration, it could be more beneficial for the project to use less area of carbon fibres and get a few millimetres more deformation to gain other

values. At least this shows that there is great potential to quickly determine where and how much carbon fibres that should be used to suit a specific project the most. The chosen elements for carbon fibre, based on the new deformation optimisation, can be seen in Figure 5.20.

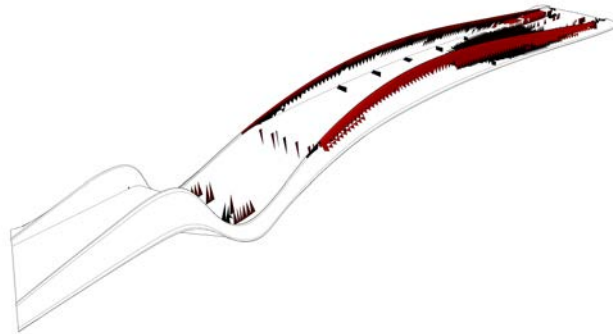


Figure 5.20: Carbon fibre arrangement based on the elements with highest stress.

The elements with the highest stresses are spread out and some of the elements are on the stiffeners, which is not desired. This would be very difficult to produce since the carbon elements are so spread out. A more suitable use of this tool is to find the general areas with the highest stresses and remove unwanted elements. A selection of grouped elements based on the highest stress analysis could look like Figure 5.21.

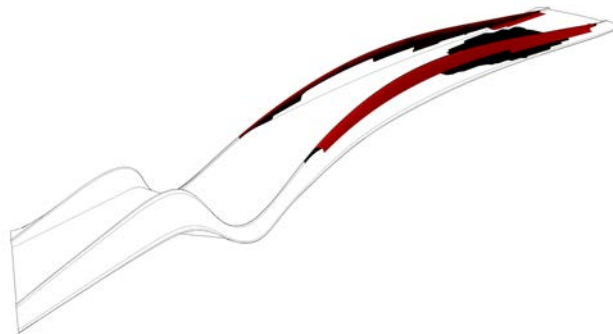


Figure 5.21: Refined carbon fibre arrangement.

This would be possible to build and covers the main high stressed areas. The total carbon fibre area is based on the optimisation with a few elements removed. The area used in the analysis was 122.7 m^2 , with a carbon fibre section thickness of 18.4 mm adding up to 4.75 t carbon fibre. Table 5.17 shows the results from this analysis.

Table 5.17: Results from refined- and unrefined carbon fibre arrangement

	Unrefined	Refined	Difference
CFRP area [m^2]	124.1	122.7	-
CFRP thickness [mm]	18.2	18.4	-
z-def [mm]	60	62	+3.3%
First freq [Hz]	2.73	2.70	-1.1 %

The difference between the refined and the optimised carbon output is fairly small. It could be considered as a suitable simplification without increasing the deformation significantly.

Perhaps the most interesting thing would be to see how little carbon fibre that could be used to reach the same deformation. Three different configurations were tried and Figure 5.22 shows the deformation for these different models with predetermined carbon fibre area, but changing carbon fibre section thickness. The alternatives analysed were:

- *Alt. 1*, 75 m² carbon fibre area.
- *Alt. 2*, 100 m² carbon fibre area.
- *Alt. 3*, 125 m² carbon fibre area.

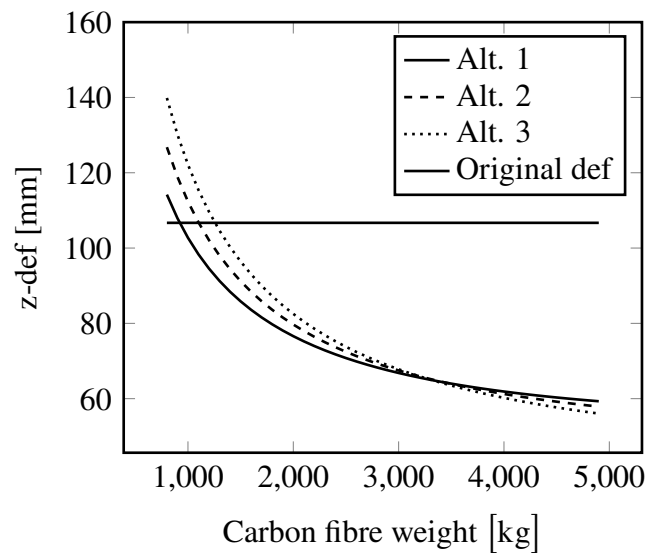


Figure 5.22: Deflection with different amount of carbon fibre for different area-thickness ratios.

The results from Figure 5.22 only takes deformation in regards, since eigenfrequencies did not give as good improvements from the optimisations. The different alternatives in Figure 5.22 were compared in Table 5.18.

Table 5.18: Result from different carbon fibre configurations

	Original	Alt.1	Alt.2	Alt.3
CFRP area [m ²]	51.9	75.0	100	125.0
CFRP thickness [mm]	51-20	5.8	5.2	4.8
Weight CFRP [t]	4.75	0.92	1.1	1.25
z-def [mm]	107	107	107	107
First freq [Hz]	2.35	2.33	2.34	2.35

Table 5.18 shows that all the three alternatives decrease the amount of carbon fibres significantly. Of the three alternatives, *Alternative 1* performed best and manage to achieve the same maximum vertical deformation with only 20% of the original carbon fibre weight.

So far, all the optimisation have been done with regards to deformation, but looking at the demands for this bridge, the vertical deformation demand $L/400 = 84$ mm is fulfilled with a margin, but the first eigenfrequency is not high enough. Again a *Galapagos* analysis can be made, this time with the aim to maximise the first eigenfrequency while the maximum vertical deformation is less than 84 mm. If the analysis is done with the original 4.75 t of carbon fibre, Figure 5.18 shows that the maximum vertical deformation is less than 84 mm when a carbon fibre arrangement between 30 – 400 m² with a carbon fibre section thickness of 5.7 – 75.4 mm is used, more clearly visualised in Figure 5.23.

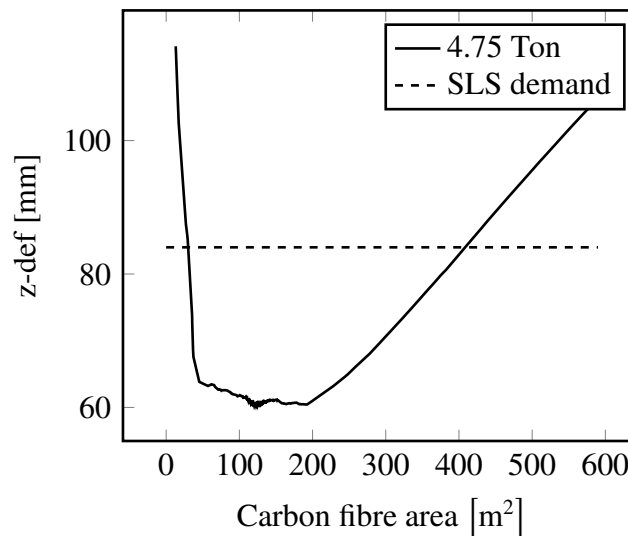


Figure 5.23: Deformation of different CFRP configurations and SLS demand.

The Galapagos optimisation with regards to maximising the first eigenfrequency can be seen in Figure 5.23. The area limits are the maximum allowed to manage the deflection requirements.

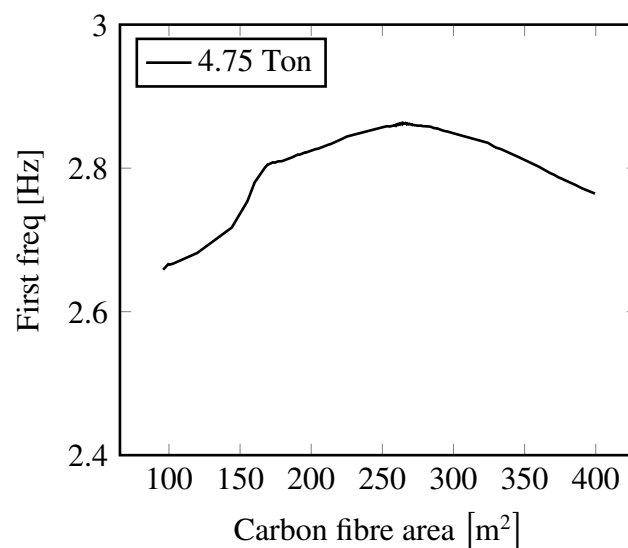


Figure 5.24: First eigenfrequency for different CFRP lay up configurations.

As can be seen in Figure 5.23 the different carbon fibre area affects the first eigenfrequency with a decent amount. In this case, where the first eigenfrequency is still far from 3.5 Hz and it is not much use for this kind of optimisation, but can be useful in other cases. In this case, a carbon fibre area of 263 m² with a corresponding carbon fibre thickness of 8.6 mm gives the highest first eigenfrequency, 2.86 Hz.

5.1.6 Fibre angle alignment

Another method to potentially decrease the deformation is by changing the direction of the fibres. When modelling the elements, the first material axis is directed in the longitudinal axis of the bridge. This is a good approximation for most of the bridges since the highest stresses often occur in the longitudinal direction. But in this case it is not optimal and not how it would be done in reality since the bridge has such a curved shape. This modelling technique could therefore be improved. Figure 5.25 shows the current first material axes for the elements in a part of the bridge.

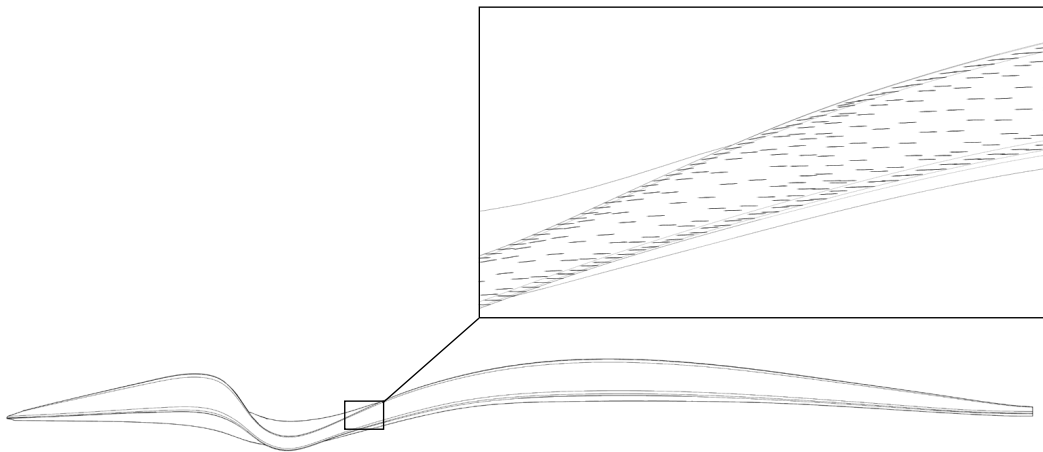


Figure 5.25: Material axis for each element, with original fibre directions.

To improve the deformation an analysis was done where each element had its first axis direction in the same direction as the highest principal stress in that element. The directions of the highest principal stresses for the same part of the bridge as in Figure 5.25 is seen in Figure 5.26.

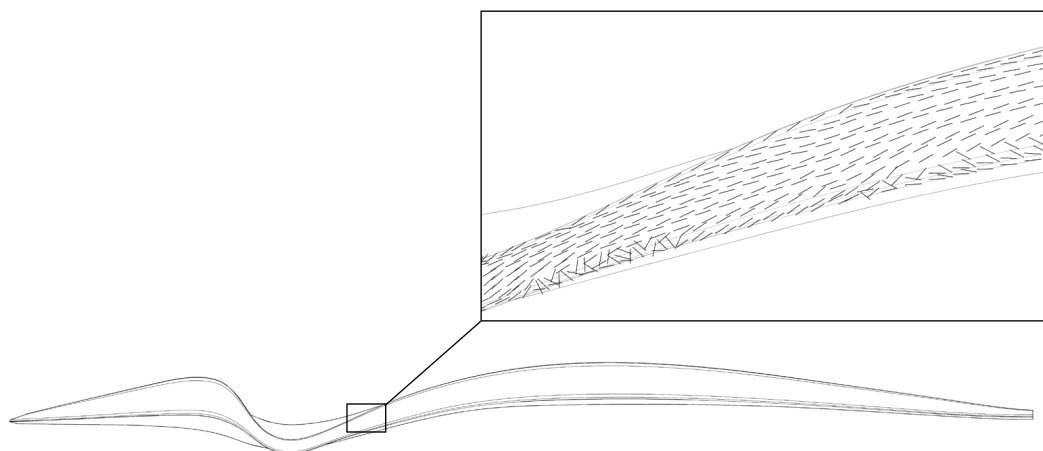


Figure 5.26: Material axis for each element, with fibre angles changed according to principal stresses.

If the material axis direction is set to the same angle as the direction of the principal stresses the results, seen in Table 5.19, were obtained. The principal stresses have been generated from an isotropic material, to get the direction of the stresses unaffected by any material.

Table 5.19: Result from original model and modelled with fibre angles changed according to principal stresses.

	Original	Changed angles	Difference
z-def [mm]	187	172	-8.0%
First freq [Hz]	1.83	1.87	+2.2 %

The fibre angle optimisation shows a good improvement of both deformation and first eigenfrequency. But this lay up would be impossible to achieve due to the difficulty to lay the fibre mattes in such intricate patterns. To improve the material direction of the laminates in a more realistic way would be to draw curves on the geometry as guides for the first axis direction, see Figure 5.27. With the component *DrawMaterialAxis* a more realistic orientation could be gained.

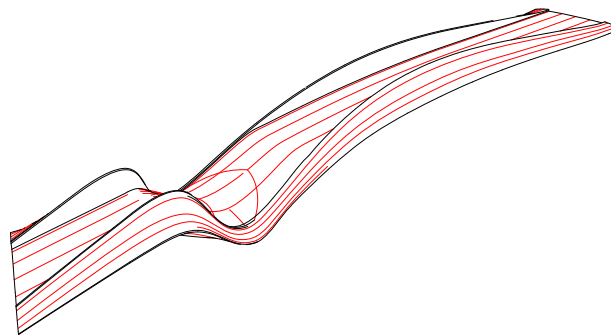


Figure 5.27: Guide curves, in red, for the elements first material axis.

Figure 5.28 shows the first material axis for a part of the bridge after the first axis direction have been modified based on the drawn guide curves.

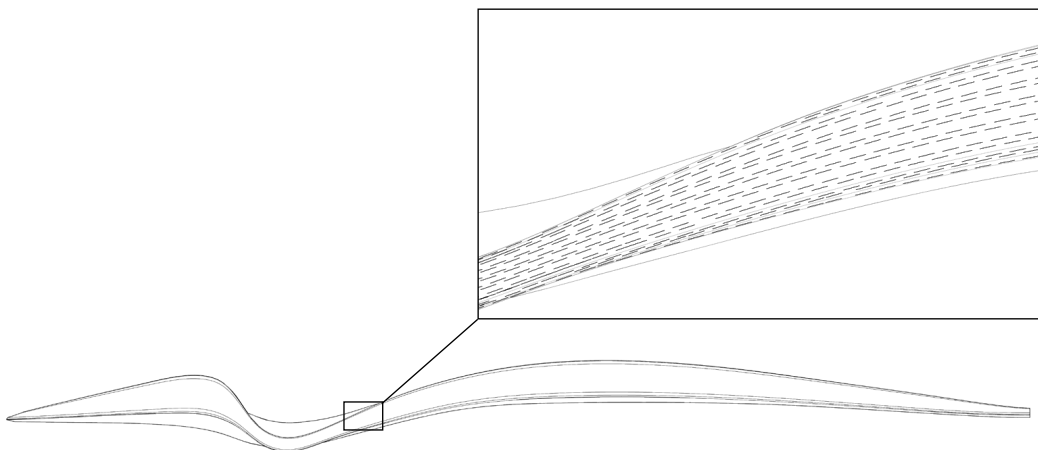


Figure 5.28: Elements material axis based on guide curves.

First a comparison with only glass fibres were made. Table 5.20 shows the results and difference between the glass fibre design in Table 5.7 and a design where the material angles have been changed based on the drawn curves.

Table 5.20: Comparison between original GFRP model and GFRP model with changed material axes

Properties	Original	Changed axis	Difference
z-def [mm]	187	181	-3.2%
First freq [Hz]	1.83	1.86	+1.6%

This method was then applied on the model with optimal refined carbon arrangement, Table 5.21 shows the result.

Table 5.21: Results for the original model and model with optimised CFRP configuration

	Original	Optimised	Difference
z-def [mm]	62	58	-6.5%
First freq [Hz]	2.70	2.78	+3.0%

The difference is slightly better than the GFRP results obtained in Table 5.20. An 6.5% decrease in deformation could be gained which is a good amount. This arrangement is more similar to how it would be produced in reality.

5.1.7 Comments

The most probable way this bridge would have been modelled and designed is a similar version to what was presented in Section 5.1.4 with additional carbon fibre on the parapets and underneath the bridge deck. According to the analyses done in this report with that configuration both the demands on vertical deformation and first eigenfrequency would have been exceeded. The final proposed configuration in this report involves both carbon fibre amount optimisation and fibre orientation optimisation. Table 5.22, shows a comparison between the proposed way to design it and the suggested way based on the optimisations done in this case study.

Table 5.22: Result from the original model and the final optimised model.

	Original	Optimised	Difference
Weight CFRP [t]	4.75	4.75	0%
z-def [mm]	107	58	-46%
First freq [Hz]	2.35	2.78	+18 %

The first eigenfrequency is still too low compared to the demands of 3.5 Hz, a way to handle that would be to use dampeners. Comparing the original model and the optimised model the difference is large, especially for the deformation.

There might be other reasons to why the suggested carbon fibre layout was done that we are not aware of and all different load cases have not been analysed. The deformations at the cantilever part could have been investigated more. Despite this, the original carbon fibre layout could probably be more efficient than the original design.

It should be noted that the self weight was included in our analysis, which it should not have been since the bridge is raised during construction to counter deformations from the self weight. The results would still with high probability be similar to the current ones. A smaller deformation at the main span would be expected. It is difficult to say exactly how the cantilever part would behave without self weight, but no large differences are expected.

The carbon fibre amount optimisation is not taking different carbon fibre thicknesses at different elements into account, this could also improve the performance of the bridge. But this would also increase the risk of error during fabrication due to a more complex fibre lay up.

5.2 Bascule bridge in Fredrikstad



Figure 5.29: Image of the bridge (courtesy of FiReCo).

As described in Section 2.4.2, the bascule bridge in Fredrikstad, Norway, is a 56 m span movable bridge of bascule type. It has no counterweights and relies solely on hydraulic pistons for the opening mechanism, and needs to be lightweight. It is therefore constructed in FRP with a combination of carbon- and glass fibres.

5.2.1 Modelling

Materials

As in the study of Kaponjärbron, the materials used in this study are E-Glass fibres/Epoxy, Carbon fibres/Epoxy and foam. Properties of said materials can be seen in Table 5.23.

Table 5.23: Material properties (Agarwal, Broutman, & Chandrashekhara, 2015)

Property	E-Glass/Epoxy	Carbon/Epoxy	Foam
E_L [GPa]	38.6	138.0	0.0
E_T [GPa]	8.27	8.96	0.0
G_{LT} [GPa]	4.14	7.1	0.0
ν [-]	0.26	0.3	0.5
ρ [kg/m ³]	1800	1600	0.0

The main ply arrangement for each laminate in the first analysis can be seen in Table 5.24, and is based on the master thesis by Chiv and Vocal (2014). It is similar to that of Kaponjärbron, apart from the thickness of the outer plies.

Table 5.24: Main GFRP laminate configuration

Laminate*		
0°	G/Ep	5 mm
45°	G/Ep	0.25 mm
-45°	G/Ep	0.25 mm
90°	G/Ep	0.25 mm
0°	Foam	30 mm
90°	G/Ep	0.25 mm
-45°	G/Ep	0.25 mm
45°	G/Ep	0.25 mm
0°	G/Ep	5 mm

* G= Glass fibres, Ep= Epoxy

The configuration of hybrid laminates is identical to that of Kaponjärbron and can be seen in Table 5.25. The sole information available on the carbon fibre laminates, is that it consists of a single skin with varying thickness, 10 mm to 38 mm (FiReCo, 2014). For simplicity, three thicknesses, t_{cf} , were chosen for the carbon fibre plies; 5 mm, 12 mm and 19 mm to give equal amounts of carbon fibre. The configuration can be seen in Table 5.25.

Table 5.25: Hybrid laminate configuration

Laminate*		
0°	C/Ep	t_{cf} mm
45°	G/Ep	0.25 mm
-45°	G/Ep	0.25 mm
90°	G/Ep	0.25 mm
0°	Foam	30 mm
90°	G/Ep	0.25 mm
-45°	G/Ep	0.25 mm
45°	G/Ep	0.25 mm
0°	C/Ep	t_{cf} mm

* C=Carbon fibre G=Glass fibre, Ep=Epoxy, t_{cf} =carbon fibre thickness

Geometry

Together with the limited written information from the FiReCo website (FiReCo, 2014), the geometry was approximated from images and generated through *Grasshopper*. Two longitudinal and 9 transversal stiffeners were added according to the drawing shown in Figure 5.31.

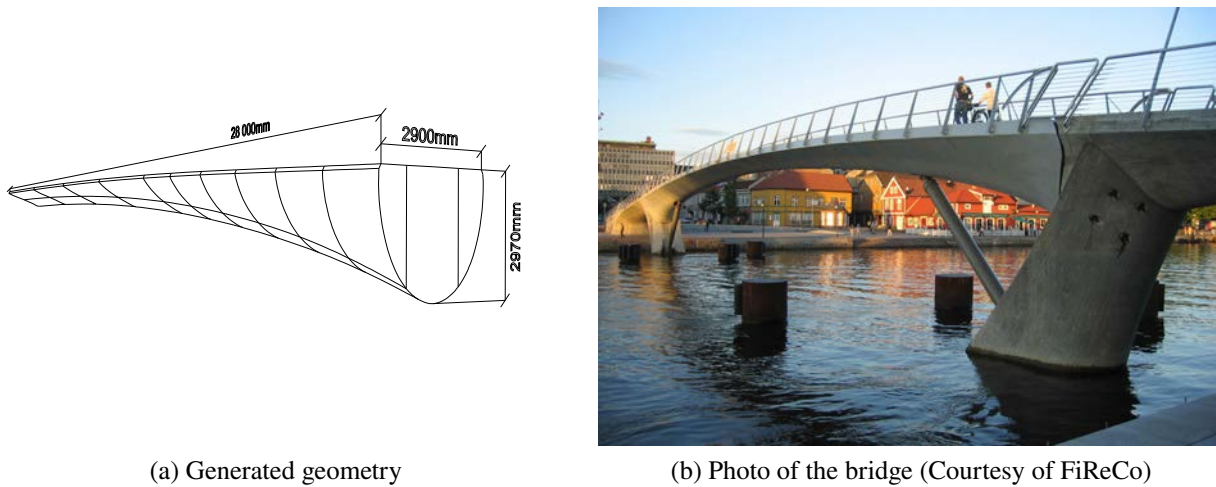


Figure 5.30: Bridge geometry.

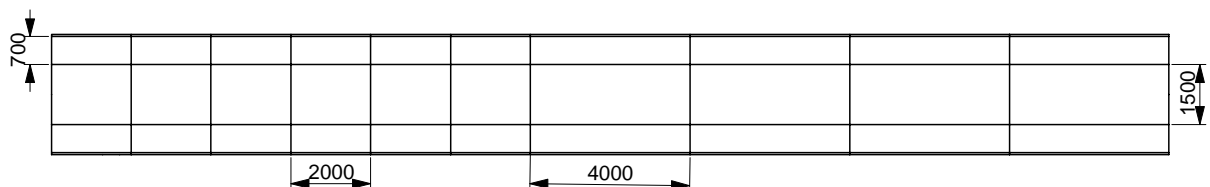


Figure 5.31: Stiffener layout, plan.

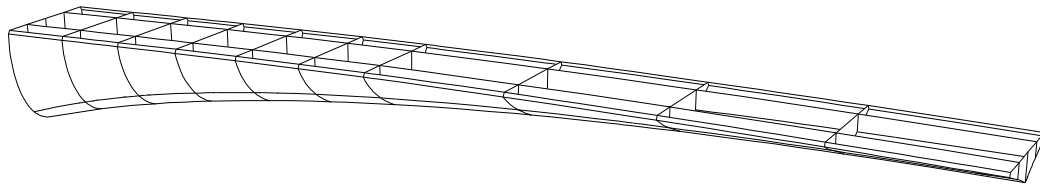


Figure 5.32: Stiffener layout, perspective.

As seen in Figure 5.33, the section changes from pointy and shallow to rounded and deep along the span. This was replicated in the model and section drawings can be seen in Figure 5.34.



Figure 5.33: Bridge geometry.

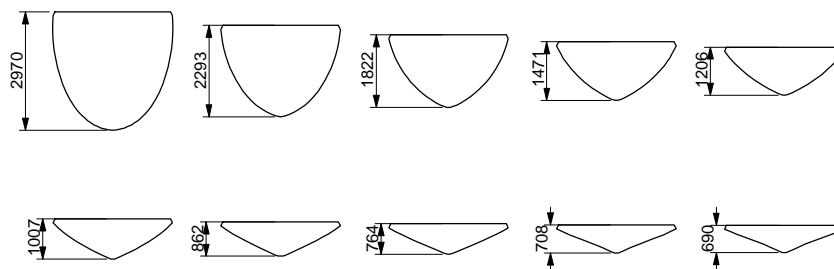


Figure 5.34: Generated sections.

Boundary Conditions

Because of its symmetry, only half of the bridge needed to be modelled. There is no interaction between the two segments apart from a shear transfer mechanism. However, since a symmetric load case is assumed to be governing, this connection was modelled as a free end. The other end was modelled as fixed as seen in Figure 5.35. In reality, the bridge is supported on diagonal pistons in the open configuration, which requires some steel detailing in order to transfer the forces to the FRP shell. This was however ignored in our analysis due to the complexity and the fact that the piston can be assumed to be unloaded during closed operation.



Figure 5.35: Boundary conditions.

Loads

Similar to Kaponjärbron, the bridge is loaded with a distributed load from pedestrians on the bridge deck. The pedestrian characteristic distributed load q_{fk} can be calculated from EN-1991-2:2003 (2003) Section 4.3.5, which gives:

$$q_{fk} = 5 \text{ kN/m}^2$$

The pedestrian load is taken into regards as a leading frequent load in this case. When analysing in serviceability limit state the variable actions Q_d from Table A2.6 in EN-1991-2:2003 (2003) gives:

$$Q_d = \psi_{1,1} q_{fk}$$

where $\psi_{1,1} = 0.4$ from Table 2.6 in EN-1990:2002/A1 (2002). The total variable load in this case would then be:

$$Q_d = 2 \text{ kN/m}^2$$

Q_d is applied on the entire bridge deck.

Mesh

The mesh was generated using *Karamba's* meshing component *Mesh Breps*, where settings for approximate element side lengths are available. A number of meshes with different side lengths were analysed to perform a convergence study. The results can be seen in Figure 5.36. For further analysis, a mesh with an element side length of 0.1 m was chosen, which corresponds to about 75000 elements, well beyond the limit of convergence at about 30000 elements.

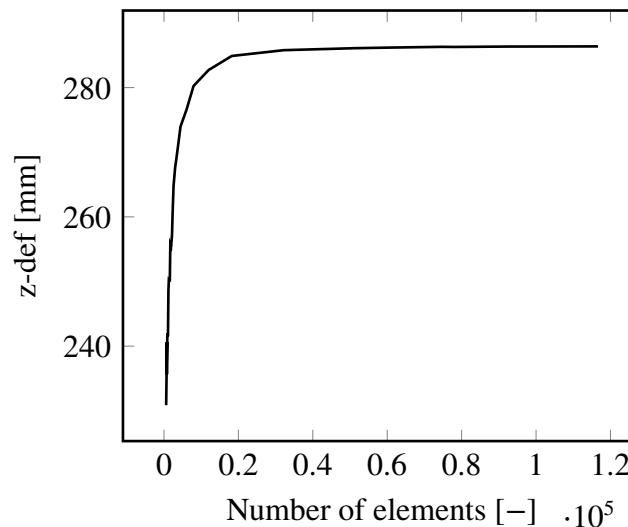


Figure 5.36: Convergence, deflection with different number of elements in mesh



Figure 5.37: Mesh used for analysis.

Model Verification

Since only *Karamba* was available for analysis, model verification had to be done with an isotropic material. See Table 5.26 for the steel material properties used in model verification. In terms of loads, only self weight was considered.

Table 5.26: Material properties for verification model

Property	Value
Young's modulus [GPa]	210
Shear modulus [GPa]	79.3
Poisson's Ratio [-]	0.3
Thickness [mm]	10
Density [kg/m ³]	7800

The results of the verification analysis can be seen in Table 5.27. The deviation of 0.68% and 0.94% in deflection and first eigenfrequency respectively, can be seen as very small and acceptable. Further, the deformation plots seen in Figure 5.38 show the same pattern, and the model can therefore be considered verified.

Table 5.27: Verification results comparison

Property	Karamba	Tortoise	Deviation
z-def	68.93 mm	68.88 mm	-0.68%
First freq	2.445 Hz	2.422 Hz	-0.94%



Figure 5.38: Deflection plots from verification analysis, scaled by 50.

5.2.2 Demands

As stated in the limitations of this thesis, only SLS demands are investigated. The allowed vertical deflection when loaded by variable loads is limited to:

$$L/400$$

where:

L = Theoretical span length in meter

according to B.3.4.2.2 TRVK-Bro-11 (2011) and EN-1991-2:2003 (2003). In this case the allowed deformation is 140 mm for the main span.

Demands concerning natural vibrations are somewhat ambiguous. Different codes state different demands, and therefore the demands set for Kaponjärbron are deemed reasonable for this bridge as well:

$$\begin{aligned} f_{1,vert} &\geq 3.5 \text{ Hz} \\ f_{1,horvid} &\geq 1.75 \text{ Hz} \end{aligned}$$

where:

$$\begin{aligned} f_{1,vert} &= \text{First vertical frequency.} \\ f_{1,horvid} &= \text{First horizontal frequency.} \end{aligned}$$

5.2.3 Analysis

Initial analysis

The model was initially analysed with an assumed carbon fibre layout seen in Figure 5.39. As stated in the limited information available online, the carbon fibre parts are located in the bottom flange of the bridge, with thickness ranging from 10 mm to 38 mm. It is not specified what the distribution of thickness is, but a rational guess would be to have the thickest parts close to the support due to moment distribution.

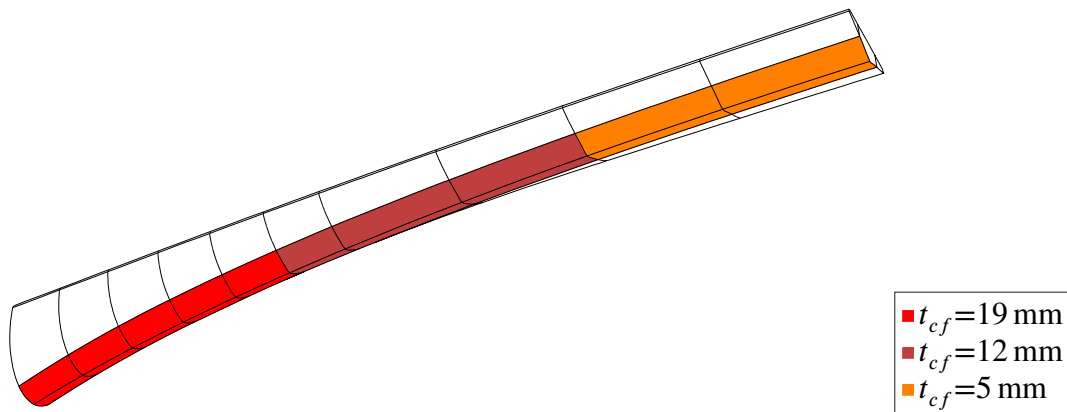


Figure 5.39: Carbon fibre arrangement.

Results from the initial analysis can be seen in Table 5.28. Plots of the stress and deflection can be seen in Figure 5.41, Figure 5.42 and Figure 5.43. As seen in Figure 5.40, the first eigenmode, as expected, corresponds to vertical deflection from loads. The frequency is slightly lower than the limit of $\geq 3.5 \text{ Hz}$.

Table 5.28: Original model compared with demands

Property	Original	Demands
z-def	134.7 mm	$\leq \frac{L}{400} = 140 \text{ mm}$
First freq	3.34 Hz	$\geq 3.5 \text{ Hz}$

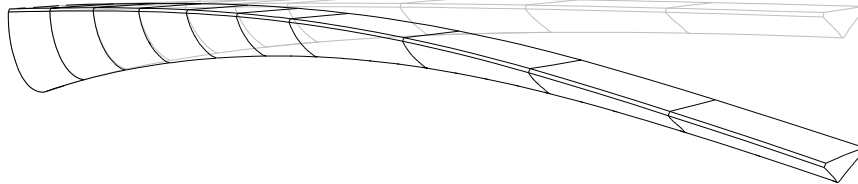


Figure 5.40: First mode shape.

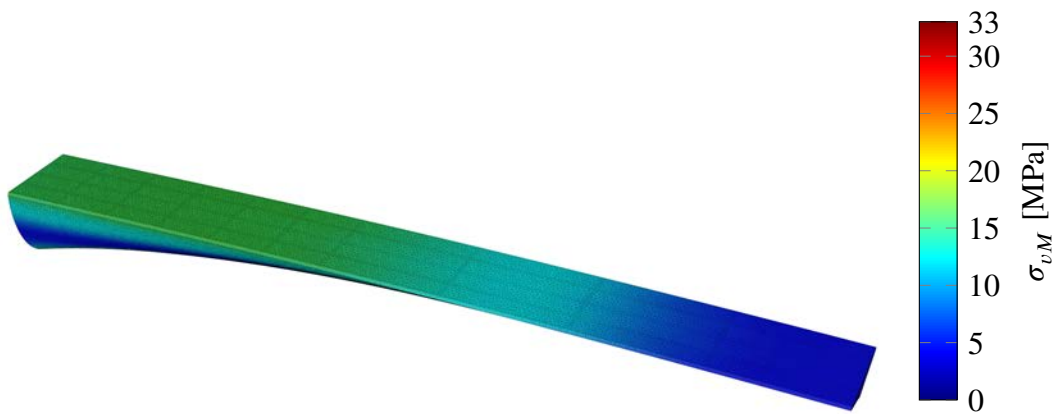


Figure 5.41: von Mises stress, top view.

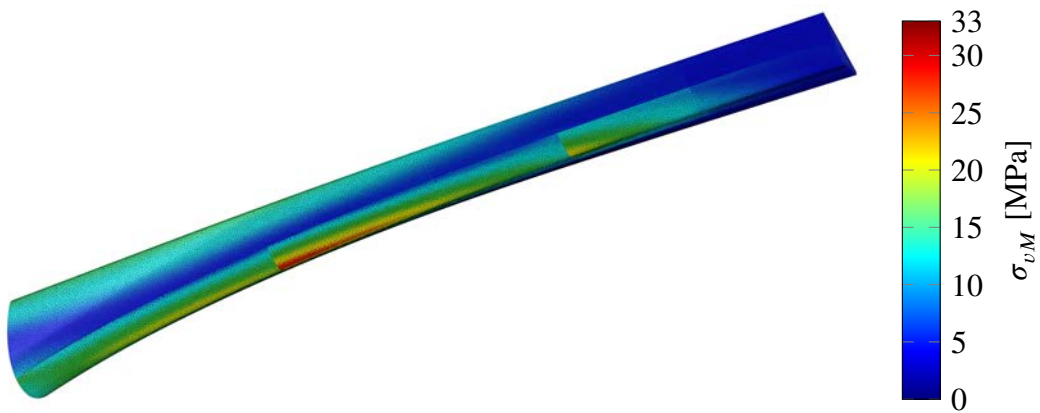


Figure 5.42: von Mises stress, bottom view.



Figure 5.43: Deflection, side view.

5.2.4 Optimisation

Optimisation was made on carbon fibre placement and geometry. The fibre alignment optimisation, performed on Kaponjärbron, was assumed to have very low impact on this bridge since the principal stress directions generally coincides with the longitudinal direction of the bridge, and was subsequently disregarded.

Carbon fibre placement

The assumptions made on the original design indicate that the bridge contains roughly 1928 kg of CFRP. While the design seems rational and the shape is rather simple, it may not be the optimal design. Similar to Kaponjärbron, the bascule bridge in Fredrikstad was optimised with regards to carbon fibre placement, with the difference being that this bridge has three different thicknesses of laminae. The optimisation was done by running a reference analysis with the main GFRP material described in Table 5.24 applied to all elements (seen in Figure 5.44), whereby the elements were ordered with respect to von Mises stress. *Galapagos* was then allowed to assign the CFRP laminate described in Table 5.25 to the most stressed elements, choosing freely between the three predefined carbon fibre lamina thicknesses of $t_{cf} = 5$ mm, $t_{cf} = 12$ mm, and $t_{cf} = 19$ mm with the restriction that the total CFRP mass remained at 1928 kg.

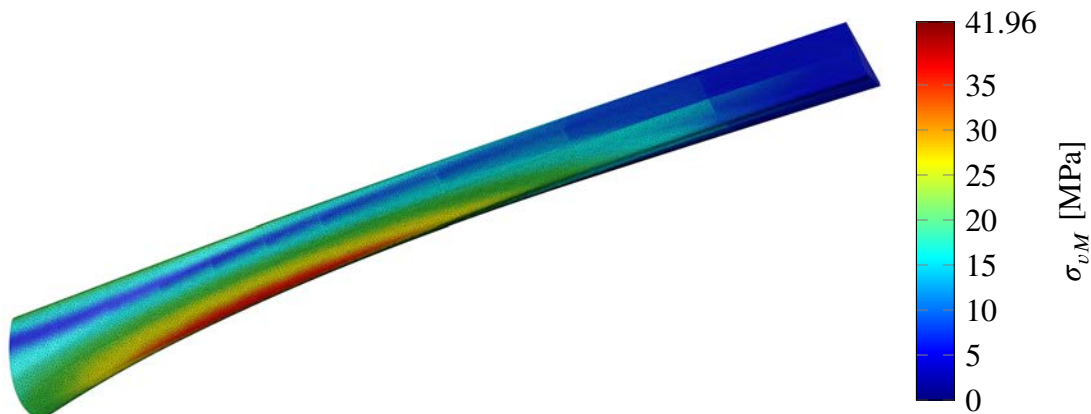


Figure 5.44: Reference model, von Mises stresses, bottom view.

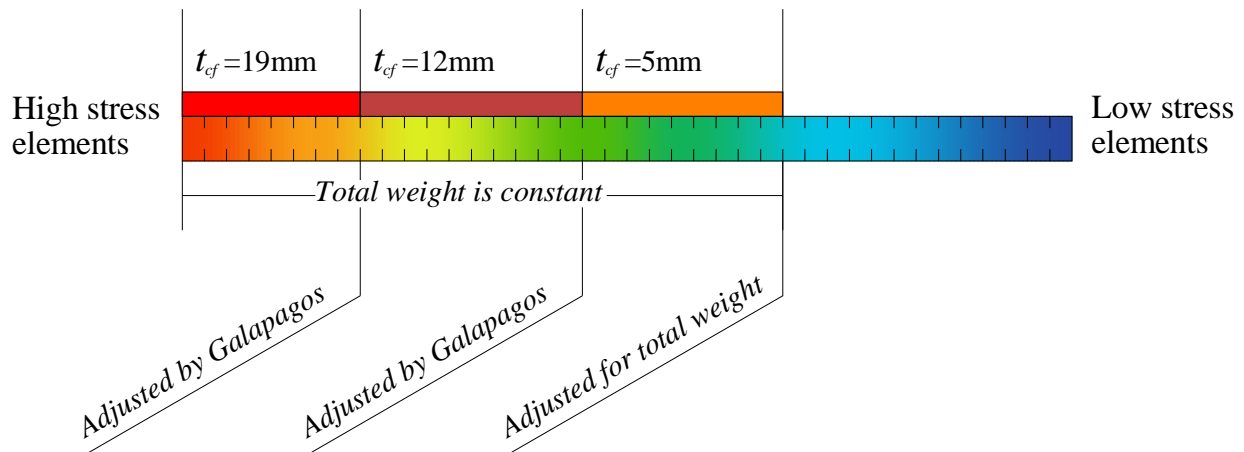


Figure 5.45: Optimisation schematic.

Results from the optimisation can be seen in Figure 5.46, where the optimal solution is marked with a red dot. With roughly 1144 kg of $t_{cf} = 5$ mm, 588 kg of $t_{cf} = 12$ mm, and 196 kg of $t_{cf} = 19$ mm, a deflection of 112.7 mm is achieved. Rather surprising is the distribution, where for example a composition of only $t_{cf} = 19$ mm results in 150 mm deflection.

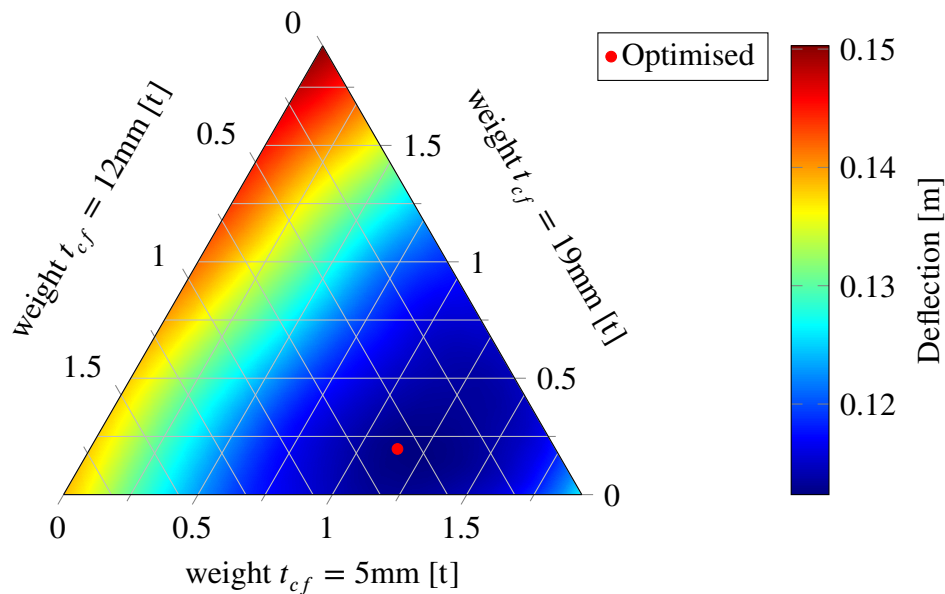


Figure 5.46: Deflection for different compositions of carbon fibre thickness.

The optimised carbon fibre layout can be seen in Figure 5.47 and Figure 5.48. Unlike the original design, the optimised layout has carbon fibre placed in the top flange, and does not concentrate the thickest parts furthest to the support.

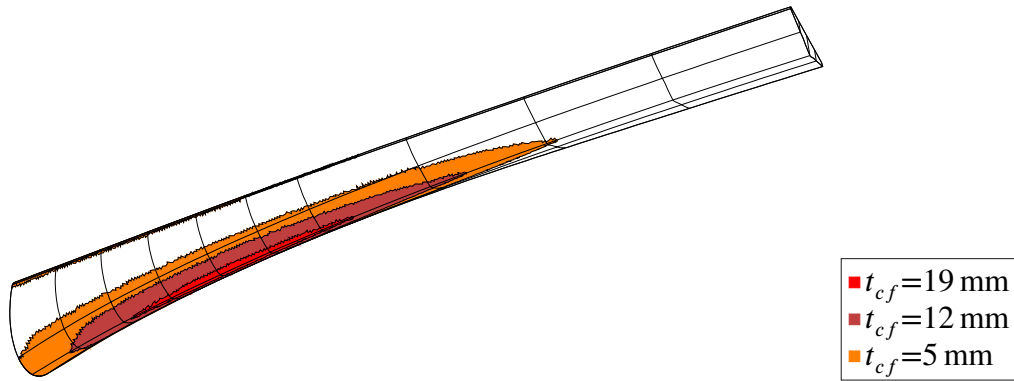


Figure 5.47: Optimised carbon fibre arrangement, bottom view.

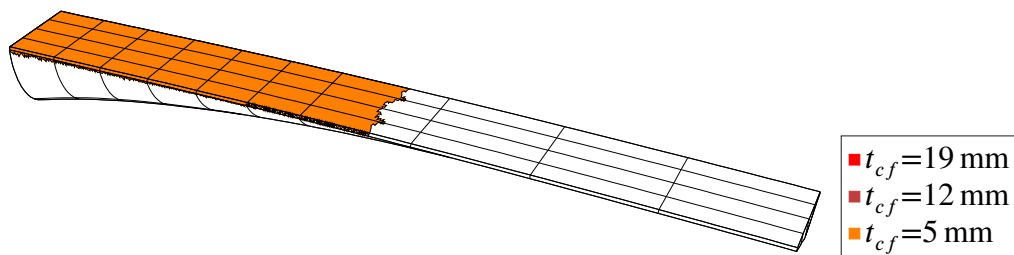


Figure 5.48: Optimised carbon fibre arrangement, top view.

Based on the optimised results, a rationalised layout was created, which can be seen in Figure 5.49 and Figure 5.50. This was done to show the results of something that could realistically be built.

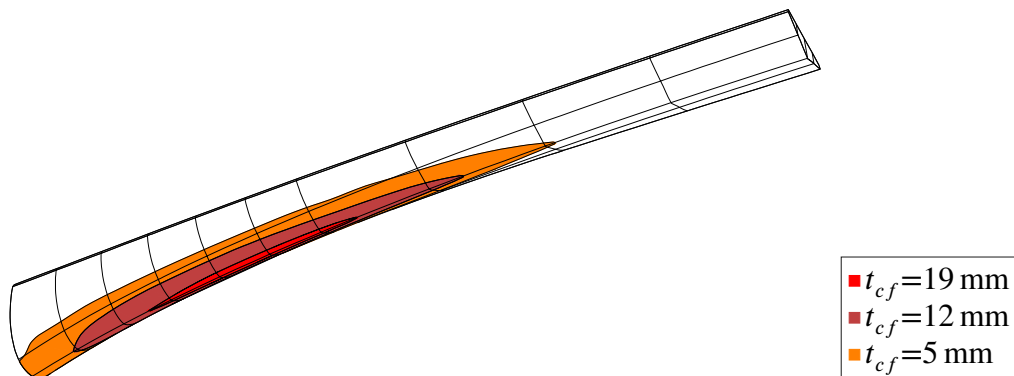


Figure 5.49: Rationalised carbon fibre arrangement, bottom view.

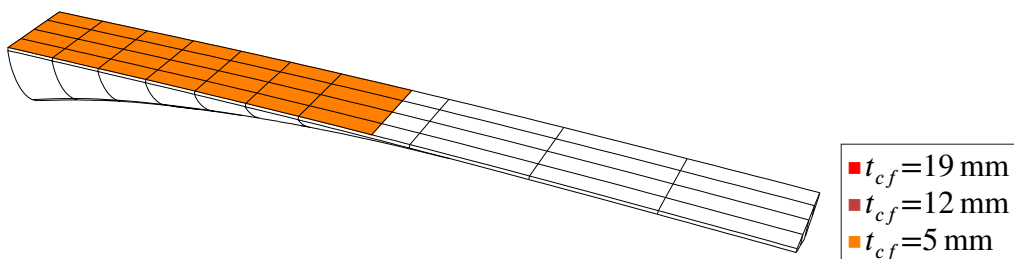


Figure 5.50: Rationalised carbon fibre arrangement, top view.

A summary of results can be seen in Table 5.29. It is clear that rather large gains can be achieved by carefully placing carbon fibre. As expected, the rationalised version does not perform as well as the optimised one, however it uses less CFRP making it less expensive.

Table 5.29: Results comparison

Property	Original design	Optimised	Optimised-rationalised	Improvement*
z-def	134.7 mm	112.7 mm	113.8 mm	-15.5%
First freq	3.34 Hz	3.72 Hz	3.69 Hz	+10.6%
CFRP weight	1928 kg	1928 kg	1736 kg	-9.96%

*Based on the fraction (optimised-rationalised) / (original design)

Geometry optimisation

The beam section height of the bridge roughly corresponds to a moment diagram of a uniformly loaded cantilever beam, namely a quadratic curve, however perhaps not the perfect shape. A geometrical optimisation was run through *Galapagos* to see if it was possible to find a more optimal shape.

The moment equation for a uniformly loaded cantilever beam can be seen in Equation (5.1)

$$M_y = q\frac{x^2}{2} - qLx + q\frac{L^2}{2} \quad (5.1)$$

where q is the uniformly distributed load and L is the length of the bridge. This was simplified to Equation (5.2)

$$h = a(\frac{x^2}{2} - x + \frac{1}{2}) + b \quad (5.2)$$

where h is the height of the section, and a and b are numbers controlled by *Galapagos*, and x is the position along the span. This equation was run through *Galapagos* to minimise the deflection by creating a more suitable shape, while still keeping the total element area smaller or equal to the original design.

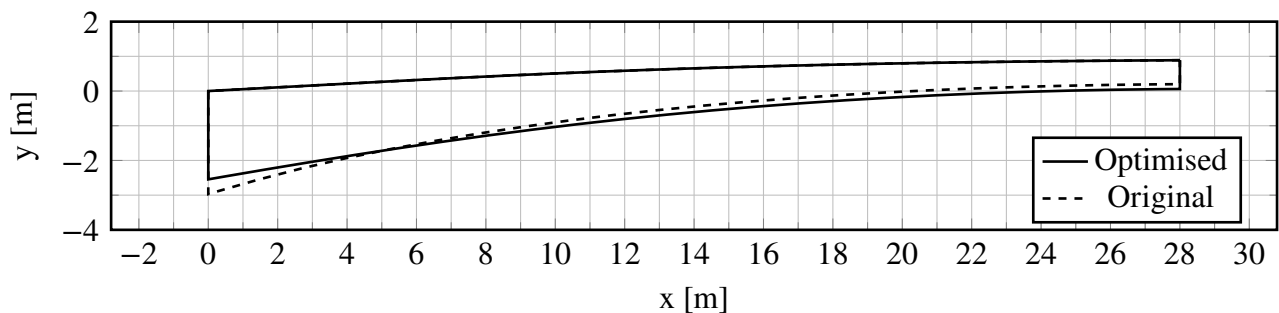


Figure 5.51: Section comparison.

As seen in Figure 5.51, the optimised shape has its section height gravitated more to the right side, giving it more of a beam-like shape. Results from the analysis can be seen in Table 5.30.

Table 5.30: Results comparison, geometry optimisation

Property	Original	Optimised	Improvement
z-def	134.6 mm	121.0 mm	-10.2%
First freq	2.42 Hz	2.52 Hz	+4.2%
CFRP area	244.9 m ²	243.16 m ²	-0.7%

5.2.5 Comments

There are some substantial gains to be made on this bridge in terms of geometry and CFRP placement. However, the comparison is not completely fair since we do not have all the necessary data. The distribution of CFRP thicknesses on the original design for instance, may be something completely different and more efficient in reality. Furthermore, the shape, which was approximated from images may in reality in fact be closer to the optimised shape than the shape the was modelled in the first case. Specific demands on for free passable height underneath the bridge could also influence the geometry.

However, the purpose of this case study was not to improve the design of this bridge, but rather show the strengths of parametric modelling in early stage FRP bridge design.

5.3 Arkitektbron

Arkitektbron is a proposal for a new pedestrian bridge, in the Haga area of Gothenburg. The bridge has a horse shoe shape with an outer radius of 24 m. The entire bridge is in FRP, a combination of both glass fibres and carbon fibres. Much like Kaponjärbron, FRP was chosen to minimise loads on the canal walls since they are weak and vulnerable.



Figure 5.52: Rendered image of Arkitektbron. Courtesy of Erik Andersson architects.

5.3.1 Modelling

Materials

As in the the previous case studies, the materials used in this study are E-Glass fibres/Epoxy, Carbon fibres/Epoxy and foam. Properties of said materials can be seen in Table 5.31.

Table 5.31: Material properties (Agarwal, Broutman, & Chandrashekhara, 2015)

Property	E-Glass/Epoxy	Carbon/Epoxy	Foam
E_L [GPa]	38.6	138.0	0.0
E_T [GPa]	8.27	8.96	0.0
G_{LT} [GPa]	4.14	7.1	0.0
ν [-]	0.26	0.3	0.5
ρ [kg/m ³]	1800	1600	0.0

The main ply arrangement for each laminate in the first analysis can be seen in Table 5.32, and is based on the master thesis by Chiv and Vocal (2014). It is similar to that of Kaponjärbron.

Table 5.32: GFRP laminate configuration.

Laminate*		
0°	G/Ep	10 mm
45°	G/Ep	0.25 mm
-45°	G/Ep	0.25 mm
90°	G/Ep	0.25 mm
0°	Foam	30 mm
90°	G/Ep	0.25 mm
-45°	G/Ep	0.25 mm
45°	G/Ep	0.25 mm
0°	G/Ep	10 mm

* G=Glass fibres, Ep=Epoxy

The configuration of hybrid laminates, carbon fibres and glass fibres, is similar to that of Kaponjärbron and the bascule bridge in Fredrikstad and can be seen in Table 5.33. The thicknesses used in this model was the same as used by the engineers that had been working on this project.

Table 5.33: Hybrid laminate configuration.

Laminate*		
0°	C/Ep	15 mm
45°	G/Ep	0.25 mm
-45°	G/Ep	0.25 mm
90°	G/Ep	0.25 mm
0°	Foam	30 mm
90°	G/Ep	0.25 mm
-45°	G/Ep	0.25 mm
45°	G/Ep	0.25 mm
0°	C/Ep	15 mm

* C=Carbon fibre, G=Glass fibre, Ep=Epoxy

Geometry

The geometry used in these analyses was made based on a simplified structural model used by Olsson and Nilsson (2015) and sections and rendered images from the architect Erik Andersson. Information on the transverse stiffeners was lacking and an assumption of transverse stiffeners every fifth meter was made. There is one longitudinal stiffener along the entire bridge centre line. The bridge deck has an inclination of 1:20 while the height of the shell structure is increased towards each side of the canal. Figure 5.54 shows the geometry used in the analysis.

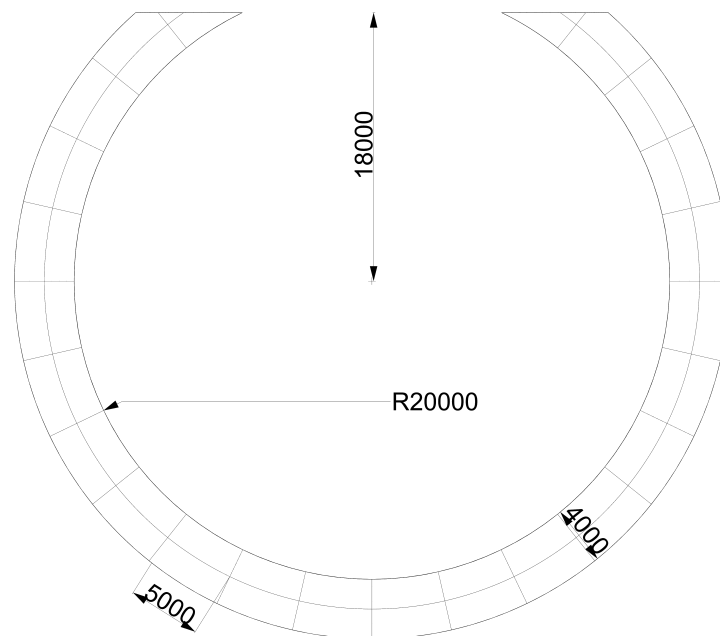


Figure 5.53: Plan view of Arkitektbron and its dimensions.

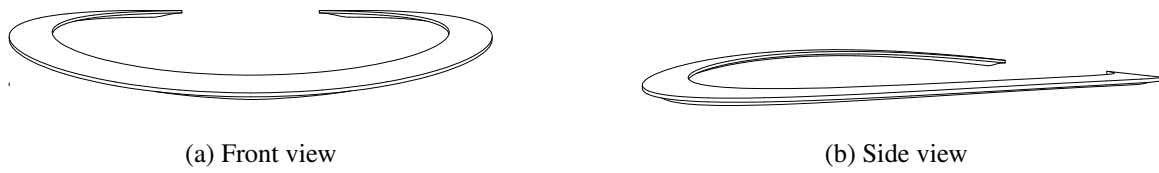


Figure 5.54: Geometry used in the analysis.

Figure 5.55 shows how the sections are changing along the bridge deck.



Figure 5.55: Sections of Arkitektbron.

Boundary conditions

Figure 5.56 shows the boundary conditions of the bridge. The bridge is fixed in all points on the edge surfaces A and B. On the other side the bridge is simply supported, resting on a line support at C.

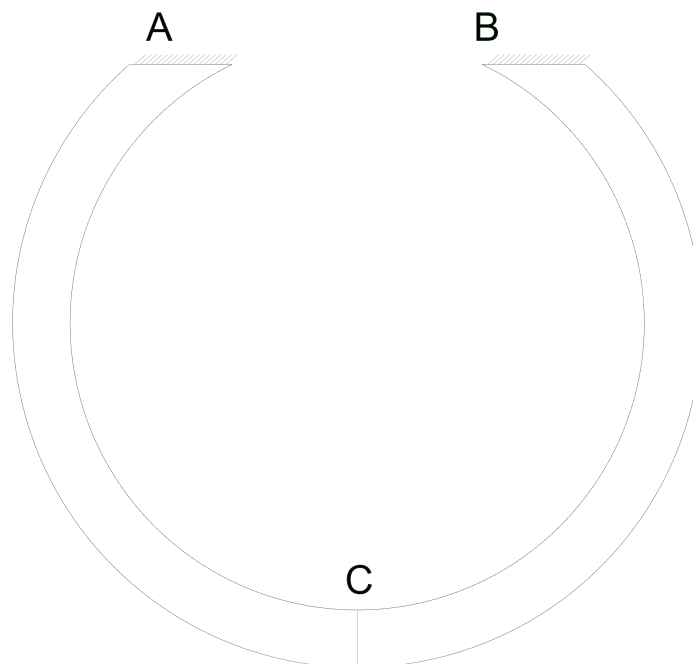


Figure 5.56: Boundary Conditions.

Loads

Similar to the previous case studies, the bridge is loaded with a distributed load Q_d from pedestrians on the bridge deck, where:

$$Q_d = 2 \text{ kN/m}^2 \quad (5.3)$$

The load case that is generating the largest vertical deformations is when Q_d is applied on one side of the bridge deck, for example between supports B and C. For the optimisation, that load can be applied on either of the halves of the bridge, and therefore the optimisation analyses were done with the load Q_d applied on both sides. The self weight of the bridge is not included in the analysis, since the deformation from this load is handled by initially raising the bridge the same amount.

Mesh

The mesh was generated using *Karamba's* meshing component *Mesh Breps*, as the previous two case studies. A number of meshes with different side lengths were analysed to perform a convergence study. The results can be seen in Figure 5.57. For further analysis, a mesh with an element side length of 0.17 m was chosen, which corresponds to about 90000 elements.

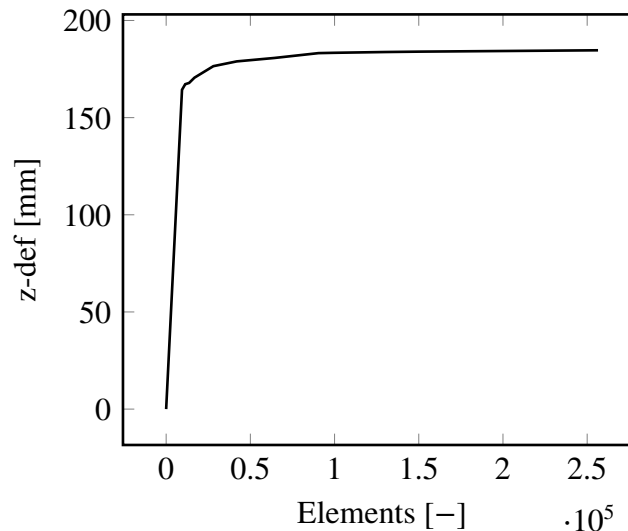


Figure 5.57: Convergence study, deformation with different size of the mesh.

Model Verification

The analysed model was as the previous two case studies compared with *Karamba*. Again, a steel material was used, with a section thickness of 30 mm and with the steel properties in Table 5.34. In terms of loads, only self weight was considered for the verification.

Table 5.34: Steel properties for verification model

Property	Value
Young's modulus [GPa]	210
Shear modulus [GPa]	79.3
Poisson's Ratio [-]	0.3
Thickness [mm]	30
Density [kg/m ³]	7800

The results of the verification analysis can be seen in Table 5.35.

Table 5.35: Results comparison of verification analysis

Property	Karamba	Tortoise	Deviation
z-def	144.7 mm	145.5 mm	0.56%
First freq	0.784 Hz	0.780 Hz	0.46%

The deviations of the deflection and the first eigenfrequency are both very small, less than 1%, and should be considered acceptable. Further, the deformation plots seen in Figure 5.58 show the same pattern, and the model with an isotropic material can therefore be considered verified.



Figure 5.58: Front view deformation plot.

5.3.2 Demands

As stated in the limitations of this thesis, only SLS demands are investigated. The allowed vertical deflection when loaded by variable loads is limited to:

$$L/400$$

where:

$$L = \text{Theoretical span length in meter}$$

according to B.3.4.2.2 TRVK-Bro-11 (2011) and EN-1991-2:2003 (2003). In this case the allowed deformation is 139 mm for the main span, where L is measured as the length of half of the bridge deck.

Demands concerning natural vibrations are somewhat ambiguous. Different codes state different demands, and therefore the demands set for Kaponjärbron are deemed reasonable for this bridge as well:

$$\begin{aligned} f_{1.vert} &\geq 3.5 \text{ Hz} \\ f_{1.horvrid} &\geq 1.75 \text{ Hz} \end{aligned}$$

where:

$$\begin{aligned} f_{1.vert} &= \text{First vertical frequency.} \\ f_{1.horvrid} &= \text{First horizontal frequency.} \end{aligned}$$

5.3.3 Analysis

Initial analysis

The model was based on the technical report by Olsson and Nilsson (2015) and talking to the engineers who had worked on this project. It was modelled to be as similar to the model in the report as possible. There were still some differences in both geometry and how materials were treated to that of the Olsson and Nilsson (2015) model. It is not fair to compare the models since the model by Olsson and Nilsson (2015) is heavily simplified.

All the vertical parts of the bridge, the side shells and stiffeners, are modelled as glass fibre laminates with the lay up from Table 5.32. The rest of the bridge, the bottom shell and the bridge deck are modelled as carbon fibre parts, with the laminate lay up from Table 5.33. Figure 5.59 shows a the carbon fibre on the bottom shell of the bridge. The bridge deck is also made of carbon fibre.

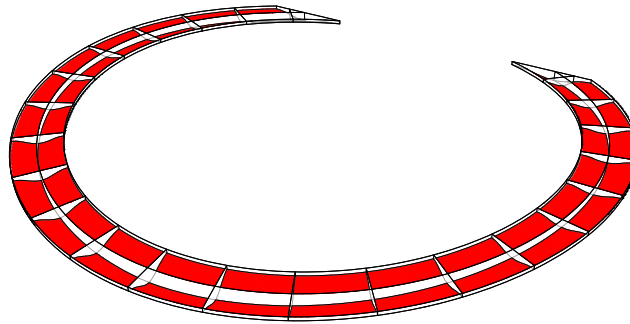


Figure 5.59: Bottom shell carbon fibre arrangement in red.

Results from the initial analysis can be seen in Table 5.36.

Table 5.36: Results from first analysis compared with demands

	Original	Demands	Utilisation
z-def [mm]	461	139*	332%
First freq [Hz]	0.48	3.5	729 %

*The distance $\frac{L}{400}$ is based on the length of the bridge deck, which is the same as in technical report by Olsson and Nilsson (2015).

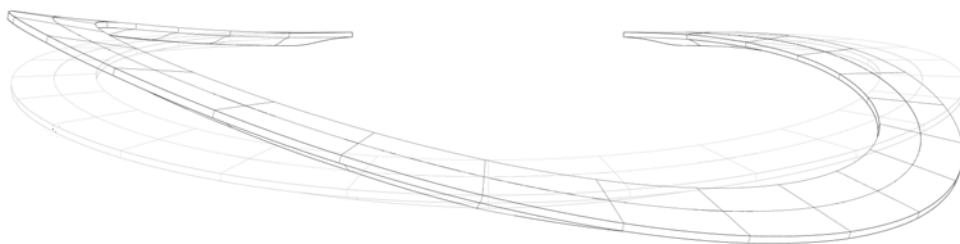


Figure 5.60: First eigenmode.

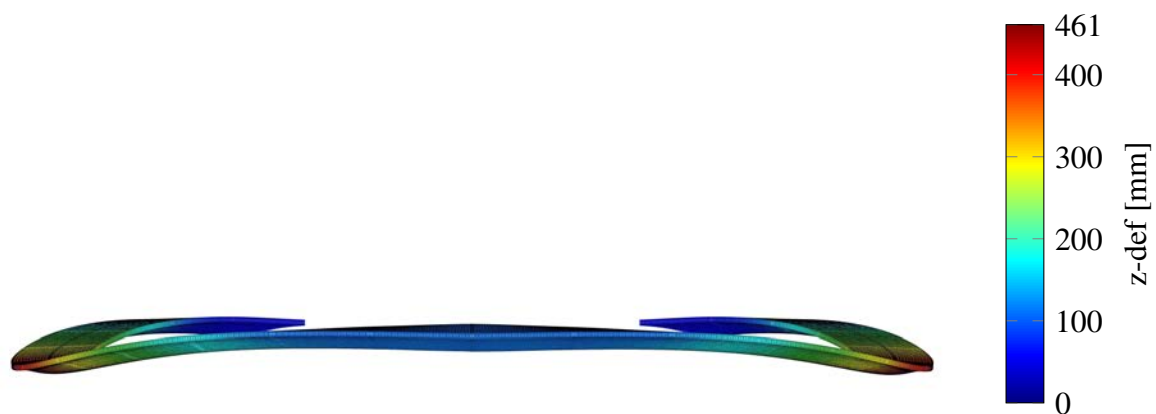


Figure 5.61: Front view deformation plot, scaled by 7.

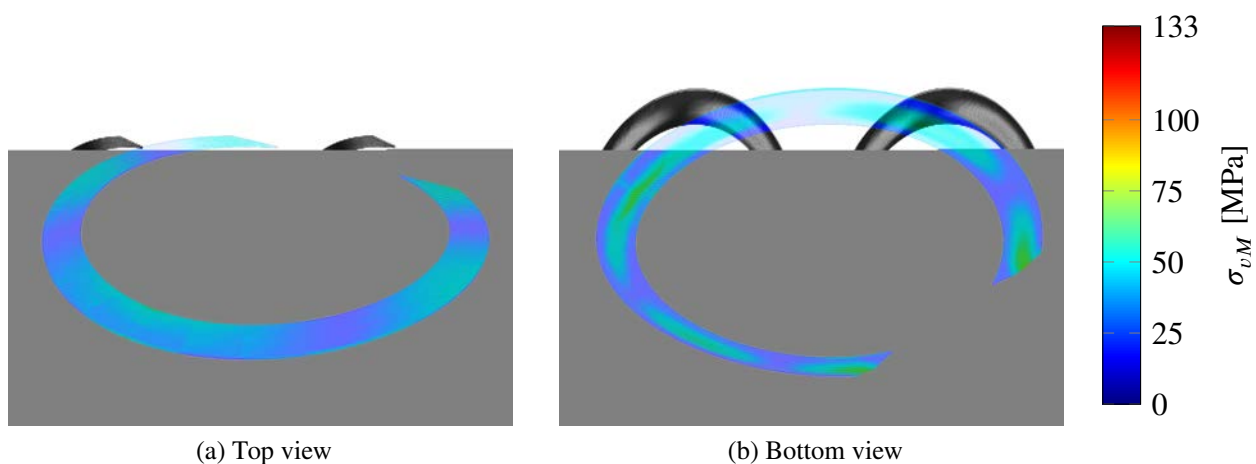


Figure 5.62: von Mises stress plot.

The deformation behaves as expected and symmetrical around the longitudinal mid axis of the bridge. No major local deformations occur. The elements on the bottom shell experience slightly higher stresses, especially around support and in the middle of the span. Elements on the bridge deck also experience stresses in similar magnitude in the same areas.

Both the deformation and vibration requirements are far from being reached. But this model does not give fair results of what the bridge can handle in reality. The fibres are as in previous case studies modelled with the first axis in the longitudinal direction of the bridge. That is definitely not how one would arrange the laminates in this case. A better way to arrange the first material axis will be investigated in the optimisation chapter.

5.3.4 Optimisation

Fibre angle alignment

The standard input in *Tortoise* and many other FE-software is to put the first axis in the x-axis direction. This is a good approximation in many cases, however in *Arkitektbron* it is not, due to the circular geometry of the bridge. The fibres can be arranged in different ways, but from the two other

case studies good results were achieved when the first material axis were similar to the direction of the highest principal stress at each element. Such a study was performed in this case as well and results can be seen in Table 5.37.

Table 5.37: Original model compared with model where elements have the first material axis based on stresses

	Original analysis	New material axis	Difference
z-def [mm]	461	98	-79%
First freq [Hz]	0.66	0.95	+44%

This arrangement of the fibres is of course not realistic, since it would take extremely long time to arrange the fibre direction for every single element. Instead patterns from the principal stresses can be seen as general directions for how the fibres should be arranged. With the component *AlignMaterialAxisWithCurves* some curves were drawn that is more representing how the fibres would be arranged in reality. The curves can be seen in Figure 5.63

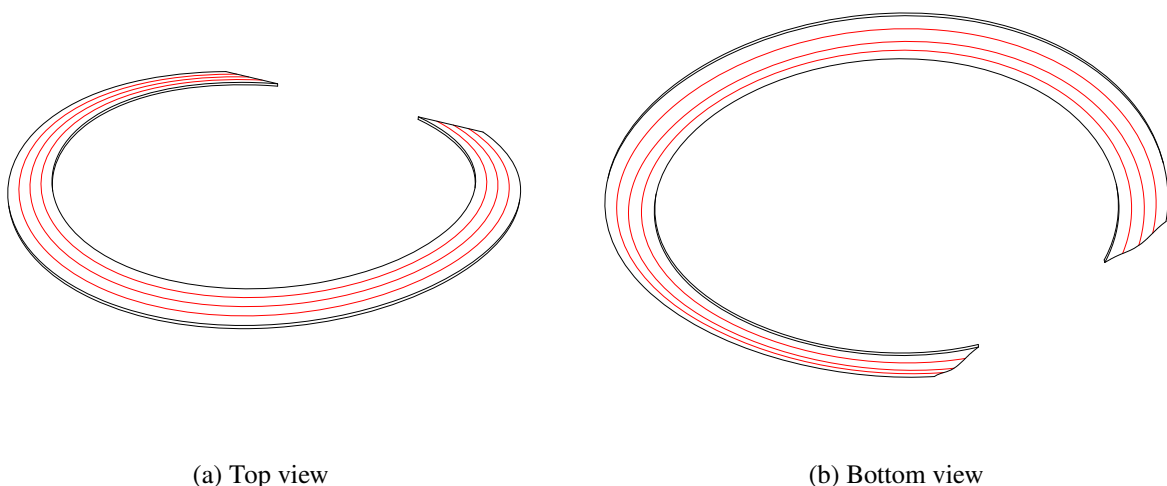


Figure 5.63: Guide curves for the elements fibre direction.

The curves were rather simplified based on the principal stress analysis and could be improved, but this arrangement gave a fibre lay up that would be easy to produce. The results with the new material axis can be seen in Table 5.38.

Table 5.38: Result comparison of original model and models with changed fibre direction based on guide curves

	Original	Aligned to principal stresses	Aligned to guide curves
z-def [mm]	461	98	135
First freq [Hz]	0.48	0.95	1.04

The guide curves drawn in *Grasshopper* gives a decent approximation from the principal stresses, but could still be improved in regards to minimising the deformation. Compared to the original model the deformation has improved 70.7% which shows that the original model is not much of use. The deformation could be improved by adding more guide curves, but this would also contribute to a more complex production. Plots of von Mises stresses can be seen in Figure 5.64.

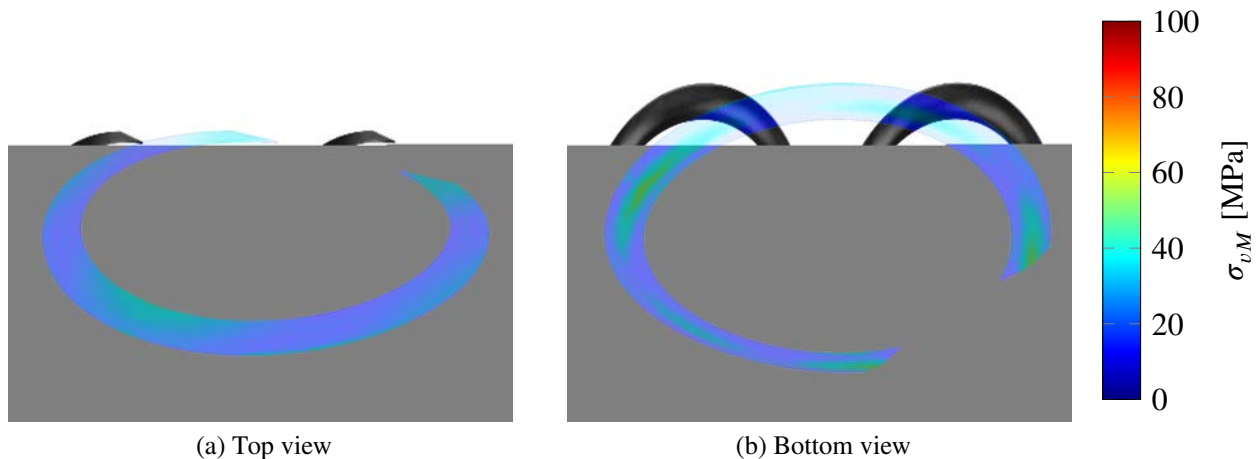


Figure 5.64: von Mises stress plot for model with fibres aligned with guide curves.

The von Mises stresses in the model with arranged fibre direction based on the guide curves have a more evenly stress distribution and the maximum stress of 100 MPa is a bit less than the original 126 MPa. This model is going to be used in the next chapter, since it gives the most realistic results compared to how it would be produced in reality.

Carbon fibre placement

The model has been optimised to minimise the amount of carbon fibre used, by changing the configuration of the carbon fibre. In the original design 43.7 t of carbon fibre was used. In these analyses the configuration of carbon fibre area and carbon fibre thickness of each element was changed to find the best solution, just as in previous case studies. By using *Galapagos* multiple different configurations could be analysed to find the best solution with regard to minimising the deformation. An analysis was made to see where the elements with the highest stresses were located and the carbon fibre were placed on those elements. Different configurations of carbon fibre section thickness versus carbon fibre area were made, all different configurations with the same weight, 43.7 t. Results can be seen in Figure 5.65.

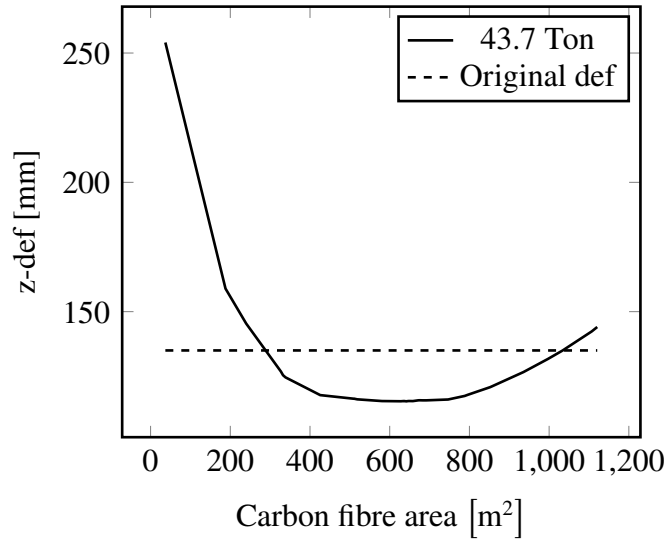


Figure 5.65: Different carbon fibre layups, each configuration has 43.7 t carbon fibres.

Based on the result from Figure 5.65 an optimised model was made, and a comparison with the original design is shown in Table 5.39.

Table 5.39: Result from original model and model with fibres aligned by guide curves

	Original*	Optimised
CFRP area [m ²]	910	642
CFRP thickness [mm]	30	43
CFRP weight [t]	43.7	43.7
z-def [mm]	135	115
First freq [Hz]	1.04	0.90

* With fibre directions based on appropriate guide curves.

The difference between the original and the optimised carbon fibre layout is not as large as in the previous case studies, but there is still a 15% difference between the models. The placement of the 642 m² carbon fibre elements is illustrated in Figure 5.66.

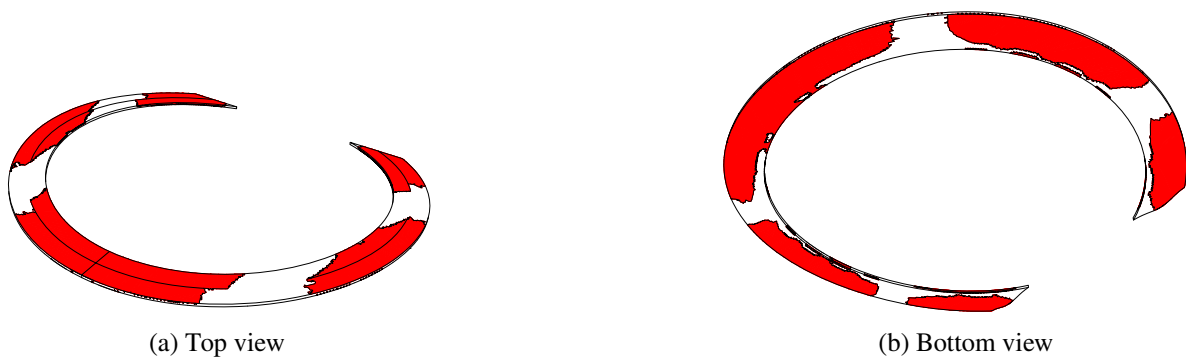


Figure 5.66: Carbon fibre arrangement based on elements with highest stresses.

Stress plots with this carbon fibre arrangement can be seen in Figure 5.67.

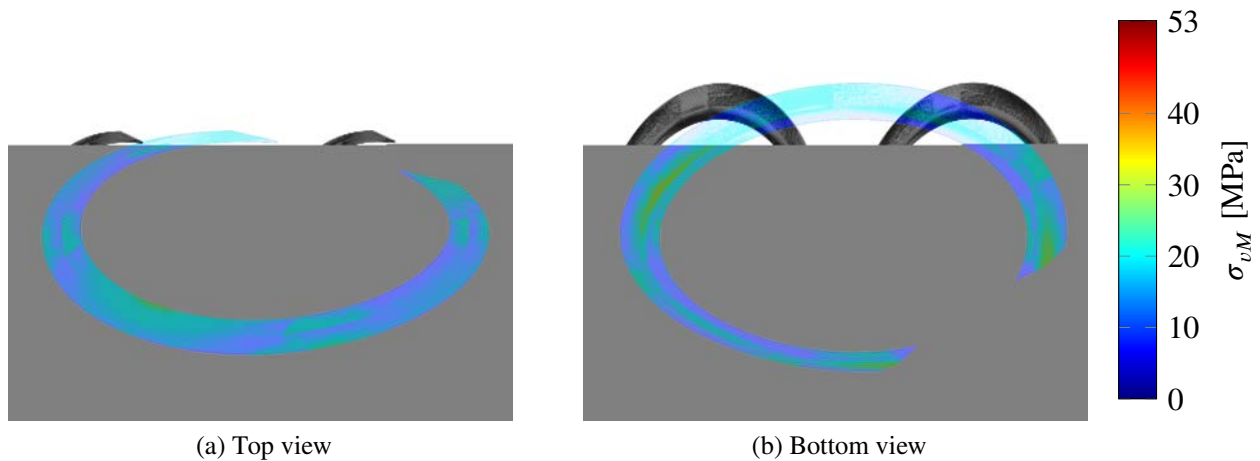


Figure 5.67: von Mises stress plot.

This arrangement is quite difficult to achieve and would need to be simplified before production. Figure 5.68 shows how the elements in Figure 5.66 could be simplified.

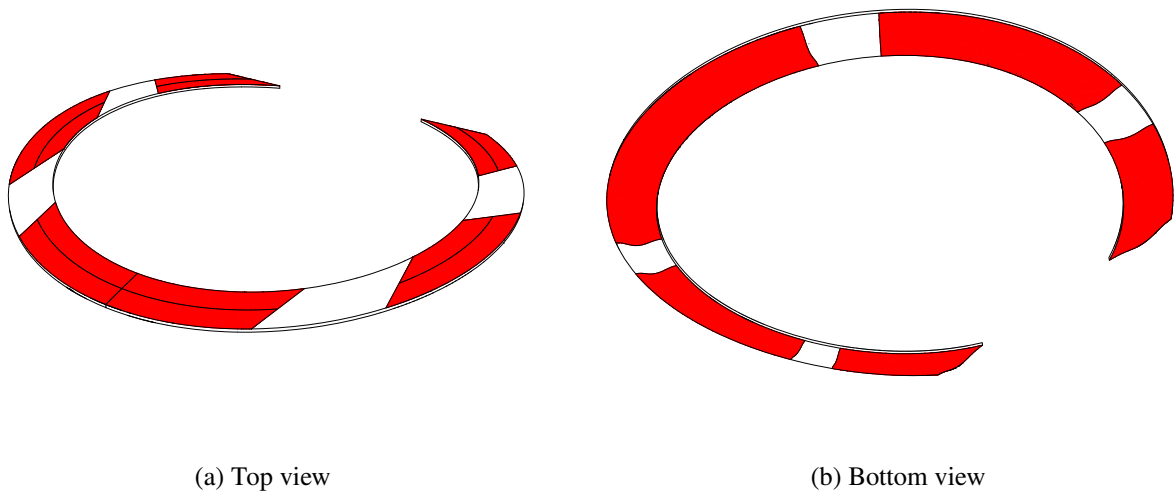


Figure 5.68: Refined carbon fibre arrangement.

Based on the unrefined configuration the amount of carbon fibre could be reduced and still achieve the same deformation as the original. Table 5.40 shows the result from the the reduced carbon fibre amount and the original design.

Table 5.40: Result comparison of original model and optimised unrefined model

	Original*	Optimised**	Difference
CFRP area [m ²]	910	642	-
CFRP thickness [mm]	30.0	34.6	-
CFRP weight [t]	43.7	35.5	-8.2 t
GFRP weight [t]	7.6	29.8	+22.2 t
z-def [mm]	135	134	-0.8%
First freq [Hz]	1.04	0.90	-13.4%

* With fibre directions from drawn curves.

**Unrefined version, see Figure 5.66.

By rearranging the carbon fibre, it can be reduced by 8.2 t. Table 5.39 shows that more glass fibre is needed, but since carbon fibre is roughly 8 times more expensive it is most likely economically worth saving 8.2 t of carbon fibre even though adding 22.2 t of glass fibre. These numbers are based on the unrefined version, and slightly more carbon fibre could be expected to be used for the refined model. The savings are not as substantial as in the case study of for example Kaponjärbron. There could also be other reasons that make it more economical to use only one material instead of using both carbon fibre and glass fibre, for example simplified production.

The dominant load case is not when the bridge is fully loaded, but instead loaded on only one side. Therefore two analyses were made with the bridge loaded on only one half, one with the original and one with the optimised design. Table 5.41 shows the results.

Table 5.41: Results from the bridge loaded on half side with reduced carbon fibre amount.

	Original*	Optimised	Difference
CFRP weight [t]	43.7	35.5	-8.2 t
z-def [mm]	351.6	444.4	+26%
First freq [Hz]	1.04	0.90	-13%

* With fibre direction based on appropriate curve guide.

There is a drastic deformation increase with the optimised configuration. To see if this configuration is useful at all for this load case an analysis were made with same carbon amount as the original model, 43.7 t. Table 5.42 shows the result from this analysis.

Table 5.42: Results from the bridge loaded on half side with same carbon fibre amount.

	Original*	Optimised	Difference
CFRP weight [t]	43.7	43.7	0 t
z-def [mm]	351.6	395.9	12.5%
First freq [Hz]	1.04	0.90	-13%

* With fibre direction based on appropriate guide curves.

It seems that this carbon fibre optimisation used for the load case where the entire bridge is loaded is not useful for the load case where only half the bridge is loaded. An optimisation analysis would need to be done for this load case as well and then mirrored to the other side. Since the carbon fibre optimisation based on the entire deck loaded did not give much improvement, it is uncertain if any improvements would be made if all the load cases were combined.

5.3.5 Comments

In this case study it was crucial to be able to align the material axis as wanted. The model with the first fibre axis in longitudinal bridge direction is basically useless. Based on the material axis curves drawn in this model there is still potential to make them more accurate according to the principal stresses direction and up to 37 mm could be gained, but again it would make the fibre lay up more complex.

The carbon fibre optimisation did not work out well for this bridge. The bridge experienced the highest stresses at different parts when loaded with the different load cases. The largest principal stresses is based on an isotropic material, and Figure 5.69 shows two stress plots from analyses with steel material, one with fully loaded bridge deck and one with the bridge deck loaded on one half.

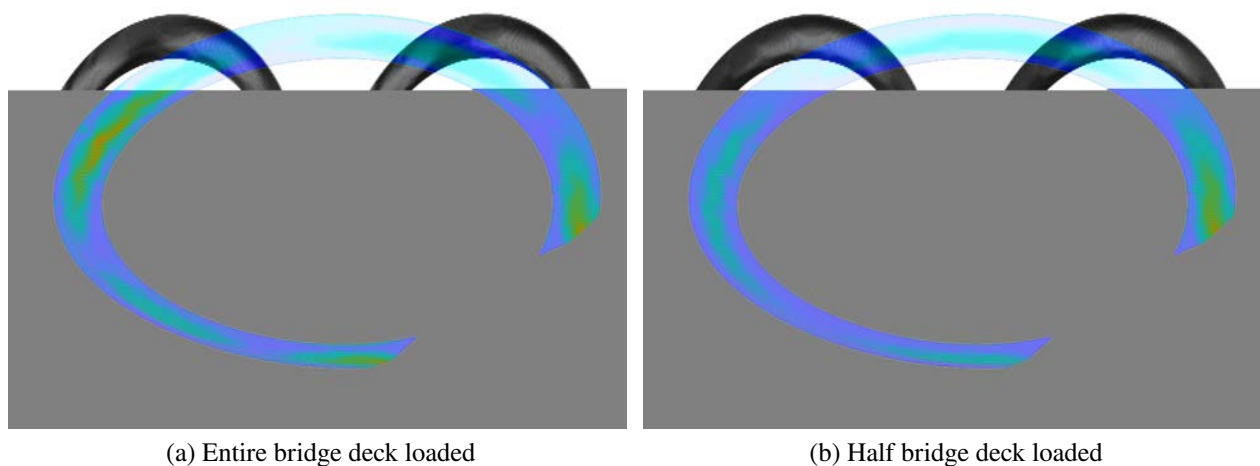


Figure 5.69: von Mises stress analysis with isotropic material for two different load cases.

The stress plots show that the highest stresses occur at different places for the two different load cases. The analyses in this chapter were made on symmetrical load case. When running analyses with a half loaded bridge deck, some parts that experience high stress are not reinforced with carbon fibre and therefore a higher deformation is reached compared with the original design.

6 Discussion

6.1 FRP and bridges

Bridges with FRP parts or fully constructed in FRP are gaining more and more popularity. In Europe quite a few FRP bridges have already been completed, and in Sweden there are several ones under way. The main constraints for building FRP bridges today is still slight higher material cost, limited knowledge of the material and a lack of structural design handbooks. Currently there is only the *EUROCOMP Design code and Handbook* and the dutch *CUR 96*. Many producers use their own design manual. A new FRP Eurocode is at final draft stage and is currently in process for acceptance. With a constantly declining prices and more FRP structures getting built, the FRP trend should keep increasing.

6.2 Parametric analysis

Throughout the process of this thesis we made many different models, both for testing purposes and case studies. All of our models were changed several times during the process due to new knowledge or realising mistakes. By having all of our models fully- or at least semi-parametrically set up, we could save a lot of time. Parametric modelling allowed us to perform three case studies and make changes in the models that would have otherwise been too time consuming. The parametric modelling was also a crucial part for making the optimisation process possible. There would be no way of analysing the different carbon configurations other than parametrically, since each optimisation changed the models hundreds of times, all automatic.

Parametric analysis is not widely used in the industry, but it is getting more and more popular. The strong benefits of not having to completely remake the entire model once a change is done at a certain place is a huge benefit, especially in the early stage when there are a lot of uncertainties and changes being done constantly. The fact that we were able to make three case study models, analysed and optimised, shows the strength and speed of this modelling technique. For the early design stage case studies the use of parametric modelling was very useful and efficient.

The main reason parametric modelling is not widely used in the industry is that it is not available in most of cases. To our knowledge, there are only a few plug-ins for *Grasshopper* that can perform parametric analysis. There is of course also the software *CATIA* and *ANSYS*, but these are not used in the construction industry. For FE-analysis, *Karamba* is the main software available, but *Karamba* can only handle isotropic materials at the time, which means it can only properly analyse steel. There is a great need for tools like *Tortoise* and other similar software, since *Tortoise* is very limited and not yet fully developed.

6.3 Optimisation techniques

6.3.1 Case studies

There are definitely arguments to be made that our optimisation techniques and results do not give justice to the designs at hand. All the case studies were done with certain limited knowledge about

the bridges and the carbon fibre setup. There might be reasons to why carbon fibre had been placed on certain places that we were not aware of. Also it should be said that our analyses disregarded many load cases, which could affect the placement of the carbon fibre.

However, the purpose of these studies was not to strictly improve current designs, but to showcase the possibilities with parametric analysis and the tools that we have developed. To quickly be able to analyse a geometry and iterate different design possibilities to find the best solution for the structure is a large advantage in early design.

6.3.2 Carbon fibre optimisation

The carbon fibre optimisation theories gave good results in general. In some cases it gave a large improvement and in other cases it did not help very much. This depends on how good the original carbon placement were, and in extension how easy it is to predict the structural behaviour of the geometry at hand. Placing carbon fibre at the most stressed elements generally seems to be a successful method, however the tool should not serve to pinpoint exactly where to place carbon fibre, but more of a guide to find the right areas. In simple cases there is likely enough knowledge to know where to place the carbon fibre (in a straight beam design for example), but when the geometry gets complex it is more difficult to place the carbon fibre on the most efficient parts. Our case studies showed that there is potential for a tool determining where to place the carbon fibres.

6.3.3 Fibre angle optimisation

The tools developed gives a more accurate model compared to the reality than by just aligning the fibres in the longitudinal direction. To our knowledge there is no easy and fast way to model the fibre directions in FE-tools like *BRIGADE/Plus*. This is very useful in some cases, for example Arkitektbron. In the technical report by Olsson and Nilsson (2015), an isotropic material was used in the basic model. If the bridge could be model as fast, or faster, in *Tortoise* and at the same time use more accurate material properties it could be of great use for the early design stage.

6.4 FE-solver

The decision to only implement shell elements is generally a large constrain, but for the investigated bridges it was suitable type of element. For most FRP structures shell elements will be enough, but for analysis of pultruded members, beam elements are a more suitable option. There is a lot of other functionality that could be added to complete the *Tortoise*-package, but the current components are a good base and have been enough for the SLS analyses in the case studies performed.

6.4.1 Performance

The tool has been fast enough to perform both regular analysis and the iterative optimisations with a mesh size large enough. Even though the analyses have been slower than *Karamba* and *BRIGADE/Plus* for large meshes, which is expected, the analyses have been performed in a reasonable time frame. No case studies have been limited in mesh size by the run time of the analyses. For more complex analyses with several load cases this could be a problem, but for the early stage design analysis the performance is good enough.

6.4.2 Verification

The components would still need more testing and be compared with other software to be completely verified. The testing has been performed on a limited number of test cases due to the time constraints of the thesis. The tests done have shown good correspondence and there have been no case where the results from *Tortoise* have differed greatly from other software. Especially the composite material components could use more testing in more complex geometries, since many test cases have been done in *Karamba*, which cannot handle anisotropic material.

7 Further investigations

7.1 Eigenfrequency optimisation

Through this thesis, the first frequency has generally been treated the same way as deflection. Only one specific optimisation of the eigenfrequency was made, and this was made from stress patterns derived from deflection due to vertical loads.

In order to truly optimise for a higher first eigenfrequency, one approach would be to derive the stresses from the first eigenmode. This could be done with the following expression:

$$\sigma = \mathbf{D}\mathbf{B}\mathbf{a}_m \quad (7.1)$$

where \mathbf{a}_m is the element deflections from the first eigenmode. This way, stiffness can be optimised for this particular deformation pattern. Usually, the first eigenmode is very similar to the deflected shape from vertical loads, but that is not necessarily always the case. In some cases the first horizontal eigenfrequency can be decisive, and thus the aforementioned approach could be beneficial.

7.2 Element definitions

The element chosen for this project does not take out of plane shear deformations into account. It is also inherently flat, meaning the surface analysed will be faceted. We do not consider any of these flaws to be severe, since out of plane shear deformations (perpendicular to the shell) play a small role in deformation of thin shells, and a sufficiently dense mesh will minimise the error from faceted elements.

However, a more precise element would allow for a faster convergence and thereby higher performance. A suitable element could be the MITC3+ element described by Lee, Jeon, Lee, and Bathe (2015).

The FE-solver could also benefit from greater functionality in terms of element types. It could potentially be useful to implement 1D elements such as beams and bars.

7.3 Ultimate limit state

This thesis is limited to investigations in serviceability limit state since this is widely regarded as the deciding factor in FRP Bridge design. However, engineers still need to check the design for ultimate limit state and better tools for this could be useful.

7.4 Second order effects

Since deformations in FRP bridges can become large, it might be useful and interesting to take second order effects into account. The FE-solver developed for this project uses linear assumptions, which may give non conservative results when deformations are large.

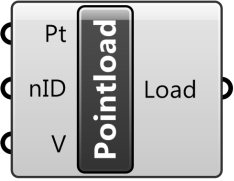


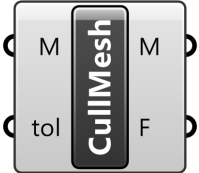
References

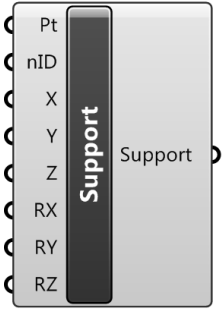
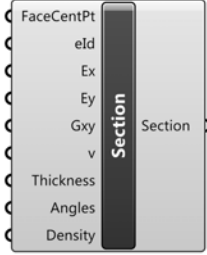
- EN-1990:2002/A1. (2002). *Eurocode: basis of structural design*. EUROPEAN COMMITTEE FOR STANDARDIZATION. (Cited on pages 41, 63).
- EN-1991-2:2003. (2003). *Eurocode 1: Actions on structure- part 2: Traffic loads on bridges*. EUROPEAN COMMITTEE FOR STANDARDIZATION. (Cited on pages 41, 63, 65, 76).
- Agarwal, B. D., Broutman, L. J., & Chandrashekhara, K. (2015). *Analysis and performance of fiber composites*. Wiley. (Cited on pages 5–8, 14, 15, 38, 49, 60, 72).
- Analytica. (2014). Analytica user guide: Parametric analysis. Retrieved May 16, 2017, from http://wiki.analytica.com/index.php?title=Parametric_analysis. (Cited on page 21)
- Ansys. (2010). *Ansys advantage, volume iv, issue 1: Driving vehicle performance*. Ansys. (Cited on page 21).
- Ansys. (2011). *Parametric analysis: The key to rapid, robust design*. Ansys. (Cited on page 21).
- Campbell, F. (2010). *Structural composite materials*. ASM International. (Cited on page 4).
- Carlsson, C. (2015). *Granskningshandling av kaponjärbron - regler för konstruktionsarbetets förutsättningar och metoder (rkfm) enligt trvk bro a.3.4*. Göteborgs Stad, Trafikkontoret. (Cited on page 43).
- Chiv, C. & Vocal, Y. (2014). *Preliminary design of a fiber reinforced polymer pedestrian bridge* (Master's thesis, Chalmers University of Technology, Division of Civil and Environmental Engineering). (Cited on pages 38, 40, 45, 60, 72).
- Chlosta, M. (2012). *Feasibility study on fiber reinforced polymer cylindrical truss bridges for heavy traffic* (Master's thesis, Delft University of Technology). (Cited on pages 5, 6).
- Damberg, H. (2001). *Komposithandboken*. Industrilitteratur AB. (Cited on pages 4–9).
- David Rutten. (2014, August 27). Grasshopper (Version 0.9.0076). Retrieved from <https://www.grasshopper3d.com>. (Cited on page 23)
- Dongyu-Fiberglass. (2014). Netherlands installs largest single-span composite bridge. Retrieved February 22, 2017, from <http://www.dongyufiberglass.com/en/news01.asp?id=3062>. (Cited on page 13)
- FiReCo. (2014). Bascule frp composite footbridge – fredrikstad. Retrieved February 22, 2017, from <http://www.fireco.no/?news=bascule-frp-composite-footbridge-fredrikstad>. (Cited on pages 13, 60, 61)
- karamba3d. (2016). Karamba - parametric engineering. Retrieved May 2, 2017, from <http://www.karamba3d.com/>. (Cited on page 24)
- Lee, Y., Jeon, H.-M., Lee, P.-S., & Bathe, K.-J. (2015). *The modal behavior of the mitc3+ triangular shell element*. Elsevier. (Cited on page 88).
- Mattsson, L. (2017). Se när norra europas första lättviktsbro lyfts på plats – i malmö. Retrieved June 13, 2017, from <https://www.sydsvenskan.se/2017-03-28/premiar-i-malmo-for-lattviktsbro>. (Cited on page 1)
- News, P. (2013). Moulded fibre reinforced plastic for bridge decks. Retrieved February 22, 2017, from <http://www.plastics.gl/construction/enter-the-dragon/>. (Cited on page 12)
- Novedge. (2017). The most powerful nurbs modeling tool with full support from mcneel. Retrieved April 28, 2017, from <https://novedge.com/products/2217>. (Cited on page 22)
- Olsson, E. & Nilsson, A. (2015). *Arkitektbron - technical description*. (Cited on pages 73, 77, 86).
- Ottosen, N. & Petersson, H. (1992). *Introduction to the finite element method*. Prentice Hall. (Cited on page 16).
- Ramböll. (2016). Kaponjärbron. Retrieved March 29, 2017, from <http://www.ramboll.se/Projekt/rse/kaponjarbron>. (Cited on page 37)

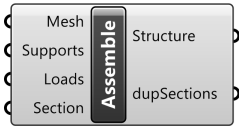
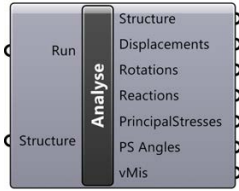
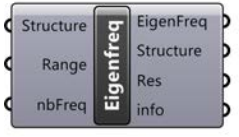
- Roylance, D. (2000). *Laminated composite plates*. MIT, Material Science and Engineering. (Cited on page 15).
- Rutten, D. (2010). Evolutionary principles applied to problem solving. Retrieved May 2, 2017, from <http://www.grasshopper3d.com/profiles/blogs/evolutionary-principles>. (Cited on page 24)
- Rutten, D. (2016). Galapagos evolutionary solver. Retrieved May 2, 2017, from <http://www.grasshopper3d.com/group/galapagos>. (Cited on page 24)
- Rutten, D. (2017). Grasshopper - algorithmic modeling for rhino. Retrieved April 28, 2017, from <http://www.grasshopper3d.com/>. (Cited on pages 22, 23)
- Summerscales, J. & Short, D. (1978). Carbon fibre and glass fibre hybrid reinforced plastics. (Cited on page 8).
- Tarek K.Hassan, E. M. & Rizkalla, S. H. (2003). Innovative 3-d frp sandwich panels for bridge decks. (Cited on page 9).
- TRVK-Bro-11. (2011). *Trvk bro 11 - trafikverkets tekniska krav bro*. Trafikverket, (cited on pages 43, 65, 76).
- Tutorialspoint. (2014). C# programming - object oriented programming. Retrieved May 2, 2017, from https://www.tutorialspoint.com/csharp/csharp_tutorial.pdf. (Cited on page 26)
- Valbona Mara, R. H. & Harryson, P. (2013). Bridge decks of fibre reinforced polymer (frp): A sustainable solution. (Cited on page 1).
- Zienkiewicz, O. & Taylor, R. (2000). *The finite element method, fifth edition*. Butterworth-Heinemann. (Cited on page 17).

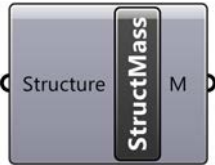
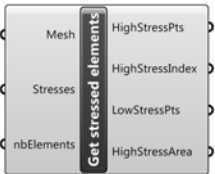
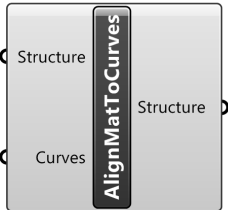
A Tortoise components

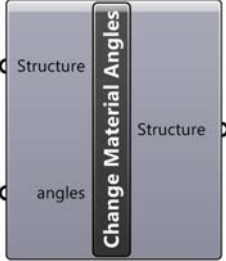
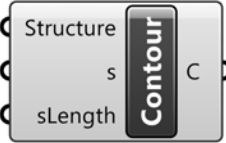

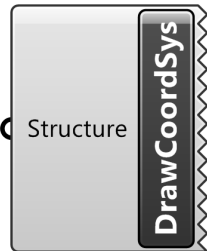
The following components are included in the *Tortoise*-package:

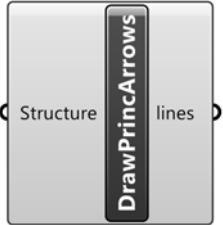

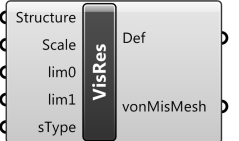
Component	Input	Output
<p>Create a point load.</p> 	<ul style="list-style-type: none"> • Pt: Points where loads are applied. • nID: Optional node ID where loads are applied. • V: Force vector in kN to be applied on points. 	<ul style="list-style-type: none"> • Load: A Tortoise point load
<p>Create a distributed load.</p> 	<ul style="list-style-type: none"> • CenPt: Face centre points where load is applied. • eID: Optional element ID where load is applied. • q: Force vector in kN to be applied to elements 	<ul style="list-style-type: none"> • Load: A Tortoise distributed load.
<p>Create a gravity load.</p> 	<ul style="list-style-type: none"> • CenPt: Face centre points where load is applied. • eID: Optional element ID where load is applied. 	<ul style="list-style-type: none"> • Load: A Tortoise gravity load.
<p>Cull duplicate vertices in mesh and remove zero area faces.</p> 	<ul style="list-style-type: none"> • M: Mesh to be culled. • tol: Distance tolerance. 	<ul style="list-style-type: none"> • M: Culled mesh. • F: Removed faces.

Component	Input	Output
<p>Create a support from vertices.</p> 	<ul style="list-style-type: none"> • Pt: Points where support is added. • X: Lock translations in X-direction. • Y: Lock translations in Y-direction. • Z: Lock translations in Z-direction. • RX: Lock rotations around X-axis. • RY: Lock rotations around Y-axis. • RZ: Lock rotations around Z-axis. 	<ul style="list-style-type: none"> • Support: A Tortoise support.
<p>Create a section from face centre points.</p> 	<ul style="list-style-type: none"> • FaceCentPt: Face centre points where section is applied. • eId: Optional element ID where section is applied. • Ex: Longitudinal E-modulus. • Ey: Transverse E-modulus. • Gxy: Longitudinal shear modulus. • v: Poisson's ratio. • Thickness: Thickness of laminae. • Angles: Angles of fibres. • Density: Density. 	<ul style="list-style-type: none"> • Section: A Tortoise section.

Component	Input	Output
<p>Assembles a structure from inputs.</p> 	<ul style="list-style-type: none"> • Mesh: Mesh to analyse. • Supports: Tortoise-supports to include. • Loads: Tortoise- loads to include. • Section: Tortoise-sections to include. 	<ul style="list-style-type: none"> • Structure: Assembled structure. • dupSections: IDs of elements with duplicate sections assigned.
<p>Analyse a Tortoise structure.</p> 	<ul style="list-style-type: none"> • Run: Toggle if analyse should run or not. • Structure: Tortoise-structure to be analysed. 	<ul style="list-style-type: none"> • Structure: Analysed structure. • Displacements: Displacement vector. • Rotations: Rotation vector. • Reactions: Solved reaction forces in kN. • PrinciplStresses: Principal stresses in MPa. • PS Angles: Angle between each elements x-axis and the largest principal stress in the element. • vMis: von Mises stresses in MPa.
<p>Calculate eigenfrequencies.</p> 	<ul style="list-style-type: none"> • Structure: Structure to analyse. • Range: Highest eigenfrequency value to look for. • nbFreq: Number of eigenfrequencies to calculate. 	<ul style="list-style-type: none"> • EigenFreq: Calculated eigenfrequencies. • Structure: Analysed structure. • Res: Residuals for each eigenvalue. • info: Feedback from the solver routine.

Component	Input	Output
<p>Calculate the total mass of a structure.</p> 	<ul style="list-style-type: none"> • Structure: Structure to weigh. 	<ul style="list-style-type: none"> • M: Mass of structure.
<p>Get the elements with the highest stresses.</p> 	<ul style="list-style-type: none"> • Mesh: Mesh to evaluate. • Stresses: Principal stresses for each element. • nbElements: Number of elements to be classified as 'High stressed'. 	<ul style="list-style-type: none"> • HighStressPts: 'High stressed' elements midpoint, based on the 'nbElements'-input. • HighStressIndex: Index of 'High stressed' elements. • LowStressPts: The rest of the elements. • HighStressArea: Area of the 'High stressed' elements.
<p>Align all elements material axis to a set of curves.</p> 	<ul style="list-style-type: none"> • Structure: Structure to analyse. • Curves: Curves to align element material axis with. 	<ul style="list-style-type: none"> • Structure: Analysed structure.

Component	Input	Output
<p>Change the material angles for the elements in a structure.</p> 	<ul style="list-style-type: none"> • Structure: Structure to change. • angles: Material orientation angle, one per element. 	<ul style="list-style-type: none"> • Structure: Analysed structure.
<p>Draw principal stress contours.</p> 	<ul style="list-style-type: none"> • Structure: Structure to analyse. • s: Start curve. • sLength: Step length. 	<ul style="list-style-type: none"> • C: Contour curves.
<p>Draws the material axis for each element.</p> 	<ul style="list-style-type: none"> • Structure: Structure to visualise. 	<ul style="list-style-type: none"> • lines: Lines indicating directions of the material directions.
<p>Draws the coordinate system for each element.</p> 	<ul style="list-style-type: none"> • Structure: Structure to visualise. 	

Component	Input	Output
<p>Draw largest principal stress arrow in each element.</p>  <p>The diagram shows a rectangular component with a vertical bar in the center labeled 'DrawPrincArrows'. To the left of the bar is the input 'Structure' and to the right is the output 'lines'.</p>	<ul style="list-style-type: none"> • Structure: Structure to analyse. 	<ul style="list-style-type: none"> • lines: Lines indicating direction of the largest principal stress in each element.
<p>Visualise eigenmodes.</p>  <p>The diagram shows a rectangular component with a vertical bar in the center labeled 'EigenModes'. To the left of the bar are inputs 'Structure' and 'ScaleFac'. To the right of the bar is the output 'EigenModes'.</p>	<ul style="list-style-type: none"> • Structure: Structure with analysed eigenfrequencies. • ScaleFac: Scale factor for the deformation. 	<ul style="list-style-type: none"> • EigenModes: Deformed mesh from the eigenmodes.
<p>Visualise deformation and von Mises stresses.</p>  <p>The diagram shows a rectangular component with a vertical bar in the center labeled 'VisRes'. To the left of the bar are inputs 'Structure', 'Scale', 'lim0', 'lim1', and 'sType'. To the right of the bar are outputs 'Def' and 'vonMisMesh'.</p>	<ul style="list-style-type: none"> • Structure: Structure to visualise. • Scale: Factor to scale the deformation with. • lim0: Lower limit for von Mises stress. • lim1: Top limit to visualise von Mises stress ($\text{lim1} < 1$). 	<ul style="list-style-type: none"> • Def: Deformed mesh. • vonMisesMesh: von Mises stress plot.

B C# types

C# types mentioned in the thesis are listed below:

C# type	Explanation
double	64-bit floating-point value
Boolean	Store the boolean values, true and false
Enum	A set of named integer constants
Vector3D	3 dimensional vector in <i>MiStrAn</i>
SparseMatrix	Matrix only storing nonzero elements
Vector	Single column vector. Not to be confused with a Euclidean vector
Node	<i>MiStrAn</i> node, Holds information for a single node in the structure
ShellElement	<i>MiStrAn</i> shell element. Stores information for a single shell element
Support	<i>MiStrAn</i> support. Stores information of support conditions for a node
Section	<i>MiStrAn</i> section. Stores information of one or multiple elements section
Load	<i>MiStrAn</i> load. Stores load information

C Tortoise accessibility

The *Tortoise* package will undergo minor bug fixing, arrangement and clean up of components before it is available to download. The package is likely to be released in June 2017, and will be available at www.food4rhino.com for free.

The entire source code is uploaded on *GitHub* and can be viewed and downloaded on the link: <https://github.com/GurraGurka/MiStrAn/>